

Bi系酸化物高温超電導銀被覆線材の研究

1992

日方威

①

Contents

1. Introduction

1-1. Superconductor 2

1-2. High-Tc oxide superconductor 4

1-3. Powder-coated Bi系酸化物高温超電導銀被覆線材の研究 7

2. Experimental

(Studies of silver sheathed Bi-based oxide high-Tc superconducting wires)

2-1. Measurement of T_c 8

2-1-1. DC method 8

2-1-2. a.c. inductive method (Cooper method) 10

2-2. Observation of structure and sample preparation 12

3. Development of Bi-based oxide superconducting wire with high Jc

3-1. Introduction 14

3-2. Homogenization of Bi-Tl phase 15

3-3. Grain definition and sintering process 17

3-4. Control of composition ratio 19

3-5. Summary 20

1992

日方 威

Takeshi Hikata

4. Studies of weak links at grain boundaries

4-1. Introduction 22

4-2. Studies of weak links by μ -probe method 24

4-3. Studies of weak links by ac inductive method 25

Contents

1. Introduction	
1-1. Superconductor	3
1-2. high-Tc Oxide superconductor	4
1-3. Powder-in-tube process	7
2. Experimental	
2-1. Measurement of J_c and T_c	9
2-1-1. 4-probe dc method	
2-1-2. SQUID	
2-1-3. a.c. inductive method (Campbell method)	
2-2. Observations of structures and sample preparations	12
3. Development of Bi-based oxide superconducting wire with high J_c	
3-1. Introduction	14
3-2. Homogenization of Bi-2223 phase	15
3-3. Double deformation and sintering process	17
3-4. Control of composition ratio	19
3-5. Summary	20
4. Studies of weak links at grain boundaries	
4-1. Introduction	22
4-2. Studies of weak links by 4-probe dc method	24
4-3. Studies of weak links by ac inductive method	26

4-4. Summary	31
5. Studies of J_c -B properties	
5-1. Introduction	32
5-2. Dominating factors of J_c -B properties	34
5-2-1. For parallel magnetic field to a-b plane	
5-2-2. For perpendicular magnetic field to a-b plane	
5-3. J_c -B properties in liquid helium	44
5-4. J_c -B properties in liquid hydrogen	44
5-5. Summary	46
6. Studies of Irreversibility lines	
6-1. Introduction	49
6-2. measurement of Irreversibility lines	50
6-3. Summary	54
7. Conclusions	
55	
Acknowledgements	59
References	61
Figure captions	66

1. Introduction

1-1. Superconductor

Superconductivity was discovered by Kamerlingh Onnes in 1911.[1-1-1] He observed the fact that the electrical resistance of mercury disappeared completely at 4.1 K using liquid helium. He concluded that the resistance state of the mercury was transformed into a new phase. The phase-transition temperature is called as critical temperature (T_c). It was found that many metals became the superconductors such as Nb and Pb at 4.2 K.

Since then many trials were attempted for getting high critical current density (J_c) for power applications. However, the metals such as Hg, Pb ($T_c=7.2$ K) and Nb ($T_c=9.2$ K) so called as type-I superconductors, did not allow high J_c and the construction of magnets generating high magnetic field because of low critical magnetic field (H_c). For example, the critical magnetic field was 400 Gauss for the first discovered superconductor -mercury- even at absolute zero temperature. The problem for low H_c was settled by discovery of the superconducting alloys such as NbTi($T_c=18$ K), Nb₃Sn ($T_c=18.3$ K) and Nb₃Ge (23.2 K) etc. (type-II superconductors) because there are a continuous increase in flux penetration starting at a lower critical field H_{c1} and reaching $B=H$ at a upper critical field H_{c2} , instead of a discontinuous break down of superconductivity in a first-order transition at H_c in type-I superconductors, and further the pinning sites were introduced to disturb the break down by the flux flow caused by Lorentz force between the

transport current and magnetic field. The H_{C2} was of the order of 10-20 Tesla for those alloy superconductors.

The superconductors have the advantages of large current without electric resistance and of large generating magnetic field for power applications. However, there were some disadvantages. Liquid helium which is inevitable for working superconductors as coolant, is expensive and restricted for resource, and it is difficult to simplify the cryostat including the cooling systems. Therefore, the applications were limited to the superconducting magnet mainly and it was difficult to apply on superconducting cables etc. because the large cooling systems were required. Now superconductivity is applied to the superconducting magnets such as in MRI devices and other various magnets by using liquid helium.

1-2. High-Tc Oxide superconductor

Since oxide high-Tc superconductors were discovered by J.G.Bednortz and K.A.Muller in 1986,[1-2-1] there have been reports of a Y-based oxide superconductor by Wu et al.[1-2-2] with a superconducting critical temperature (T_c) in the 90 K class, followed by 110 K class Bi-based oxide superconductor by H.Maeda et al.[1-2-3] and a 125 K class Tl-based oxide superconductor by A.M.Hermann et al. [1-2-4], thus making it possible to use liquid nitrogen (where boiling temperature at 1 atm. is 77.3 K) as the coolant. Since a new oxide superconductor, Bi-Sr-Ca-Cu-O system with a high-Tc phase (110 K) and a low-Tc phase (80 K) was reported by Maeda et al., there

have been many investigations for homogenization of each phase.

For high-Tc phase, it was reported that substituting a part of Bi for Pb produced a stable high-Tc phase.[1-2-5] Bi-based high-Tc oxide superconductors with a high-Tc phase was expected to have a higher Jc because of a larger margin between its Tc and the liquid nitrogen temperature (77.3 K) than a low-Tc phase. However, it was difficult for the high-Tc phase to produce the single phase because the low-Tc phase was included.

Not only is liquid nitrogen easy to use and inexpensive, but it also makes it possible to simplify the cryostat and features a large heat flux. It is expected that the actual use of a superconductor at the temperature of liquid nitrogen will greatly affect such fields as energy and electronics.[1-2-6] For power applications, for example, the superconducting cable which can transfer the large electric current with much smaller volume and voltage than the cables by the copper or aluminum conductors, can be used in low magnetic field below 0.1 Tesla. The superconducting magnets which can be used for MRI device or MAGREV (magnetic revitator), are used in high magnetic field over 1 Tesla. Therefore, it was the most important subject for the development of oxide superconducting wire to increase the critical current density (Jc) in each operating magnetic field.

The author has made an early start on research into the development of Bi-based high-Tc oxide superconducting wires. In this thesis the author represents the studied of the silver sheathed Bi-based high-Tc oxide superconducting wires.

Bi-based high-Tc superconductor has two kinds of the phases which have critical temperatures exceeding 77.3 K. That is, the

phase with the chemical formula of $\text{Bi}_2\text{Sr}_2\text{Ca}_2\text{Cu}_3\text{O}_y$ is called as 2223 phase ($T_c=110$ K), and the other phase with the formula of $\text{Bi}_2\text{Sr}_2\text{CaCu}_2\text{O}_y$ is called as 2212 phase ($T_c=80$ K). 2212 phase is homogenized by melt processing and 2223 phase is homogenized by solid reaction process.

Before the advent of Bi-based oxide superconductor, the oxide superconducting wires by Y-based oxide superconductor with high J_c over 10^4 A/cm² could not be obtained at 77.3 K. The major cause was the presence of weak links at the grain boundaries. The oxide superconductor is composed of polycrystalline with the crystallites size in range from a few microns to several tens microns in the wire. Therefore when the transport current flow across the grain boundaries, it is restricted to decrease by barriers and micro-bridges at the grain boundaries because of the short coherence length of superconducting carrier and flux creep. The weak link effect has been shown by some researchers[1-2-7,8]. The peculiar characteristics are rapid decrease of J_c by applying the slight magnetic field (<100 Gauss) and hysteresis phenomena in J_c vs. magnetic field during increase and decrease of magnetic field. These phenomena were improved for the first time through the development of Bi-based oxide superconducting wires in the author's research.

In the early stage of the research, it was not much expected to obtain high- J_c Bi-based oxide superconductor because of the fact that the possibility of flux-lattice melting in the wide range of temperature was indicated through the measurement of magnetization at 77.3 K and the temperature dependence of stiffness of magnetic flux lattice using a high-Q mechanical

oscillator.[1-2-9] ΔM disappeared at about only 0.5 Tesla in M-H curve by magnetization measurement at 77.3 K. While ΔM of other oxide superconductors, such as Y-based and Tl-based superconductors remained over 1 Tesla.[1-2-10,11] And the softening of the flux lattice was measured. Bi-based oxide superconductor has higher anisotropic structure composed of each layer such as Bi-,Sr-,Ca- and Cu- oxide. The reason is that $(\text{Bi-O})_2$ planes in the unit cell show the nonmetallic nature, while the CuO_2 planes are conductive.[1-2-12]

1-3. Powder-in-tube Process

It is widely accepted that the promising process for fabricating long wire is only powder-in-tube method now[1-3-1,2]. The manufacturing process is as follows. The superconducting powder is filled in metal pipes, drawn to a round wire, rolled or pressed into a flat tape shape wire and then sintered, as shown in Fig.1-3-1. Therefore, the wire is composed of the metal sheath and the superconductor. So far, silver has been successfully applied as the sheath material. There are following two reasons for it; (1) Silver does not react with oxide superconductors and (2) silver does not oxidize, even at high temperature and in oxygen gas. If copper sheath was used, the oxide superconductor would react, be deoxidized and not exhibit superconducting properties.

Powder-in-tube process has advantages such as; (1) for processing metallic wire drawing, rolling and other conventional techniques are used, so it is possible to obtain long unit

length and fine wire with small cross section, and (2) the metal sheath can be used as a stabilizer (a bypass for the current in the case of partial breakage of the superconductivity).[1-3-3]

2. Experimental

2-1. Measurement of J_c and T_c

2-1-1. 4-probe dc method

The criterion for critical-current (I_c) determination was defined as $1 - 0.1 \mu\text{V}/\text{cm}$ for 4 probe dc method. Expressed as electrical resistivity, $1 \mu\text{V}/\text{cm}$ is equivalent to approximately $4 \times 10^{-5} \mu\Omega \text{ cm}$ for the typical tape with about $4 \text{ mm}^w \times 0.15 \text{ mm}^t$ and silver-superconductor ratio ~ 3.5 , which is an adequate value when compared to the electrical resistance of silver, which is $3 \times 10^{-1} \mu\Omega \text{ cm}$ at 77.3 K. J_c was calculated through dividing I_c by the cross section area of superconducting section in the silver sheathed tape. [2-1-1]

2-1-2. SQUID

The magnetization measurements were carried out by using a superconducting quantum interference devices (SQUID) magnetometer with a 2 cm scan length, where the field inhomogeneity is estimated to be no greater than 0.01 %.[2-1-2] The data are taken by measuring the magnetization versus temperature at various fixed magnetic fields in the temperature range from the irreversible temperature to 300 K. Background signals and normal-state magnetization were carefully subtracted using the extrapolation of a curve fitted to the measured magnetic moment-versus-temperature data between 200 and 300 K.

2-1-3. a.c. inductive method (Campbell method)

a.c. inductive method was conceived by A.M.Campbell.[2-1-3]
The features of this method is to piled up the minute a.c. magnetic field to d.c. magnetic field and to be able to obtain the more spacious data by penetration of the a.c. magnetic field than d.c. magnetization method. Therefore, this method is useful for the polycrystal high-Tc oxide superconductors with the complex current path, such as the transport critical current density through the grain boundaries and the local critical current density within the grains through the measurement of the spacious distribution of a.c. magnetic flux for penetration depth.[2-1-4]

Figure 2-1-1(a) shows the flux distribution in the slab superconductor which is placed parallelly to y-z plane with thickness; d, and infinite width for y-z direction when the a.c. field is piled up on the minute a.c field. Constant d.c. field, B_e and minute a.c. field are applied to z-direction in the process increasing d.c. field. It is defined that the amplitude, Φ of a.c. field is applied to the sample at the d.c. field B_e , and the penetrated region reaches the depth, λ' to x direction from the surface. When b increases by δb , Φ and λ' increases by $\delta\Phi$ and $\delta\lambda'$, respectively. $\delta\Phi$ corresponds to the hatching in Fig.2-1-1(a). When it is based on the critical state model, it is introduced as follows;

$$\mu_0 J_c = \delta b / \delta \lambda' \quad (2-1-1)$$

Therefore, J_c can be estimated from the function of b for λ' .

For quantitative calculation, the width of a sample is assumed as w for the y -direction. The $\delta\phi$ becomes,

$$\delta\phi = 2w\delta b\lambda' \quad (2-1-2)$$

In the case of slab superconductor, $\delta\phi$ exhibits the flux which penetrates from both surfaces. If $\delta b \rightarrow 0$, equation (2-1-2) becomes

$$\lambda' = 1/2w (d\phi/db) \quad (2-1-3)$$

Therefore, each relationship of λ' for b is introduced by measurement of ϕ for b and calculation by the function (2-1-3).

Figure 2-1-2 shows the measurement system of a.c. inductive method. A superconducting sample and pick up coil are placed in the minute a.c. field piled up to the constant bias d.c. field.

A cancel coil is placed at the empty space in the a.c and d.c. fields. The cancel coil acts for canceling the inductive signal in the space without the superconducting sample. The measurement frequency was 35 Hz.

When an amplitude of the a.c. field, b is applied, the inductive voltage appears for the pick up (V_p) and cancels coils (V_c), respectively as follows;

$$V_p = -N_p(S_p - S_s) db/dt - N_p d\phi/dt, \quad (2-1-4)$$

$$V_c = -aN_c db/dt, \quad (2-1-5)$$

where N_p and N_c are the number of turns of the coils, and S_p , S_c and S_s are cross section areas perpendicular to the applied field of the pick up coil, cancel coil and the sample, respectively. a -value ($0 < a \leq 1$) exhibits the partial voltage by voltage divider. The term of db/dt can be canceled by adjustment of a -value. $d\phi/dt$ is obtained as follows,

$$d\phi/dt = (V_c - V_p) / N_p. \quad (2-1-6)$$

2-2. Observations of structures and sample preparations

TEM (Transmission Electron Microscope), SEM (Scanning Electron Microscope), EDX (Energy Dispersive X-ray analysis) and X-ray diffraction analysis were used for the observation of morphologies of samples. [2-2-1]

Sample preparations were as follows. For the TEM observation, the silver sheathed tapes were peeled off from the sheath and were cut perpendicularly to the tape plane and ground down to below 20-30 μm in thickness. And then the samples set on the single core mesh, were ground by an ion etching device to below sub-micron in thickness. TEM observations were carried out in view along tape planes.

For SEM and EDX, the silver sheathed tapes buried in the epoxy

resin, were ground to flat surface and polished by aluminum powder in alcohol.

X-ray diffraction analysis using Cu-K α radiation was performed on the tape surface of each oxide superconductor after the silver sheathes were peeled off.

Results of the X-ray diffraction analysis of the Bi-2223 oxide superconductor, which has two kinds of phases, 70-80 K class phase (2112) and 8-10 K class phase (2202), revealed that the Bi-2223 oxide superconductor has two kinds of phases, 70-80 K class phase (2112) and 8-10 K class phase (2202), indicating liquid nitrogen superconductivity. Since the Bi-2223 oxide superconductor has two kinds of phases, the high-T_c phase (2112) is the main phase and the low-T_c phase (2202) is the secondary phase. In order to improve the high-T_c phase, an addition of excess Cu and Bi (1-1.5, 2), high pressure oxygen treatment (1200°C) and prolonged sintering (3-4 d) were attempted. For example, when the Bi-2223 oxide superconductor was sintered at 850°C for 4 d, the ratio of 2112 phase (81-220) increased through the partial substitution of Bi for Bi (11-2-3). However, the Bi-2223 phase (81-220) still contained in Bi (11-2-3) oxide superconductor. Therefore, it was expected to obtain high T_c of 77 K by substitution of the low T_c phase non-superconducting materials and was tried at the grain boundaries.

In the early period, Bi-2223 oxide superconductor was not well reported to exhibit high T_c because the main phase was not the 2112 phase. The substitution of Bi for Bi (11-2-3) was reported to improve the superconductivity of Bi-2223 oxide superconductor. The Bi-2223 oxide superconductor was reported to exhibit high T_c of 77 K by substitution of the low T_c phase non-superconducting materials and was tried at the grain boundaries.

3. Development of Bi-based oxide superconducting wires with high J_c

3-1. Introduction

Maeda et. al who discovered Bi-Sr-Ca-Cu oxide superconductor, exhibited that the Bi-based oxide superconductor had two kinds of phases, $T_c=80$ K class phase (2212) and $T_c=110$ K class phase (2223), exceeding liquid nitrogen temperature.[1-2-3] Since the discovery, much effort had been made to single out the high- T_c phase, Bi-2223. In order to increase the high- T_c phase, an addition of excess Ca and Cu [3-1-1,2], high pressure oxygen treatment [3-1-3] and prolonged sintering [3-1-4], were attempted, for example, about 1 week. Among these efforts, it was reported to increase the ratio of 110 K phase (Bi-2223) through the partial substitution of Pb for Bi [1-2-5]. However, the 80 K phase (Bi-2212) still remained in Bi(Pb)-Sr-Ca-Cu-O bulk samples. Therefore, it was impossible to obtain high J_c at 77.3 K by disturbance of the low T_c phase, non-superconducting materials and weak links at the grain boundaries.

In the early period, Bi-based oxide superconductor was not much expected to obtain high J_c because the weak pinning force was indicated through the measurements of magnetization at 77.3 K compared to other oxide superconductor such as Y-based and Tl-based superconductors. ΔM disappeared at about only 0.5 Tesla in M-H curve by magnetization measurement. However the transport J_c over 10^4 A/cm² has been obtained at 77.3 K and at 1 Tesla for $(\text{Bi,Pb})_2\text{Sr}_2\text{Ca}_2\text{Cu}_3\text{O}_x$ silver sheathed tapes by the

author's studies. After the author's study, many researchers had participated in the researching J_c for Bi-based oxide superconductor. In following sections, the author describes how the Bi-2223 superconducting wires with high J_c were developed.

3-2. Homogenization of Bi-2223 phase

The oxide superconducting powder was put into a silver tube. This powder was produced by mixing the powders of the composition ratio of 1,1,1 and 2 for Bi, Sr, Ca and Cu from Bi_2O_3 , SrCO_3 , CaCO_3 and CuO , respectively. This ratio was reported first by Maeda et.al.[1-2-3] It was known also that the partial substitution of bismuth by lead increases the high- T_c phase.[1-2-5] The powder of the composition ratio of 0.8, 0.2, 1, 1 and 2 for Bi, Pb, Sr, Ca and Cu from Bi_2O_3 , PbO , SrCO_3 , CaCO_3 and CuO , respectively, was produced.[3-2-1] Then the powders were mixed and calcined and sintered before putting into the silver tube. The sintered powder was composed of low- T_c phase (80-K phase) rather than high- T_c phase (110-K phase). After reduction of the diameter by drawing, they were introduced to a press process. The drawing process can not increase the density of oxide powder enough because the strength of the silver sheath is not sufficient to squeeze the inner powder. The press process which is extensively used to make bulk material is adequate for controlling the pressure for the inside powder when pressure is applied to the silver sheathed wire. The length of wire which is limited by a pressure die head, is 30-50 mm, sufficient to

measure J_c . Milling by rolls can produce long lengthen tape conductors, where the material elongates in a longitudinal direction, and this process was not adequate for experiments in controlling the pressure. In the press process, the oxide powder in the silver tube are elongated in the transverse direction of the conductor length. The elongation in the longitudinal direction is highly restricted by the friction between silver surface and pressure die head. The cross section slightly changes in accordance with the increase of inner powder density. This means that the pressure goes to the inside powder effectively by press process using a sheath conductor. All press processing was performed at room temperature. The tapes after pressing were sintered. The heat treatment is necessary to obtain J_c . J_c and T_c were measured through 4-probe dc method.

J_c did not change in the $\text{BiSrCaCu}_2\text{O}_x$ superconductor with silver sheath for the load before heat treatment as shown in Fig. 3-2-1. In this $\text{BiSrCaCu}_2\text{O}_x$ silver sheathed wire without Pb, J_c could be increased by using heat treatment around the melting point for short period rather than using press processing. However the produced superconducting phase was low T_c phase (Bi-2212 phase; 80 K class) only. Figure 3-2-2 shows that the J_c rapidly increases at 880 C for 1 hr sintering. In this case it was observed that the oxide became dense by melting. The maximum J_c was 426 A/cm^2 at 77.3 K and $T_{c(R=0)}$ was 84 K.

When Pb was partially substituted to the bismuth, the phenomenon drastically changed. The oxide superconductor of $\text{Bi}_{1.8}\text{Pb}_{0.2}\text{SrCaCu}_2\text{O}_x$ with silver sheath exhibited that the

thickness of the wire becomes thinner when increasing the load by pressing, and then J_c increases rapidly as the press load increases and the maximum value was $1,850 \text{ A/cm}^2$ at 77.3 K in zero magnetic field as shown in Fig.3-2-3. When the tapes become too thin, J_c decreased rapidly. The reason is due to damage of superconducting phase through the gas inflation from inner oxide.

The $T_c(R=0)$ of the sample with $1,850 \text{ A/cm}^2$ was 104 K, thus the high- T_c phase (Bi-2223 phase) was dominant in this $\text{Bi}_{1.8}\text{Pb}_{0.2}\text{SrCaCu}_2\text{O}_x$ silver sheathed wire. The susceptibility of this sample after removing the silver sheath was measured. The result is shown in Fig. 3-2-4. The onset of T_c was 110 K and the low temperature phase could not be seen for this sample. It was thought before that it was difficult to obtain the single high- T_c phase, and the long heat treatment (for example, for longer than 1 week) was necessary to obtain a large volume of high- T_c phase from the bulk material experiments, but all samples in this experiment were sintered for 24 hours. The formation of high- T_c phase was accelerated by press processing and the silver sheath.

Previously, lengthy period over 1 week was required for the sintering time[3-1-4]. U.Endo et al. produced single phase by sintering under low oxygen pressure, 1/13 atm at 842 C for 84 hours. [3-2-2] The author succeeded to produce the single phase for a very short time, only 24 hours under atmosphere without controlling the oxygen partial pressure.

3-3. Double deformation and sintering process

Figure 1-3-1 shows the fabricating process of $(\text{Bi,Pb})_2\text{Sr}_2\text{Ca}_2\text{Cu}_3\text{O}_y$ silver sheathed wire.[2-2-2,3-3-1] Oxide or carbonate powder of Bi, Pb, Sr, Ca and Cu with the each composition ratio is mixed with $(\text{Bi,Pb})_2\text{Sr}_2\text{Ca}_2\text{Cu}_3\text{O}_x$ and calcined from 750 to 860 C.

The powder is filled in a silver pipe, and then the composite is drawn and rolled to a tape shape, typically 0.1~0.2 mm in thickness and 2~5 mm in width. After then the wires are sintered at about 850 C and deformed again by rolling or pressing and finally sintered again.

It was found that this double deformation and sintering process had the different functions for each step. At the first step, the filled powder is homogenized to 2223 phase (110 K phase) for growing large grains as shown in Fig.3-3-1(a). At the second step, the platelet grains are connected strongly by the deformation and sintering again. If the sintering process was conducted once only, the J_c would decrease rapidly in a slight magnetic field because the grains grow to the large straight planes with misorientation to each other and the grain boundaries are composed of the point contacts which become the origin of the rapid decrease of J_c in low field by the weak links as shown for sample C in Fig. 3-3-2. In this case the J_c -B properties exhibit the 2-step decrease and especially decreases to over 1/10 at only about 100 Gauss as shown in Fig.3-3-3. The improvement of J_c and J_c -B properties can be executed by repetition of deformation and sintering, and the 2-step decrease phenomena of J_c -B disappears as shown as samples A and B in Fig.3-3-3. It was shown that J_c was increased and J_c -B properties were improved

by the second sintering. The grain boundaries are connected at the c-plane to each other with slight bending as shown in Fig. 3-3-1(b).

Figure 3-3-4 shows the X-ray diffraction pattern for the specimen with J_c of $5,500 \text{ A/cm}^2$. The series of peaks of the low- T_c phase with the characteristic (002) peak at $2\theta=5.7$ and 7.2 degree could not be observed. Therefore, the only superconducting phase of this specimen was the 110 K phase. However, it was observed that the non-superconducting phase, Ca_2PbO_4 , remained. The grains in the 110 K phase were found to be oriented with the c-axis perpendicular to the wide plane of the specimen.

3-4. Control of the composition ratio

The optimization of composition ratio was carried out for getting higher J_c . [3-4-1] Figures 3-4-1(a) and 3-4-1(b) show the SEM photographs on the polished surface of the cross section of sample A ($J_c(77.3 \text{ K}, 0\text{T})=14,300 \text{ A/cm}^2$) and B ($J_c(77.3 \text{ K}, 0\text{T})=5,500 \text{ A/cm}^2$). The composition ratio of sample A was $\text{Bi}_{1.8}\text{Pb}_{0.4}\text{Sr}_2\text{Ca}_{2.2}\text{Cu}_3\text{O}_x$ and that of sample B was $\text{Bi}_{1.6}\text{Pb}_{0.4}\text{Sr}_2\text{Ca}_2\text{Cu}_3\text{O}_x$. $T_c(R=0)$ of sample A was 106 K. $T_c(R=0)$ of sample B was 104 K. By increasing the composition ratio of Bi and Ca, the volume of the non-superconducting phases in sample A was reduced to a half of those in sample B. The optimized composition ratio might be shifted to higher composition ratio of Bi and Ca from the complete composition ratio, $(\text{Bi}, \text{Pb})_2\text{Br}_2\text{Ca}_2\text{Cu}_3\text{O}_x$ for increasing J_c .

Through the improvement by the optimized composition ratio and fabricating process, J_C achieved 4.7×10^4 A/cm² at 77.3K and a zero magnetic field. This wire exhibited $J_C=1.1 \times 10^4$ A/cm² at 1 Tesla as shown in Fig. 3-4-2. For actual applications, J_C was required to be over 10^4 A/cm² at least in each operating magnetic field. It is shown that the J_C of BiPbSrCaCuO silver-sheathed wire is close to the useful level of the cables and magnets.

3-5. Summary

It was found that the J_C and J_C -B properties were improved by the homogenization of high- T_c phase (110 K phase), alignment of the superconducting grains and the good contact at the grain boundaries through the double deformation and sintering process.

For homogenization of high- T_c phase, it was found that the silver sheath accelerated the formation of high T_c phase (2223 phase).

For double deformation and sintering process, it was found that the filling powder was homogenized to 2223 phase (110 K phase) for growing large grains at the first step and the platelet grains were connected strongly by the deformation and sintering again.

For controll of the composition ratio, it was found that the volume of the non-superconducting phases ($CaPbO_4$, Ca_2CuO_3 , etc.) were reduced through the control of composition ratio by increasing Bi and Ca.

As a result, J_c became first exceeding 10^4 A/cm² in zero magnetic field at 77.3 K through the improvement of these morphologies. These data exhibited that the Bi-2223 silver sheathed wire had high potentiality for the practical use to power applications.

4. Studies of weak links at grain boundaries and the history effect

4-1. Introduction

It was observed that the sintered polycrystalline samples of high- T_c oxide superconductors had low J_c and showed hysteresis of J_c in low magnetic field during increase and decrease of the magnetic field (history effect).[1-2-7] It is empirically known that the history effect is caused by weak couplings at the grain boundaries in superconductors.[4-1-1]

The history effect was exhibited for metal superconductors by T.Aomine et al.[4-1-2] They produce a micro bridge for granular Al, In, Nb, NbN etc. as shown in Fig.4-1-1. The two superconducting banks are connected through the bridge. When the bridge length is shorter than coherence length, $\xi(T)$, Josephson effect appears. In this case, the bridge length is longer than $\xi(T)$. The history effect of granular Al with $2 \mu\text{m} > L > (T)$, $3 \mu\text{m} > W > 1 \mu\text{m}$, $2,000 \mu\text{m} > W_{\text{bank}} > 20 \mu\text{m}$, $800 \mu\text{m} > d > 44 \mu\text{m}$ was observed, where L , W , W_{bank} and d indicate the bridge length, width, bank width and thickness, respectively. The characteristics of history effect for the micro bridge were summarized as follows:

- (1) the history effect became small when the bridge length became large and the width became large;
- (2) magnetic field with the maximum value of J_c , and H_p became large when the bank width became large;
- (3) the history effect did not appear for the samples without the

bridge;

(4) the history effect became larger when the thickness at the banks became larger than at the micro bridge. They exhibited that the micro bridge model could apply to the polycrystalline Y-Ba-Cu-O high-Tc oxide superconductors.[4-1-3]

The history effect was explained also through the Josephson type weak links of polycrystalline $\text{YBa}_2\text{Cu}_3\text{O}_7$ by E.Evetts et al.[4-1-4]. They explained that an interpretation of the complex dependence of critical current on applied field and sample microstructure was given in terms of the hysteretic properties of a Josephson-junction network mediated by trapped flux which was retained by strong pinning regions.

The weak link problems at grain boundaries with history effect of the silver sheathed wire was serious for the development of practice superconducting wires. Silver sheathed Y-based oxide superconducting wires were fabricated by the powder-in-tube method. Even if J_c was $4,140 \text{ a/cm}^2$ at 77.3 K in zero magnetic field for $\text{YBa}_2\text{Cu}_3\text{O}_{7-\delta}$, it was decreased rapidly to 1/100 at slight magnetic field of about $2 \times 10^{-2} \text{ Tesla}$. [4-1-5] Polycrystalline $\text{YBa}_2\text{Cu}_3\text{O}_{7-\delta}$ has granular grains and it is difficult to align the grains in a-b plane. D.Dimos et al. reported that the J_c decreased as a function of misorientation in a-b plane of bicrystal of $\text{YBa}_2\text{Cu}_3\text{O}_{7-\delta}$. [4-1-6] Therefore, it was very important for good connection at grain boundaries to align the grains. The author describes about the relationship between J_c and weak links through the history effect and the temperature dependence.

4-2. Studies of weak links by 4-probe dc method

In Fig. 3-3-3, sample C has a two-step decrease in J_c against H , while samples A and B have only a one-step decrease in the higher magnetic field.[2-2-1] Sample C is from the first process only (rolling-sintering) in the double deformation and sintering process (deformation-sintering-deformation-sintering).

Samples A and B are from the complete double deformation and sintering process. The difference was revealed in the observation of SEM photographs of the fracture surfaces of sample B and C in Fig.3-3-1. It was found that sample C has the grain boundaries composed of the point contacts with different orientation in a-b planes by straight platelet grains as shown in Fig.3-3-1(a). Sample B has grain boundaries which are connected at the c-plane to each other with slight bending as shown in Fig. 3-3-1(b). Therefore the transport current flows smoothly through the grain boundaries securely along the aligned a-b plane. The rapid decrease disappeared in the low magnetic field at about 100 gauss since the magnetic field never penetrated easily into the grain boundaries by the strong bonding at the grain boundaries.

Figure 3-3-2 shows the history effect of J_c during the increase and decrease of the magnetic field.[3-4-1] The hysteresis appeared at a low magnetic field below 0.1 Tesla and showed anisotropy for the magnetic field direction, parallel and perpendicular to the tape surface. The hysteresis of sample A was small, while sample C had large hysteresis. Therefore the hysteresis must be caused mainly by the weak links at the grain

boundaries.

Figure 4-2-1 shows the relationship between the magnetic field dependence and history effect of J_c of Bi-based oxide superconducting wire. In the low magnetic field below 0.1 T, it was found that the magnetic field dependence and history effect of J_c were improved with the increase of J_c in a zero magnetic field. The history effect disappeared for the wire with J_c above 2.5×10^4 A/cm² in a zero magnetic field. This indicates the disappearance of the weak links which led the history effect by improvement of the contact at the grain boundaries. [4-2-1]

Fig. 4-2-2 shows the magnetic field dependence of J_c of various samples at 4.2 K. J_c at 77.3 K for each specimen were (A) 2.8×10^4 A/cm², (B) 2.5×10^4 A/cm², (C) 1.8×10^4 A/cm² and (D) 1.4×10^4 A/cm². J_c at 23 T was 4.6×10^4 A/cm² ($I_c = 54$ A) at 4.2 K for sample A. The history effect was observed during the increase and decrease of magnetic field.

The magnetic field dependence of J_c and history effect were improved also with the increase of J_c in a zero magnetic field at 4.2 K. The wire B with 2.5×10^4 A/cm² did not exhibit the history effect in 77.3 K as shown in Fig. 4-2-1, but exhibited it clearly at 4.2 K. It is considered that the magnetic field dependence of J_c is influenced more strongly by the weak links at the grain boundaries at 4.2 K than 77.3 K.

The temperature dependence of history effect of J_c was measured at the temperature range from 4.2 K to 20 K by using liquid helium and hydrogen for the samples with $J_c=16,000-30,000$ A/cm² at which the history effect did not appear at 77.3 K. [4-

2-2] Figure 4-2-3 shows the magnetic field dependence of J_c at 4.2 K, 15 K and 20 K for the sample with $J_c=30,000 \text{ A/cm}^2$. The history effect is quite evident at 4.2 K, less so at 15 K and virtually nonexistent at 20 K. Therefore it was found that the history effect appeared again at temperature range below 20 K for the sample without the history effect at 77.3 K. It is known that the history effect appears by weak links with microbridge at grain boundaries. Therefore these data suggest that the weak links appear again at the temperature below 20 K.

4-3. Studies of weak links by a.c. inductive method

Figure 4-3-1 shows the λ' -b line of the Bi-based oxide superconducting silver sheathed wire through a.c. inductive method. The horizontal axis exhibits the amplitude of a.c. field and the vertical axis exhibits the penetration depth of the magnetic field from the sample surface. The gradient, $d\lambda'/db$ exhibits as $1/\mu_0 J_c$ in eq.2-1-1. In this case, there are 2 kinds for gradient. These data show the 2 kinds of J_c with different current path such as inter- and intra- J_c for superconducting grains. In this section, the author discusses J_c through the inter-grain.

Figure 4-3-2 shows the comparison of J_c -B properties measured at 77.3 K for silver-sheathed BiPbSrCaCuO wires by a.c. inductive method and 4 probe dc method.[4-3-1] J_c of these wires was $1.7 \times 10^4 \text{ A/cm}^2$ in a zero magnetic field measured by the 4 probe d.c. method. J_c -B properties are almost the same for the two measurements, a.c inductive method and 4-probe d.c. method.

This result shows that the magnetic field dependence of the transport J_C can be described by ac inductive method as well as 4 probe dc method. This means that it is possible to easily measure the temperature dependence of J_C -B properties (J_C -B-T) of the wires with high critical current without the influence of heating at the transport current terminals in flowing gas helium. The transport critical current of 233 A ($J_C=2.1 \times 10^5$ A/cm²) at 4.2 K in a wire with the dimension of 4.2mm^w x 0.15mm^t was achieved, so the large heat flux for coolant or extremely low resistive joints are required in the case of transport current measurements by 4 probe dc method. [4-2-2]

Figure 4-3-3 shows the temperature dependence of J_C in 0.2, 1.0 and 2.0T for sample #1 ($J_C(77.3K, 0T)=2.5 \times 10^4$ A/cm²) by a.c. inductive method. It was found that the J_C decreased largely in the temperature region over about 20 K with the increase of magnetic field from 0.2 to 2 Tesla. Figure 4-3-4 shows the magnetic field dependence of J_C up to 4 Tesla and 60 K. At 4.2K and 25 K, the magnetic field dependence of J_C is small and especially small around 4 Tesla, while at 60 K J_C has large field dependence. J_C can be represented under a fixed magnetic field as follows:

$$J_C \propto B_{C2}^m(T) \propto [1-(T/T_C)^2]^m, \quad (4-2-1)$$

using an empirical temperature dependence of $B_{C2}(T) \propto 1-(T/T_C)^2$ [4-2-3]. m-value is usually a parameter determined by the sort of pinning sites. Figures 4-3-5 and 4-3-6 show the double logarithmic plots of J_C vs $1-(T/T_C)^2$ for sample #1 and sample #2

($J_C(77.3K, 0T) = 6.3 \times 10^3 \text{ A/cm}^2$). For sample #1, m is 3.43 at high temperature region and 10.05 at low temperature region. For sample #2, m -value is 2.75 and 16.3 at high and low temperature regions, respectively. These data exhibit that the J_C -B properties were dominated by more than 2 kinds of pinning mechanism at least. Normally $m \sim 1.5$ is obtained for plane pinning sites and $m \sim 4$ for point pinning sites.[4-2-4] However, these are not fitted in this case in the low temperature region. The effects of another factors, such as change of properties of weak links and flux creep, should be taken into account for more comprehensive understanding of pinning. In low temperature region, the influence by weak links is large because m value was decreased much from 16.3 to 10.5 with the increase of J_C (77.3K) from $2.5 \times 10^4 \text{ A/cm}^2$ to $6.3 \times 10^3 \text{ A/cm}^2$.

Figures 4-3-7 and 4-3-8 show the history effects of J_C -B properties for sample #3 ($J_C(77.3K, 0T) = 3.0 \times 10^4 \text{ A/cm}^2$) and sample #2 at 4.2 K and 20 K. Solid circles indicate the increasing procedure of magnetic field and open circles indicate the decreasing one in the case of a zero field cooling. The obtained critical current density takes a smaller value in the increasing field procedure than the decreasing one. This data is also consistent qualitatively with 4 probe dc method [4-3-1]. However, in the case of decreasing magnetic field, the external field does not penetrated into the center of the superconducting grains. Therefore, it needs to penetrate the field into the center of grains by getting the field cooling measurement. Open squares indicate J_C -B properties in the field cooling procedure. In this case, the intragrain shielding

currents were not induced, and so J_C was not influenced by the weak links at the grain boundaries. Therefore, in the field cooling case, J_C must be taken as an intermediate value of those in increasing and decreasing (major) lines. In sample #3 with high J_C , the field cooling line is in approximately intermediate region, while in sample #2 with low J_C , the field cooling line is larger than the decreasing field line in a zero field cooling procedure. It is considered that when the history effect exists up to much higher magnetic field than the maximum field in the present measurement, the decreasing field line can not return completely to the major decreasing line. That is, the history effect shown in Fig. 4-3-8 is smaller than true one. Here the degree of history effect is represented by the difference in J_C between major increasing line and field cooling line, $[\Delta J_C = J_C(FC) - J_C(\text{increasing})]$. This difference, ΔJ_C , in low J_C sample is larger than those in the higher J_C samples. However this figure shows that the history effect almost simultaneously disappears near 20 K for both samples at 3 Tesla, which can be seen in Fig. 4-3-9. Figure 4-3-10 shows the temperature dependence of history effect, $(J_{C_{FC}} - J_{C_{inc}}) / J_{C_{inc}}$ at 0.5 Tesla. It is shown that the history effect is reduced with increasing temperature and disappears at near 30 K. These data are consistent with temperature dependence of transport J_C -B by using liq. He and Liq. H₂ in Fig 4-2-3.

Figure 4-3-10 exhibits that the hysteresis becomes small with the increase of J_C . Figures 4-3-5 and 4-3-6 shows also that the m value which represents the decreasing rate of J_C , becomes small in low temperature region with the increase of J_C . These

results suggest that a further improvement in J_c can be attained by improvement of weak coupling at the grain boundaries. Furthermore, the strong temperature dependence of J_c for m value, indicates differently from the temperature dependence predicted from the pinning mechanism. Therefore the equation (4-2-1) as which m value is defined, is meaningless. However, the equation can be meaningful by exchanging H_{c2} to the irreversibility field (H_{irr}) because H_{irr} has the J_c dependence as well as in this case as shown in Chapter 6.

Figure 4-3-11 and 4-3-12 represent the results in the low temperature region of Figs. 4-3-5 and 4-3-6. These results show that deviation from the straight line in the higher temperature region starts at about 30 K at 0.2 Tesla and at about 20-30 K with decreasing temperature for the both samples.[4-3-2] Hence the strong temperature dependence of J_c coincides with that of the history effect in the low temperature region. It can be concluded that both the rapid decrease in J_c with elevating temperature and the history effect originate from weak links in the samples.

The rapid decrease in J_c is considered to be caused by degradation of superconductivity in weak link region with increase of temperature. These regions seem to lose the superconductivity completely above 20-30 K and remain as a strong coupling region only at the grain boundaries. Hence, the variation in J_c becomes more gradual and is accompanied by the disappearance of the history effect. The disappearance of the history effect at higher temperature does not originate from better coupling due to longer coherence length but from the fact

that the current flows only through the strong coupling region without the history effect.

4-4. Summary

It was corroborated that the rapid decrease of J_c in low magnetic field region was dominated by the weak link at the grain boundaries, and the history effect could disappear by double sintering process (deformation-sintering-deformation-sintering) and the improvement of morphologies including non-superconducting phases with increasing of J_c .

The temperature dependence of J_c -B properties and the history effect were measured effectively in wide temperature range on BiPbSrCaCuO silver sheathed wires with various level of critical current density. The results were obtained as follows;

(1) Both the rapid decrease in J_c with increasing temperature and the history effect of J_c appeared in the same temperature region, below 20-30 K. In the low temperature region, it was observed clearly that J_c was influenced by weak links with the history effect. It is concluded from the coincidence of the two temperature regions that these phenomena are caused by the low temperature weak links in the silver sheathed Bi-based oxide superconducting tapes.

(2) In the samples with a smaller J_c , the history effect is relatively larger and the temperature dependence of J_c in the low temperature region is stronger. Therefore, J_c in this state is still thought to be influenced by the weak links and the improvement of weak coupling is necessary in order to improve J_c further at the grain boundaries.

5. Studies of Jc-B properties

5-1. Introduction

Since the discovery of high-Tc oxide superconductors exceeding liquid nitrogen, many efforts have been attempted to get higher Jc for power applications. At the beginning, it was difficult to get the polycrystalline oxide superconductors such as Y-based high-Tc superconductors. For Bi-2223 oxide superconductor, Jc was low and magnetic field dependence of Jc had two-step decrease. The low field decrease was improved by solution of weak links problems as described in previous chapter 4. However, the decrease of Jc in the higher magnetic field remains. Usually, Jc-B properties in the higher magnetic field were explained by pinning mechanism.

Type II superconductor has mixed state allowing penetrating quantum fluxoids between H_{C1} and H_{C2} . When the current flows in the state, the quantum fluxoids move by Lorentz force and induce the voltage. However, the fluxoid's motion by Lorentz force can be restrained through the pinning sites composed of separating fine non-superconducting phases and lattice defects etc. Therefore the fluxoids were trapped in the valley of potential of pinning sites against Lorentz force, and do not induce the voltage through movement of fluxoids. For increasing Jc, The effective pinning sites have been investigated.

Pinning mechanism of metal superconductors such as NbTi were investigated quantitatively.[5-1-1,2] When the quantum fluxoid

lattice is assumed as a continuous medium, the elastic properties are represented by elastic modulus tensor as follows;

$$C_{44} = (B_{C2}^2 / \mu_0) b^2, \quad (5-1-1)$$

$$C_{66} = (B_{C2}^2 / \mu_0) G_{66}(b), \quad (5-1-2)$$

where $G_{66}(b) = (1/8K^2)(1-K^2/2)b(1-b)^2(1-0.58b+0.29b^2)$, $b = B/B_{C2}$ and $K = \lambda/\xi$ (GL parameter). When a quantum fluxoid moves slightly as shown in Fig. 5-1-1(a), the surrounding fluxoids were moved together to the same orientation. Radius of the correlating region is represented as l_{66} for shear motion of quantum fluxoid. The correlating length is represented as l_{44} for the bending motion as shown in Fig. 5-1-1(b). l_{44} and l_{66} are written respectively as follows,

$$l_{44} = (C_{44}/\alpha)^{1/2}, \quad (5-1-3)$$

$$l_{66} = (C_{66}/\alpha)^{1/2}, \quad (5-1-4)$$

where α is Labusch parameter determined by pinning potential, U_0 . [5-1-3] When Lorentz force density, F_L increases as the transport current, the pinned fluxoid get out of the pinning sites and begins to slip against other pinned one. The relative restrain force is proportional to the shear modulus of flux lattice, C_{66} . Therefore the slip of fluxoids begins when F_L is equal to F_p ,

$$F_p = C_{66}/2\pi a_f, \quad (5-1-3)$$

where $a_f = (2\Phi_0/\sqrt{3B})^{1/2}$ ($\Phi_0 = h/2e$). Therefore, F_p is dependent on the properties of flux lattice.

For high-Tc oxide superconductors, dominating factors of Jc-B properties were not clear enough because of the strong anisotropy of superconducting properties such as the short coherence length, penetration depth and high thermal activation energy in high temperature region. The author discusses later the dominating factors and mechanism of Jc-B properties through the difference of Jc-B properties for Jc values and applied magnetic field directions of polycrystalline Bi-based oxide superconductors.

5-2. Dominating factors of Jc-B properties

5-2-1. Parallel magnetic field to a-b plane

Figure 5-2-1 shows the magnetic field dependence of Jc at 77.3 K, which are normalized by Jc in a zero magnetic field from 1.7×10^4 to 3.0×10^4 A/cm². [4-2-1] The magnetic field was applied perpendicularly to a transport current, and parallelly to the wide plane of the wires at 77.3 K. The magnetic field dependence of Jc was improved with the increase of Jc in a zero magnetic field. The sample with Jc = 3.0×10^4 A/cm² (Ic=35 A) in a zero magnetic field has Jc = 1.5×10^4 A/cm² at 0.1 Tesla, which is considered for usage with the superconducting cables and has Jc = 3.3×10^3 A/cm² at 1 Tesla which is the field used

for the magnets. While, when the magnetic field applied perpendicularly to the tape surface, the improved tendency at the high J_c region is much smaller than that in parallel field as shown in Fig. 5-2-16. Therefore it was found that the magnetic field dependence of J_c had different tendency for the directions of the applied magnetic field with respect to the tape surface.

Figure 5-2-2 shows J_c in each magnetic field compared to J_c in a zero magnetic field. It was found that the improved tendency of the magnetic field dependence of J_c was enhanced better simultaneously in the low magnetic field area below 0.1 Tesla and the high magnetic field area above 1 Tesla. In the magnetic field from 0.1 to 1 Tesla, the improved tendency of the magnetic field dependence of J_c was the same because the lines for the region from 0.1 Tesla to 1 Tesla were parallel to each other as shown in Fig. 5-2-2. However, the tendency is much larger at 2 Tesla than that below 1 Tesla.

Figure 5-2-3 shows the magnetic field dependence of pinning force ($J_c \times B$) for wires having each levels of J_c , (a) $47,000 \text{ A/cm}^2$, (b) $18,000 \text{ A/cm}^2$ and (c) $5,500 \text{ A/cm}^2$. Pinning force increased in whole range up to 3 T with the increase of J_c in a zero magnetic field. The magnetic field at which the pinning force becomes the maximum value, does not change.

Figure 5-2-4 shows the pinning force normalized with maximum pinning force value. The magnetic field dependence of the pinning force was improved especially large in the high magnetic field region. This means that the pinning force becomes large relatively at high magnetic field region. Figure 5-2-5 shows

the SEM photographs of superconducting section of wires having J_C of (a) 5,500 A/cm², (b) 10,600 A/cm² and (c) 22,200 A/cm². In sample (a) with low J_C , three kinds of non-superconducting phases, such as phase I (SrCaCuO), phase II ((Ca,Sr)₂PbO₄) and phase III (Ca₂CuO₃), were found with large granular shape. In sample (b), phase I disappeared, and phase II became small and thin shape. However, phase III remained with the large size. In sample (c) with high J_C , all non-superconducting phases were dispersed in fine and thin shape.

The fine dispersed non-superconducting phases were observed through TEM. Figure 5-2-6 shows the TEM image of thin non-superconducting phase at a gap in a-b planes viewed along the a-b plane, which was found in the sample B. The thickness is about several nm. The boundary between the high-T_c phase with $c/2=1.8$ nm and the non-superconducting phase is clear, and the arrangement of atoms in the high-T_c phase does not show any disorder. These phases found through TEM were platelet shaped, and aligned along the plane of the wire. Therefore they are expected to function as the pinning sites for the Lorentz force along c-axis. The superconducting grains connect smoothly with gentle bending toward each other.

The fine granular non-superconducting phase was found, as shown in Fig.5-2-7. This granular non-superconducting phase may act as the point pinning sites which become effective when the magnetic field applied perpendicularly to a-b plane. However, it must be noted that the weak links are produced simultaneously at the grain boundaries including the non-superconducting phases since the a-b planes at both side of the

grain boundary have misorientation.

The grain boundaries which did not include the non-superconducting phases, were observed along a-b plane of Bi-2223 oxide superconductor through TEM. Three types of grain boundaries were observed as shown in Figs. 5-2-8 and 5-2-9. Figure 5-2-8 shows the twist boundary which was composed of the aligned grains rotated around c-axis since the arrangement of atoms was clear for the only upper grain through high resolution TEM. Figure 5-2-9 shows the misfitted grain boundaries with small angle as shown in the electron diffraction pattern. The boundary is sharp and clear because it does not include the non-superconducting phase. Figure 5-2-7 shows the grain boundary in a-b plane with different orientation by small angle. Each arrangement of atoms was connected smoothly through the grain boundary. The area of these clean and sharp grain boundaries as shown in Figs. 5-2-8 and 5-2-9 increases and the current path through the grain boundary connections becomes smooth with decreasing the non-superconducting phases.

The volume ratio of non-superconducting phases to high-T_c phase was estimated by observation through EDX measurement to be 30% for sample(a), 20% for sample(b) and 8% for sample(c) through Fig. 5-2-5. The improvement of J_c-B properties of the wires in Fig. 5-2-1 have strong relationship with the improvement of morphology.

In the low magnetic field below 0.1 T, the magnetic field dependence and history effect of J_c were improved with the increase of J_c in a zero magnetic field through history effect as shown in Fig. 4-2-1. These data correspond the improvement

of the contact at the grain boundaries. The decrease of J_c in the high magnetic field area around 1 T was shifted to a higher magnetic field as shown in Fig.5-2-1. It looks like that the improvement of the weak links at the grain boundaries corresponds to the improvement of J_c -B in a high magnetic field when it is applied parallelly to the plane of the wire.

Figure 5-2-10 shows the magnetic field dependence of J_c for the wire of $J_c = 2.5 \times 10^4$ A/cm² at 77.3 K. When the magnetic field was applied parallelly to the plane of the taped wire, it was found that the wire exhibits the same magnetic field dependence of J_c for both directions, parallel and perpendicular to the transport current. This means that the J_c -B properties are dominated by the same mechanism for parallel and perpendicular directions to the transport current.

The BiPbSrCaCuO superconductor was composed of platelet grains with a few hundreds nm in thickness piled up along the c-axis as shown in Fig. 3-3-1(b). The transport current in the wire must have the two kinds of components along the c-axis direction when it crosses the grain boundaries and along the a- or b-axis directions when it flows in a platelet grains.

Usually, the magnetic field dependence of J_c in the higher magnetic field have been understood by pinning theory which dominates the pinning force estimated by the size and interval distance of pinning sites through Lorentz force between the transport current and magnetic field. However, the author discusses later about the presence of the other dominating factors of J_c -B properties.

The author considered how Lorentz force acted and the

magnetic flux flowed in polycrystallines of Bi-2223 oxide superconductor when the transport current flowed through the grains as shown in Fig. 3-3-1(a). In this case, the grains were composed of straight platelet shape. Therefore the grain boundaries have misorientation and a point contact. The Jc-B properties in high magnetic field region are improved by the second deformation and sintering process as shown in Fig. 3-3-3.

It was found that Bi-2223 oxide superconductor in silver sheathed wire has large anisotropy by large two-dimensional fluctuation in the magnetization measurements.[5-2-1,2] The magnetization in high fields from 1 to 5 Tesla displays good scaling behavior as function of $4\pi M / (TH)^{1/2} = A[T - T_c(H)] / (TH)^{1/2}$, which can be explained by Ginzburg-Landau fluctuation theory for a two-dimensional system as shown in Fig.5-2-11(a). For three dimensional scaling law, it was not fitted as shown in Fig.5-2-11(b). While, for $YBa_2Cu_3O_7$, it was fitted as function of $4\pi M / (TH)^{3/2} = A[T - T_c(H)] / (TH)^{3/2}$, which can be explained as three-dimensional system as shown in Fig. 5-2-12 by U.Welp et al. [5-2-3] These data mean that the correlation between layers of a-b plane of Bi-2223 oxide superconductor is much weaker than that in a-b plane.

The flux lattice softening was observed through loss peaks of a high-Q mechanical oscillator by Gammel et al. as shown in Fig.5-2-13. For Bi-based oxide superconductor (2212 phase) single crystal, the softening temperature exhibited $T_s / T_c = 0.32$. The magnetic flux lattice becomes soft at 77.3 K. Furthermore, when the flux flows at a few Tesla, the flux flow resistivity is

very low at 77.3 K because the flux-flow resistivity, R_f is represented by the simplest Bardeen-Stephen model[5-2-6] as follows:

$$R_f(T) = \rho_n B / \mu_0 H_{C2}(T),$$

where ρ_n is the normal-state resistivity at measuring temperature. The term of $B / \mu_0 H_{C2}(T)$ means that the flux-flow resistivity is proportional to the area of the normal core of a vortex. At 77.3 K, $\mu_0 H_{C2}$ is determined as 128 Tesla through the measurement of M-H curve. The flux resistivity becomes about 1/32 of ρ_n when the flux flow appears at 4 Tesla.

When the flux moves along a-b plane, the correlation length of flux lattice, l_{44} (bending motion) and l_{66} (shear motion) is short and the elastic modulus of flux lattice, C_{44} (bending motion) and C_{66} (shear motion) is small. Therefore, local flux-flow can occur perpendicularly to c-axis through the weak correlations.

Through the above considerations, the author proposes a model for the magnetic field dependence of J_c of BiPbSrCaCuO silver sheathed wire at 77.3 K as follows.

Figure 5-2-14 shows the model for the interactions between magnetic field and transport current. In the wire, the transport current flows along c-plane in the grains, and when the transport current crosses the grain boundaries, it flows along c-axis. Therefore the interaction between transport current and magnetic field must be considered for two kinds of

transport current.

When the magnetic field was applied parallelly to the taped plane and perpendicularly to the current, the Lorentz force was generated parallelly to c-axis for current along a-b plane and perpendicularly to c-axis for current along c-axis as shown in Fig. 5-2-14(a).

Bi-based oxide superconductor has strong anisotropy and short coherence length. The coherence length was measured through the magnetization measurement on the silver sheathed wire with the magnetic field parallel to the c axis. The coherence length, $\xi(0)_{ab}=0.96$ nm and $\xi_c(0)=0.02$ nm was estimated by a reversible M-H curve, where $\xi(0)_c$ was calculated by using the anisotropy ratio for Bi-based superconductor, (≈ 50). [5-2-2,4] The temperature dependence of $H_{C2}(T)$ was estimated as shown in Fig 5-2-15. $H_{C2}(0)$ and $H_{C2}(77.3$ K) was estimated as 297 Tesla and 128 Tesla, respectively.

It must be considered that the pinning force has anisotropy with respect to crystal orientation. The reasons are as follows.

Many possible pinning sites such as a thin non-superconducting phases and intergrowth layers as shown in Fig.5-2-6 and the twist grain boundaries as shown in Fig.5-2-8 were observed perpendicularly to c-axis. While, there are few pinning sites along c-axis. Furthermore, the grains are aligned to c-axis, and coherence length and penetration depth of Bi-2223 oxide superconductor have large anisotropy.

Therefore it is considered that J_c -B characteristics are influenced by Lorentz force along a-b plane generated by current with c-axis component and the applied magnetic field. The

relationship between the improvement of J_c - B characteristics and history effect is explained as follows: When the current path becomes narrow at the grain boundaries with weak links, magnetic field enters easily in the grain boundary and history effect occurs by difference of shielding current during increase and decrease of magnetic field.[1-2-8,5-2-5] At these grain boundaries, the transport current along c-axis concentrates at the narrow weak link path in the magnetic field, and Lorentz force is generated strongly perpendicular to c-axis for the weak links. When the history effect is improved with the increase of J_c , the current path becomes wide and the bending becomes strong at the grain boundaries and the influence of magnetic field may become small for it.

In more macroscopic scale, the sample with low J_c involves the big size non-superconducting phases such as CaCuO , CaSrPbO and SrCaCuO as shown in Figs. 5-2-5 (a) and (b). The transport current with c-axis component occurs around the non-superconducting phases. The transport current density along the c-axis becomes relatively large around those phases and the Lorentz force works parallelly to the a-b plane with wide area as shown in Figs.5-2-5(a) and (b). The transport current density along c-axis becomes small and the area with c-axis current becomes small with the decrease of the size of non-superconducting phases as shown in Fig. 5-2-5 (c), relatively. Therefore the Lorentz force which works parallelly to the a-b plane becomes small. The J_c - B characteristics are dominated by the current with c-axis component at the grain boundaries. When local flux flow along a-b plane appears at

a few Tesla and 77.3 K, the flux-flow resistivity is small and stabilizes by the high H_{C2} .

5-2-2. Perpendicular magnetic field to a-b plane

Figure 5-2-16 shows the magnetic field dependencies of J_c when the magnetic field was applied perpendicularly to the plane.

The magnetic field dependence of J_c in the low magnetic field region was improved, but it was not improved in the high magnetic field region. The feature is quite different from the case of the parallel magnetic field as shown in Fig. 5-2-1.

Therefore, the factors which dominate J_c -B characteristics are different between the applied magnetic field parallelly and perpendicularly to the tape plane. The magnetic field is applied perpendicularly to the a-b plane as shown in Fig. 5-2-14 (c), the Lorentz force works parallelly to the a-b plane for the transport current in the a-b plane and it hardly works on the c-axis component transport current.

J_c -B characteristics correspond to the magnetic field dependence of ΔM by VSM (Vibrating sample magnetometer) as shown in Fig. 5-2-17.

The magnetization curve corresponds to the J_c -B characteristics in the grains which has much larger J_c than the transport J_c through grain boundaries.

Because J_c -B characteristics must be dominated by the intrinsic pinning sites along c-axis in each grain with the large volume, they were not dependent on the grain boundary characteristics in high field region. For the improvement of J_c -B characteristics when the magnetic field is applied

perpendicularly to the tape plane, it is necessary for the increase of pinning force to introduce the effective pinning sites along c-axis. Accordingly, the flux flows along a-b plane when the magnetic field is applied along c-axis.

5-3. J_c -B properties in liquid helium

Figure 5-3-1 shows the magnetic field dependence of J_c at 4.2 K for tape wires having J_c of 1.4×10^4 to 4.4×10^4 A/cm² in a zero magnetic field and at 77.3K. [5-3-1] The magnetic field was applied parallelly to the tape plane up to 23 Tesla. J_c changed little in the magnetic field from 5 to 23 Tesla. The J_c at 4.2K was also increased with the improvement of J_c at 77.3 K. The wire with $J_c(77.3K) = 4.4 \times 10^4$ A/cm² has a J_c of 1.03×10^5 A/cm² at 23 Tesla. Figure 5-3-2 shows the magnetic field direction dependence of the wires with $J_c(77.3K) = 2.8 \times 10^4$ A/cm². When the magnetic field was applied parallelly to the tape plane, $J_c(4.2K, 23T)$ was 4.6×10^4 A/cm². When the magnetic field was applied perpendicularly to the tape plane, $J_c(4.2K, 23T)$ was 3.5×10^4 A/cm². Accordingly it was found that the difference was only about 30%. These properties are much more excellent than the metallic superconductors such as Nb₃Sn because J_c of the metallic superconductor becomes smaller around 20 Tesla as shown in Fig.5-3-3. Therefore it was found that BiPbSrCaCuO sheathed wires had a sufficient high potentiality for the application in super-high magnetic field over 20 Tesla at 4.2 K.

5-4. J_c -B properties in liquid hydrogen

The cooling system would be simplified if the superconducting magnets could generate by using the other coolants for liquid helium. The operation in liquid hydrogen has large merit from the points of running cost and the operating technique if the superconducting magnets are operated at 15-20 K by using liquid hydrogen. [4-2-2, 5-4-1]

For this measurement, a two-specimen sample holder was built to be used in a cryostat containing a bath of boiling liquid hydrogen. The sample holder is equipped with three current leads, two sets of voltage taps, and two carbon-resistor liquid-level indicators. Because of safety requirements, all the vapor is vented outdoors through a pumping system that can maintain a constant cryostat pressure. In the experiments, the leads could safely carry currents up to 21 A at 100 torr (15 K for hydrogen) cryostat pressure.

The typical measurement procedure consisted of two basic steps: (1) hydrogen runs at 20 K and 15 K (2) helium run at 4.2 K, the sample holder was placed in a cryostat containing liquid hydrogen (1.5-2 liters), and the 20 K data were taken at the magnetic field up to 19.75 Tesla. The 20 K measurements were immediately followed by the 15 K measurements with the cryostat operated at a pressure of 99-100 torr; the same field sequence was used. After completion of the hydrogen runs, the cryostat with the sample holder was removed from the magnet and taken outdoors.

Figure 5-4-1 represents three separate sets of I_c vs. T plots, for the three groups of tapes. No 4.2 K data were taken

for Tape 1 and 2 as shown in Table 5-4-1. The magnetic field direction is parallel to the tape's flat surface and perpendicular to the current direction. Tape 3 in the table, for example, has a I_c of 60.6 A at 19.75 Tesla and 20 K, which corresponds to a critical current density (over the superconductor cross section area of 0.110 mm^2) of $55,100 \text{ A/cm}^2$, a value significantly higher than that at 19.75 Tesla and 4.2 K achievable by the best Nb_3Sn conductor now available. This sample shows $J_c=103,000 \text{ A/cm}^2$ at 4.2 K and 23 Tesla. Figure 5-4-2 shows the comparison of J_c -B properties at 4.2 K and 20 K. The V-I trace taken for this tape at 19.75 Tesla and 4.2 K shows that the conductor's index number n is 29. (n is the exponent appearing in the V-I relationship near I_c : $V \propto (I/I_c)^n$.) These properties suggest that the J_c -B properties not only at 4.2 K but also at 20 K, are much more excellent than the metallic superconductors such as Nb_3Sn as shown in Fig.5-4-2.

The critical current values achieved with these tapes now make the construction of "high- T_c " superconducting magnets of engineering interest feasible, at least when operated below ~ 20 K. Although the operating of high- T_c superconducting magnets in the temperature range below ~ 20 K seems, at first glance, less appealing than that at liquid-nitrogen temperature, when requirements of stability and protection for engineering devices are included in magnet design[5-4-2], this lower temperature range operation may appear desirable. A high value of n obtained at 19.75 Tesla and 4.2 K also strongly suggests that BiPbSrCaCuO , when operated at 4.2 K, may ultimately become the best conductor material for persistent-mode, high-field (>29

Tesla) or high proton-frequency (>900 MHz) nuclear magnetic resonance (NMR) superconducting magnets.

5-5. Summary

It was found that the J_c -B properties have different dominating factors for the parallel and perpendicular magnetic field to the tape plane of Bi-based high-Tc oxide superconducting wires. The factors dominating the magnetic field dependence of J_c of silver sheathed polycrystalline BiPbSrCaCuO (Bi-2223) wire were investigated. The following model was proposed to interpret the results data. When the magnetic field is applied parallelly to the wide plane of the wire, J_c -B characteristics are dominated by the c-axis component of the transport current crossing the grain boundaries. When the magnetic field is applied perpendicularly to the wide plane of the wire, the J_c -B characteristics are dominated by the current in the a-b plane. For both cases, the fluxoid flows along a-b plane.

The magnetic field dependence of J_c was measured at 4.2 K. It was found that the J_c was much larger at 4.2 K than at 77.3 K and increased up to over 10^5 A/cm² at 23 Tesla. The magnetic field dependence of J_c was small in the magnetic field from 5 to 23 Tesla. The J_c at 4.2K was also increased with the improvement of J_c at 77.3 K.

The magnetic field direction dependence of the wire was measured. The difference between parallel and perpendicular to the tape plane was only 30 %. These properties are much more excellent than the metal superconductors such as Nb₃Sn and NbTi.

Therefore it was found that BiPbSrCaCuO sheathed wires had a very high potential for the application in super-high magnetic field over 20 Tesla at 4.2 K.

Jc-B properties were measured in high magnetic field until 19.75 Tesla in liquid hydrogen. High Jc and n-value were obtained for construction of high-Tc superconducting magnets which made it feasible for engineering interest, at least when operated at 20 K.

6. Studies of Irreversibility lines

6-1. Introduction

It was represented as shown in the previous chapters that the influence of the weak links at grain boundaries were decreased for Bi-based oxide superconductor. Very high J_c was achieved up to very high magnetic field at low temperature region below 20 K. However, these values fall off rapidly with increasing field at high temperature such as liquid nitrogen temperature. These data means that the lack of such effective pinning centers restricts the critical current property at high temperature as shown in Fig. 6-1-1. This property is characterized by the so-called irreversibility line, i.e., the boundary between the reversible ($J_c=0$) and irreversible ($J_c>0$) regions in the temperature versus magnetic field space.

For the design of a superconducting magnet, irreversibility magnetic field $H_{irr}(T)$ and temperature $T_{irr}(H)$ are important because the critical current is dominated by the $H_{irr}(T)$ rather than the critical magnetic field $H_{c2}(T)$. The irreversibility field, $H_{irr}(T)$, is obtained as the inverse relation of the irreversibility temperature, $T_{irr}(H)$.

This phenomenon was first noted by Muller et al. [6-1-1] They showed that there is a significant temperature range below the mean-field critical magnetic field $H_{c2}(T)$ in which the magnetization of bulk La-Sr-Cu-O is reversible during a warming and cooling cycle in the magnetic field. The low-temperature boundary of this reversible range is called the irreversibility

temperature $T_{irr}(H)$ or irreversibility magnetic field $H_{irr}(T)$, which depends on T as

$$H_{irr}(T) \propto [1 - T/T_c(0)]^{3/2}.$$

Based on this and other related observations, they proposed the existence of a superconducting glass state.

On the other hand, Yeshurun and Molozemoff, who observed a similar relationship between $T_{irr}(H)$ and H for a single crystal of $YBa_2Cu_3O_7$, argued that this magnetization behavior could be described by a conventional flux-creep model. [6-1-2]

The highly movable flux lines have also been studied by measurements of the broadening of the resistive superconducting transition under magnetic field [6-1-3] and of the complex ac susceptibility near the critical temperature, $T_c(H)$. [6-1-4] The results of these studies were generally explained by the thermally assisted flux motion under the Lorentz force.

Thus, it was not clearly established whether this dissipative magnetic state is a consequence of a phase transformation in the flux-line lattice or is due to thermally activated motion of flux lines (depinning fluxoids).

In this chapter, the author describes the measurements of irreversibility line and the dependence for critical current density.

6-2. Measurement and discussion of irreversibility lines

Five test samples with 3 levels of J_{C0} at 77.3 K and zero

magnetic field, (No. 1,2 and 3: 300 A/mm^2 , No. 4: 220 A/mm^2 and No. 5: 130 A/mm^2) were prepared. [6-2-1,2] (Note that test samples 2 and 3 are provided from the same tape.) The critical temperature, T_C , of each tape was 106 K. The overall dimensions, including silver sheath, were 4 mm in width, 0.15 mm in thickness. A sample holder, housed in a temperature controlled adiabatic chamber, was used for these measurements. In the holder, test samples 1, 2, 4, and 5 were oriented to align each tape plane parallel to the applied magnetic field direction, while test sample 3 was aligned in such a way that the tape plane was perpendicular to the applied field. The experimental procedure was as follows. For a given temperature, the applied magnetic field, H_a was swept at a constant rate ($\mu_0 dH_a/dt=0.16\sim 1$ Tesla/min) starting at a field considerably below H_{irr} corresponding to the temperature. For a given magnetic field setting, the temperature was increased at a constant rate from 4.2 K to 120 K. The 4-probe dc technique, with a constant measurement current of 100 mA ($J=0.9 \text{ A/mm}^2$ over the superconductor cross section) for sample 1 and 200 mA ($J=1.5 \text{ A/mm}^2$) for samples 2, 3, 4, and 5, were used to measure voltage. H_{irr} and T_{irr} were defined by a resistive electric field of 1 $\mu\text{V/cm}$. This electric field is equivalent to an effective resistivity of $7 \times 10^{-11} \Omega \cdot \text{m}$, whose value is much lower than $3 \times 10^{-9} \Omega \cdot \text{m}$, the resistivity of silver at 77 K.

Figure 6-2-1 shows $\mu_0 H_{irr}$ vs T plots for test samples 1 (open symbols) and 2 (solid symbol) with $J_{C0}=300 \text{ A/mm}^2$. The sweep rate dependency of magnetic field on H_{irr} was measured with 0.16 (open triangles), 0.4 (open circles) and 0.8 Tesla/min (reversed open

triangles) for sample 1. $T_{irr}(H)$ (open squares) was evaluated with a temperature sweep rate of 5 K/min. For sample 2 (solid circles), $\mu_0 H_{irr}$ was measured up to 30 Tesla with a 1 Tesla/min sweep rate. As shown in Fig.6-2-1, it was found that the irreversibility lines were not changed with the different measurement procedures.

Figure 6-2-2 shows $\mu_0 H_{irr}$ vs T plots for test sample 2 (open circles), 3(solid circles), 4(open squares) and 5(open triangles). $H_{irr}(55\text{ K})$ values were obtained at 27.9 T for sample 2, 22.8 Tesla for sample 4 and 18.2 Tesla for sample 5, with the magnetic field parallel to the tape plane. The data clearly show that H_{irr} increases with J_{C0} .

Figure 6-2-3 shows the relation between irreversibility field at 77.3 K and J_c at the same temperature without magnetic field. The samples has $J_c=3.01 \times 10^4$ A/cm² ($T_c=107.7$ K) for #3, 1.39×10^4 A/cm² ($T_c=109.1$ K) for #4 and 0.78×10^4 A/cm² ($T_c=108.8$ k) for #5, respectively.[6-2-3] For these samples, the irreversibility fields, were determined by the temperature at which the voltage of 0.1 μ V was detected between the voltage terminals of 3 mm. In the figure, open symbols indicate the bulk samples for comparison. [6-2-4] This also clearly shows that the H_{irr} increases monotonically with increasing critical current density.

The author described in the previous chapter that an increase in J_{C0} suggests an improvement of morphology in BiPbSrCaCuO caused by a decrease in weak links at grain boundaries and a fine dispersion of nonsuperconducting phases. These data suggest that H_{irr} apparently increases with improved morphology of the high- T_c superconducting section in the silver-sheathed tapes.

Therefore the improvement to the high field and high temperature region for irreversibility line suggests that the line is dominated by the depinning process with the improvement of morphology in the superconducting phase. These data indicate that the irreversibility field can be increased by the improvement of morphology.

For test samples 2 and 3 from the same tape, with which the effect of field direction on H_{irr} was examined, the data clearly show anisotropy in relation to field direction. With the tape plane perpendicular to applied field (test sample 3, solid circle in Fig. 6-2-2, $\mu_0 H_{irr}(33\text{ K})$ was 17 Tesla, which shows a lower irreversibility field than that of sample 2. The H_{irr} begins to increase steeply at about 50 K as temperature is lowered. With a parallel applied field (test sample 2, open circle in Fig. 6-2-1), this steep increase begins at about 80 K.

It is known that $H_{irr}(T) \propto (1-T/T_c)^n$, where $T_c=106\text{ K}$ for the tapes of sample 1, 2 and 3. Figure 6-2-4 shows $\ln(\mu H_{irr})$ vs $\ln(1-T/T_c)$ plots for test sample 1 (open circle) and 4 (solid circle), with $\mu_0 H_{irr}$ in Tesla. From these data, using the least-squares method, we obtain the values of n for the two orientations. For the perpendicular-field orientation, $n=3.0$ for the temperature range from 55 K to 90 K; for the parallel-field orientation, $n=2.8$ for the range from 33 K to 90 K. The dotted lines in Fig. 6-2-4 correspond to these n -values. It is known that the irreversibility line is given by $H \propto (1-T/T_c)^{1.5}$ for $\text{YBa}_2\text{Cu}_3\text{O}_7$ superconductor[6-1-2]. However the n -value of Bi-2223 oxide superconductor did not correspond for the case of Y-based oxide superconductors.

6-4. Summary

The irreversibility lines of BiPbSrCaCuO silver sheathed tapes were measured as a function of temperature. The high irreversibility fields were obtained for Bi-2223 oxide superconductors. For the sample with $J_{C0}(77.3\text{ K})=30,000\text{ A/cm}^2$, H_0H_{irr} was 27.9 Tesla at 55 K.

It was found that the irreversibility magnetic field (H_{irr}) increased with J_{C0} . The dependence of H_{irr} on J_{C0} suggests to originate from depinning mechanism rather than the phase transition for fluxoids.

Irreversibility lines were fitted by the function of $H_{irr}(T)\propto(1-T/T_c)^n$. n-values were obtained with 3.0 for the perpendicular field to tape plane and 2.8 for the parallel field. These values were larger than that of Y-based superconductors etc.

7. Conclusions

For the development of Bi-based oxide superconducting wire with high J_c , it was found that the J_c and J_c -B properties were improved by the homogenization of high- T_c phase (110 K phase), control of composition ratio, and the alignment of the superconducting grains and the good contact at the grain boundaries through the double deformation and sintering process. For homogenization of high- T_c phase, it was found that the silver sheath accelerated the formation of high T_c phase (2223 phase). For double deformation and sintering process, it was found that the filling powder was homogenized to 2223 phase (110 K phase) for growing large grains at the first step and the platelet grains were connected strongly by the deformation and sintering again. For control of the composition ratio, it was found that the volume of the non-superconducting phases (CaPbO_4 , Ca_2CuO_3 , etc.) were reduced through the control of composition ratio by increasing Bi and Ca. As a result, J_c over 10^4 A/cm² in zero magnetic field was obtained in the sample with $J_c=4.7 \times 10^4$ A/cm² at 77.3 K and 0 Tesla through the improvement of morphologies.

These data exhibit that the Bi-2223 silver sheathed wire has high potentiality for the practical use to power applications.

For studies of weak links at grain boundaries, It was corroborated that the rapid decrease of J_c in low magnetic field region was dominated by the weak links at the grain boundaries, and the history effect could disappear by double sintering process (deformation-sintering-deformation-sintering) and the improvement of morphologies including non-superconducting phases

with increasing of J_c .

The temperature dependence of J_c -B properties and the history effect were measured effectively in wide temperature range on BiPbSrCaCuO silver sheathed wires with various level of critical current density. The results were obtained as follows;

(1) Both the rapid decrease in J_c with increasing temperature and the history effect of J_c appeared in the same temperature region, below 20-30 K. In the low temperature region, it was found that J_c was influenced by weak links with the history effect observed clearly. It is concluded from the coincidence of the two temperature regions that these phenomena are caused by the low temperature weak links in the silver sheathed Bi-based oxide superconducting tapes.

(2) In the samples with a smaller J_c , the history effect is relatively larger and the temperature dependence of J_c in the low temperature region is stronger. Therefore, J_c in this state is still thought to be influenced by the weak links and the improvement of weak coupling is necessary in order to improve J_c further at the grain boundaries.

For studies of J_c -B properties, the factors dominating the magnetic field dependence of J_c of silver sheathed polycrystalline BiPbSrCaCuO wire were investigated and the following model was proposed. When the magnetic field is applied parallelly to the wide plane of the wire, J_c -B characteristics are dominated by the c-axis component of the transport current. When the magnetic field is applied perpendicularly to the wide plane of the wire, the J_c -B characteristics are dominated by the current in the a-b plane.

For both cases, the flux flows along a-b plane.

The magnetic field dependence of J_c was measured at 4.2 K. It was found that the J_c increased much larger at 4.2 K than at 77.3 K and changed little in the magnetic field from 5 to 23 Tesla. The J_c at 4.2K was also increased with the improvement of J_c at 77.3 K. The magnetic field direction dependence of the wires was also investigated. The difference between parallel and perpendicular to the tape plane was only 30 %. These properties are much more excellent than the metallic superconductors such as Nb_3Sn and $NbTi$. Therefore it was found that $BiPbSrCaCuO$ sheathed wires had a sufficient high potentiality for the application in super-high magnetic field over 20 Tesla at 4.2 K.

J_c -B properties were measured first in high magnetic field until 19.75 Tesla in liquid hydrogen. High J_c and n-value was obtained for construction of high- T_c superconducting magnets making engineering interest feasible, at least when operated at 20 K.

For studies of irreversibility lines, the irreversibility lines of $BiPbSrCaCuO$ silver sheathed tapes were measured as a function of temperature. The high irreversibility fields were obtained for Bi-2223 oxide superconductors. For the sample with $J_{c0}(77.3\text{ K})=30,000\text{ A/cm}^2$, $\mu_0 H_{irr}$ was 27.9 Tesla at 55 K. It was found that the irreversibility magnetic field (H_{irr}) increased with J_{c0} . The dependence of H_{irr} on J_{c0} suggests for the irreversibility line to be originated from depinning mechanism rather than the phase transition for fluxoids.

Irreversibility lines were fitted by the function of

Acknowledgements

The author would like to thank Dr.T.Matsushita, Dr.E.S.Otobe (Kyushu Institute of Technoloy), Dr.K.Yamafuji (Kyushu University) and Dr.B.Ni (Fukuoka Institute of Technology) for the available advices and leading to the measurement of a.c inductive metod and the theoretical discussion. The author would like to thank Dr.Y.Iwasa (Massachusetts Institute of Technology) and Dr.M.Suenaga (Brookhaven National Laboratory) for their useful suggestions to the cryogenics technologies and discussions. The author would like to thank the leaders of the research, Dr.M.Kawashima, Mr.H.Hitotsuyanagi, Mr.M.Nagata, and Mr.K.Sato (Sumitomo Electric Ind. Ltd.) for their valuable instructions. The author would like to express his gratitude to Mr.K.Okura, Mr.N.Shibuta, Mr.H.Mukai, Mr.M.Ueyama, Mr.T.Kato, Mr.J.Fujikami, Mr.K.Muranaka and Mr.T.Nishikawa (Sumitomo Electric Ind. Ltd.) for their sincere collaborations. The author would like to be grateful to Dr.K.Watanabe (Tohoku University) and Dr.L.Rubin (Massachusetts Institute of Technology) for their valuable advices in high magnetic field experiments. The author would like to be grateful to Mr.B.Brandt, Mr.P.Zhao and Mr.V.Adzovie (Massachusetts Institute Technology) for dedicated and skilled technical assistances on the high field experiments. The author would like to thank Mr.T.Nakayama for his valuable advices on producing this thesis. The author would like to thank Dr.I.Iguchi and Dr.H.Uwe (Tsukuba University) for the useful discussions on writing this thesis. The author finally would like to express a deep sense of his

gratitude to Dr.T.Suzuki and Dr.R.Yoshizaki (Tsukuba University) for the opportunity and useful suggestions to write this thesis.

1-1-1) H. Sawafuchi, *Journal of Polymer Science*, **55**, 1345 (1962).

1-1-2) S. Ueda, *Journal of Polymer Science*, **55**, 1345 (1962).

1-1-3) K. S. Lee, J. S. Johnson, C. F. Thomas, W. H. Jones, R. L. Shrago, L. Cox, R. J. Shrago, E. Wang and C. N. Chou, *High. Pres. Low. Temp.*, **33**(1987)1908.

1-1-4) H. Sasaki, T. Otsuka, K. Yamamoto and T. Yamada, *Jpn. J. Appl. Phys.*, **27**(1988)1204.

1-1-5) T. O. Cheng and S. C. Barlow, *Polym. J.*, **17**(1985)155.

1-1-6) H. Tamura, A. Sasaki, K. Oda, K. Hasegawa, Y. Minato, T. Sasaki, T. Otsu and T. Yamada, *Jpn. J. Appl. Phys.*, **27**(1988)1304.

1-1-7) T. Yamada, *Journal of Polymer Science*, **37**(1959)11.

1-1-8) K. Ito, H. Fujino, K. Yamamoto, T. Yamada, T. Koyanagi, T. Otsu, T. Sasaki, H. Suga, Y. Koyama, H. Fujimori and T. Otsu, *Journal of Polymer Science*, **18**(1957)125.

1-1-9) L. D. Swift and S. A. Chiriac, *Cryogenics*, **23**(1983)541.

1-1-10) P. L. Rowell, L. F. Chiriac, J. F. Johnson and S. A. Chiriac, *Polym. Dev. Lett.*, **6**(1968)1150.

1-1-11) H. Yamada, K. Yamamoto, H. Sasaki, T. Yamada, T. Otsu, T. Yamada, H. Yamamoto, *Journal of Polymer Science*, **28**(1958)144.

1-1-12) H. Sasaki, T. Otsu, H. Fujino, T. Yamada, K. Ito, H. Kishiyama and T. Otsu, *Polym. J.*, **17**(1985)155.

1-1-13) H. Sasaki, H. Yamamoto, K. Yamamoto, T. Yamada, H. Yamamoto, H. Yamamoto, H. Yamamoto, H. Yamamoto and H. Yamamoto, *J. Appl. Phys.*, **62**(1987)475.

References

- 1-1-1) H.Kamerlingh Onnes, Leiden Comm. 120b, 122b, 124c (1911).
- 1-2-1) J.G.Gednortz and K.A.Muller, Z.Phys., B-Condenced Matter 64(1986)189.
- 1-2-2) M.K.Wu, J.R.Ashburn, C.J.Thorng, P.H.Hor, R.L.Meng, L.Gao, Z.J.Huang, Q.Wang and C.W.Chu, Phys.Rev.Lett. 58(1987)908.
- 1-2-3) H.Maeda, Y.Tanaka, M.Fukutomi and T.Asano, Jpn. J. Appl. Phys., 27(1988)L209.
- 1-2-4) Z.Z.Sheng and A.M.Hermann, Nature 322(1988)55.
- 1-2-5) M.Takano, J.Takada, K.Oda, H.Kitaguchi, Y.Miura, Y.Ikeda, Y.Tomii and H.Mazaki, Jpn.J.Appl.Phys. 27(1988)L1041.
- 1-2-6) T.Nakahara, Sumitomo Electric Tech. Rev., 134(1989)1.
- 1-2-7) K.Noto, H.Morita, K.Watanabe, T.Murakami, Y.Koyanagi, I.Yoshii, I.Sato, H.Sugawara, N.Kobayashi, H.Fujimori and Y.Muto, Physica 148 B+C[1-3] (1987)239.
- 1-2-8) E.Evetts and B.A.Glowacki, Cryogenics, 28(1988)641.
- 1-2-9) P.L.Gammel, L.F.Schneemeyer, J.V.Waszczak and D.J.Bishop, Phys. Rev. Lett. 61(1988)1666.
- 1-2-10) M.Nagata, K.Ohmatsu, H.Mukai, T.Hikata, Y.Hosoda, N.Shibuta, M.Kawashima; Sumitomo Electric Tech. Rev. 28(1989)44.
- 1-2-11) H.Takei, Y.Torii, H.Kugai, T.Hikata, K.Sato, H.Hitotsuyanagi and K.Tada; Proc. of 2nd Sym. on Supercond. (ISS'89) (Springer Tokyo, 1990)359.
- 1-2-12) M.Tanaka, S.Yamazaki, M.Fujinami, T.Takahashi, H.Katayama-Yoshida, W.Mizutani, K.Kajimura and M.Ono; J. Vac. Soc. Techno. A8(1990)475.

- 1-3-1) R.Flukiger, T.Muller, W.Goldacker, T.Wolf, E.Seibt, I.Apfelstedt, H.Kupfer and W.Schauer, Physica C 153-155(1988)1574.
- 1-3-2) K.Sato, T.Hikata, M.Ueyama, H.Mukai, N.Shibuta, T.Kato and T.Masuda; Cryogenics 31(1991)687.
- 2-1-1) T.Hikata, H.Mukai, K.Sato and H.Hitotsuyanagi, Sumitomo Electric Technical Review 29(1990)45.
- 2-1-2) Q.Li, M.Suenaga, J.Gohng, D.K.Finnemore, T.Hikata, M.Ueyama and K.Sato; Phys. Rev. B 46(1992)3195.
- 2-1-3) A.M.Campbell, J. Phys. C2(1969)1492.
- 2-1-4) T.Matsushita, B.Ni, K.Yamafuji, K.Watanabe, K.Noto, H.Morita, H.Fujimori, Y.Muto, Advances in Superconductivity (Eds K.Kitazawa and T.Ishiguro) Springer-Verlag, Tokyo, Japan (1989)393.
- 2-2-1) T.Hikata, K.Sato and H.Hitotsuyanagi; Jpn. J. Appl. Phys. 28(1989)L82.
- 3-1-1) A.Sumiyama, T.Yoshitoshi, H.Endo, J.Tsuchiya, N.Kijima, M.Mizuno and Y.Oguri, Jpn. J. Appl. Phys. 27(1988)L542.
- 3-1-2) N.Kijima, H.Endo, J.Tsuchiya, A.Sumiyama, M.Mizuno and Y.Oguri, Jpn. J. Appl. Phys. 27(1988)L821.
- 3-1-3) K.Kitazawa, S.Yaegashi, K.Kishio, T.Hashegawa, N.Kanazawa, K.Park and K.Fueki, Adv. Ceram. Mater.
- 3-1-4) H.Nobumasa, K.Shimizu, Y.Kitano and T.Kawai, Jpn. J. Appl. Phys. 27(1988)L846.
- 3-2-1) M.Kawashima, M.Nagata, Y.Hosoda, S.Takano, N.Shibuta, H.Mukai and T.Hikata; IEEE Trans. Mag., 25(1989)2168.
- 3-2-2) U.Endo, S.Koyama and T.Kawai; Jpn. J. Appl. Phys. 27(1988)L1476.

- 3-3-1) K.Sato, T.Hikata, H.Mukai, T.Masuda, M.Ueyama, H.Hitotsuyanagi, T.Mitsui and M.Kawashima; Proc. of 2nd Int. Sym. on Superconductivity (ISS'89) (Springer Tokyo 1990)p.335.
- 3-4-1) T.Hikata, T.Nishikawa, H.Mukai, K.Sato and H.Hitotsuyanagi, Jpn. J. Appl. Phys. 28(1989)L1204.
- 4-1-1) T.Matsushita, B.Ni, K.Yamafuji, K.Watanabe, K.Noto, H.Morita, H.Fujimori and Y.Muto, Advances in Superconductivity (Eds. K.Kitazawa and T.Ishiguro) Springer-Verlag, Tokyo, Japan (1989)393-397.
- 4-1-2) T.Aomine and A.Yonekura, phys. Lett. 114A(1986)16.
- 4-1-3) K.Watanabe, K.Noto, H.Morita, H.Fujimori, K.Mizuno, T.Aomine, B.Ni, T.Matsushita, K.Yamafuji and Y.Muto.
- 4-1-4) J.E.Evetts and B.A.Glowacki, Cryogenics 28(1988)641.
- 4-1-5) H.Mukai, N.Shibuta, T.Hikata, K.Sato, M.Nagata and H.Hitotsuyanagi, New developments in Applied Superconductivity, ed. Y.Murakami(World Scientific, Singapore,1989)p.101.
- 4-1-6) D.Dimos, P.Chaudhari, J.Mannhart and F.K.LeGoues, Phys. Rev. Lett., 61(1988)219.
- 4-2-1) T.Hikata, M.Ueyama, H.Mukai and K.Sato; Cryogenics 30(1990)924.
- 4-2-2) K.Sato, T.Hikata and Y.Iwasa; Appl. Phys. Lett. 57(1990)1928.
- 4-2-3) A.M.Campbell and J.E.Evetts: Adv. Phys. 21(1972)358.
- 4-2-4) T.Matsushita, E.S.Otobe, B.Ni, K.Kimura, M.Morita, M.Tanaka, M.Kimura, K.Miyamoto and K.Sawano; Jpn. J. Appl. Phys. 30(1990)L342.

- 4-3-1) T.Hikata, K.Sato, B.Ni, E.S.Otobe, T.Matsushita, M.Takeo and K.Yamafuji: Adv. Supercond. III (springer, Tokyo,1991)p.511.
- 4-3-2) T.Matsushita, E.S.Otobe, B.Ni, T.Hikata and K.Sato; Cryogenics 31(1991)949.
- 5-1-1) T.Matsushita, T.Fujimori, K.Toko and K.Yamafuji; Appl. Phys. Lett. 45(1990)2039.
- 5-1-2) A.M.Campbell; J.Phys. C2 (1969)1492.
- 5-1-3) R.Lubusch; Phys. Stat. Sol. 32(1969)439.
- 5-2-1) Q.Li, M.Suenaga, T.Hikata and K.Sato, Phys. Rev. B 46(1992)5857.
- 5-2-2) Q.Li, M.Suenaga, J.Gohng, D.K.Finnemore, T.Hikata and K.Sato, Phys. Rev. B 46(1992)3195.
- 5-2-3) U.Welp, S.Fleshler, W.K.Kwok, R.A.Klemm, V.M.Vinokur, J.Downey, B.Veal and G.W.Crabtree; Phys. Rev. Lett. 25(1991)3180.
- 5-2-4) D.E.Farrel, J.P.Rice, D.M.Ginsburg and J.Z.Liu, Phys. Rev. Lett. 64(1990)1573.
- 5-2-5) K.Mizuno and T.Aomine: J. Phys. Soc. Jpn. 52(1983)4311.
- 5-2-6) J.Bardeen and M.J.Stephen: Phys. Rev. A 140(1965)1197.
- 5-3-1) T.Hikata, M.Ueyama, H.Mukai, N.Shibuta, T.Kato and K.Sato: Proc. 3rd Int. Sym. on Superconductivity (ISS'90), Sendai (Springer-Verlag) 1991,p.515.
- 5-4-1) K.Sato, N.Shibuta, T.Hikata, T.Kato and Y.Iwasa: Appl. Phys. Lett. 61(1992)714.
- 5-4-2) Y.Iwasa and Y.M.Butt; Cryogenics 30(1990)37.
- 6-1-1) K.A.Muller, M.Takashige and J.G.Bednorz; Phys. Rev. Lett. 58(1987)1143.

- 6-1-2) Y.Yeshurun and A.P.Malozemoff; Phys. Rev. Lett.
60(1988)2202.
- 6-1-3) T.T.Palstra, B.Balrogg, R.B.Van Dover, L.F. Schneemeyer
and J.V. Wszczak; Phys. Rev. Lett. 61(1988) 1662.
- 6-1-4) T.K. Worthington, W.J.Gallagher and T.R.Dinger; Phys. Rev.
Lett. 59(1987)1160.
- 6-2-1) T.Hikata, K.Sato and Y.Iwasa; Physica C 185-189(1991)2363.
- 6-2-2) T.Hikata, K.Sato and Y.Iwasa: Jpn.J.Appl.Phys.
30(1991)L1271.
- 6-2-3) T.Matsushita, E.S.Otabe, M.Kiuchi, B.Ni, T.Hikata and
K.Sato; Physica C 201(1992)151.
- 6-2-4) T.Umemura, K.Egawa, M.Wakata, S.Utsunomiya, B.Ni, M.Takeo,
K.Yamafuji, E.S.Otabe and T.MATSUSHITA; Adv. Supercond.
III (springer, Tokyo,1991)p.507.

Figure captions

- Fig.1-3-1 Fabricating process of silver sheathed BiPbSrCaCuO oxide superconducting wire.
- Fig.2-1-1 Arrangement of specimen and magnetic field for (a) ac inductive measurement for critical current density and (b) resistive measurement by 4-probe dc method.
- Fig.2-1-2 measuring system of ac inductive method.
- Fig.3-2-1 J_c vs. press load for $Y_1Ba_2Cu_3O_{7-x}$ and $BiSrCaCu_2O_x$ silver sheathed oxide superconducting wires.
- Fig.3-2-2 Critical current density vs. sintering temperature for $BiSrCaCu_2O_x$ oxide superconductor. Sintering time is 1 hour.
- Fig.3-2-3 J_c vs. tape thickness for silver sheathed $Bi_{0.8}Pb_{0.2}SrCaCu_2O_x$ superconductor. This size in the figure are the wire diameter before press processing.
- Fig.3-2-4 dc susceptibility vs. temperature for silver sheathed $Bi_{0.8}Pb_{0.2}SrCaCu_2O_x$ superconducting wire.
- Fig.3-3-1 Fracture surface of BiPbSrCaCuO oxide superconductor inside silver sheathed tapes. a) Sample C. b) Sample B.
- Fig.3-3-2 The history effect of J_c during the increase and decrease of H for samples A and C. a) H parallel to wide plane of the tapes. b) H perpendicular to wide plane of the tapes. Solid circles and triangles represent J_c during an increase in the magnetic field ; open circles and triangle represent it during a decrease in the field.

- Fig.3-3-3 Magnetic field dependence of critical current density of sample A ($J_c(77.3 \text{ K}, 0 \text{ T})=6,930 \text{ A/cm}^2$), B ($5,500 \text{ A/cm}^2$) and C ($1,650 \text{ A/cm}^2$) during increase of the magnetic field. Lines are drawn as guide for the eye.
- Fig.3-3-4 X-ray diffraction pattern for the wide surface of BiPbSrCaCuO specimen with $J_c=5,500 \text{ A/cm}^2$ after stripping of the Ag-sheath.
- Fig.3-4-1 SEM images of the polished surfaces on the cross sections in (a) sample A ($14,300 \text{ A/cm}^2$) and (b) sample B ($5,500 \text{ A/cm}^2$).
- Fig.3-4-2 Magnetic field dependence of J_c of BiPbSrCaCuO silver sheathed wire ($J_c(77.3 \text{ K}, 0 \text{ T})=47,000 \text{ A/cm}^2$).
- Fig.4-1-1 Schematic diagram of superconducting bridge.
- Fig.4-2-1 Magnetic field dependence of J_c of the wires with J_c from $1,650 \text{ A/cm}^2$ to $25,000 \text{ A/cm}^2$ during increase of magnetic field.
- Fig.4-2-2 History effect of J_c at 4.2 K for the wires (A: $J_c(77.3 \text{ K})= 2.8 \times 10^4 \text{ A/cm}^2$, B: $2.5 \times 10^4 \text{ A/cm}^2$, C: $1.8 \times 10^4 \text{ A/cm}^2$ and D: $1.4 \times 10^4 \text{ A/cm}^2$).
- Fig.4-2-3 J_c vs. B plots for tape 3 at $4.2, 15$ and 20 K for increasing ($0 \rightarrow 19.75 \text{ T}$) and decreasing ($19.75 \rightarrow 0 \text{ T}$) field sequences.
- Fig.4-3-1 λ' vs. b_0 of a silver sheathed BiPbSrCaCuO oxide superconducting wire at 77.3 K by ac inductive method.
- Fig.4-3-2 Magnetic field dependence of J_c for BiPbSrCaCuO silver sheathed wire with $1.7 \times 10^4 \text{ A/cm}^2$ by 4-probe dc method and ac inductive method.
- Fig.4-3-3 Temperature dependence of J_c of sample #1 in 0.2 T ,

1.0 T and 2.0 T by ac inductive method.

Fig.4-3-4 Magnetic field dependence of J_c in 4.2 K, 25 K and 60 K.

Fig.4-3-5 Logarithmic plots of J_c vs. $1-(T/T_c)^2$ at 0.2 T, 1 T and 2 T for samples #1.

Fig.4-3-6 Logarithmic plots of J_c vs. $1-(T/T_c)^2$ at 0.2 T, 1 T and 2 T for sample #2.

Fig.4-3-7 History effects of sample #3 in 4.2 K and 20 K.

Fig.4-3-8 History effects of sample #2 in 4.2 K and 20 K.

Fig.4-3-9 Temperature dependence of history effect for sample #2(\diamond : $J_c(77.3 \text{ K})=6.3 \times 10^3 \text{ A/cm}^2$) and #3(\blacksquare : $J_c(77.3 \text{ K})=3.0 \times 10^4 \text{ A/cm}^2$) at 3 T.

Fig.4-3-10 Temperature dependence of history effect for sample #1, #2 and #3 at 0.5 T

Fig.4-3-11 Replots of the results in low temperature region for Logarithmic plots of J_c vs. $1-(T/T_c)^2$ at 0.2 T, 1 T and 2 T for samples #1.

Fig.4-3-12 Replots of the results in low temperature region for Logarithmic plots of J_c vs. $1-(T/T_c)^2$ at 0.2 T, 1 T and 2 T for samples #2.

Fig.5-1-1 Concept of the correlation length of the fluxoids (a) shearing correlation length, (b) bending length.

Fig.5-2-1 Magnetic field dependence of J_c normalized by J_{c0} at 77.3 K for magnetic field applied parallel to the plane of the specimens. $J_{c0}(\text{A/cm}^2)$: \blacksquare ; 1.0×10^3 , Δ ; 1.7×10^3 , \bullet ; 5.5×10^3 and \circ ; $3.0 \times 10^4 \text{ A/cm}^2$.

Fig.5-2-2 J_c in each magnetic field vs. J_c in zero magnetic field applied parallel to the plane of

tapes; ●: 0.1 T, Δ: 0.5 T, ■: 1 T and ○: 2 T.

Fig.5-2-3 Magnetic field dependence of pinning force for sample (a),(b) and (c).

Fig.5-2-4 Magnetic field dependence of normalized pinning force for sample (a), (b) and (c).

Fig.5-2-5 SEM photographs of polished surface for sample (a) 5,500 A/cm², (b)10,600 A/cm² and (c) 47,000 A/cm².

Fig.5-2-6 TEM photograph viewed along the plane of the BiPbSrCaCuO wire.

Fig.5-2-7 TEM photograph viewed along the plane of the BiPbSrCaCuO wire.

Fig.5-2-8 TEM photograph viewed along the plane of the BiPbSrCaCuO wire.

Fig.5-2-9 TEM photograph viewed along the plane of the BiPbSrCaCuO wire.

Fig.5-2-10 Magnetic field dependence of critical current density ($J_{c0}=2.5 \times 10^4$ A/cm²) for magnetic field in three directions, where H = magnetic field and I = transport current.

Fig.5-2-11 (a) 2D scaling of the magnetization data for Bi(2223), measured at 10,000, 30,000 and 50,000 Oe. (b) 3D scaling of the same magnetization data as shown in (a).

Fig.5-2-12 (a) 2D scaling of the magnetization data for $Y_1Ba_2Cu_3O_{7-x}$, measured at 10,000, 30,000 and 50,000 Oe.

(b) 3D scaling of the same magnetization data as shown in (a).

- Fig.5-2-13 The frequency and dissipation of the silicon oscillator as a function of temperature. The vortex mobility transition occurs at the peak in the attenuation.
- The Meissner signal and softening temperature of flux lattice for single crystal BSCCO.
- Fig.5-2-14 Model for the factor dominated J_c -B characteristics: (a) $H \perp I$ and $H //$ tape plane; (b) $H // I$ and $H //$ tape plane (c) $H \perp I$ and $H \perp$ tape plane.
- Fig.5-2-15 Temperature dependence of H_{c2} for Bi(2223), where solid and open symbols correspond to the values derived with a constant $\kappa_c(170.4)$ and linearly varying κ_c , respectively.
- Fig.5-2-16 Magnetic field dependence of J_c normalized by J_{c0} at 77.3 K for magnetic field applied perpendicular to the plane of the specimens. $J_{c0}(A/cm^2)$: Δ ; 1.7×10^3 , \bullet ; 5.5×10^3 and \circ ; 3.0×10^4 A/cm².
- Fig.5-2-17 Magnetization curve of the specimen with $J_{c0} = 2.2 \times 10^4$ A/cm² at 77.3 K.
- Fig.5-3-1 Magnetic field dependence of J_c at 4.2 K for samples a ($J_c(77.3 \text{ K}) = 47,000$ A/cm², b (25,000 A/cm², c(18,000 A/cm²) and d (14,000 A/cm²).
- Fig.5-3-2 Magnetic field dependences of J_c at 4.2 K for magnetic field applied parallel (\bullet, \circ) and perpendicular (Δ, Δ) to the tape plane. The magnetic field was increased (solid symbols) to 23 T and decreased (open symbols).
- Fig.5-3-3 Magnetic field dependences of J_c at 77.3 K and 4.2 K

compared with NbTi and Nb₃Sn.

Fig.5-4-1 I_c vs. T plots at 0, 5, 10 and 19.75 T for three groups of silver sheathed Bi_{1.8}Pb_{0.4}Sr₂Ca_{2.2}Cu₃O_x tapes.

Fig.5-4-2 Comparison of J_c - B properties at 4.2 K and 20 K.

Fig.6-1-1 Irreversibility field in Magnetization curve.

Fig.6-2-1 Irreversibility line data for samples with $J_c(77.3 \text{ K}, 0 \text{ T}) = 30,000 \text{ A/cm}^2$.

Fig.6-2-2 $\mu_0 H_{irr}(T)$ data for four test samples (1: circle, 2: square, 3: triangle and 4: solid circle). Open symbols indicate that the applied magnetic field is parallel to the tape plane, while the solid symbols indicate a perpendicular magnetic field. The lines provide a guide for the eye.

Fig.6-2-3 Relation between irreversibility field at 77.3 K and critical current density at the same temperature without magnetic field. The open symbols show experimental data for bulk Bi-2223 specimens.

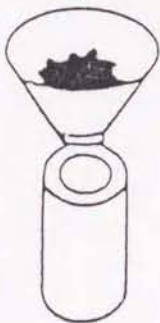
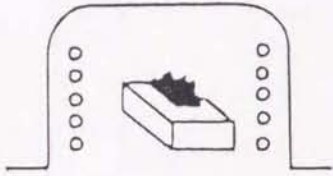
Fig.6-2-4 $\ln(\mu_0 H_{irr})$ vs. $(1-T/T_c)$ data for test sample 1 (circle) and 4 (solid circle). Note that $\mu_0 H_{irr}$ is in Tesla and $T_c = 106 \text{ K}$.

PROCESS FOR
Ag/BiPbSrCaCuO SUPERCONDUCTING WIRE

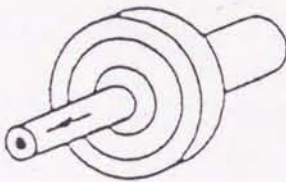
SINTERING OF POWDER

Bi:Pb:Sr:Ca:Cu

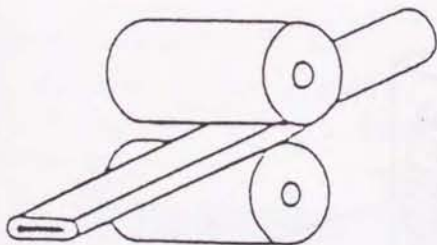
1.8:0.4:2.0:2.2:3.0



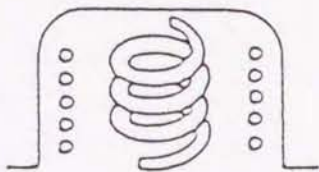
FILLING UP POWDER
TO Ag-PIPE



PLASTIC DEFORMATION
(ROUND WIRE)

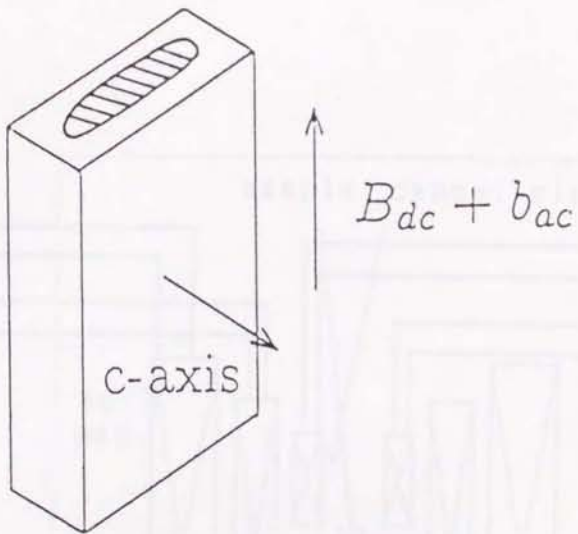


PLASTIC DEFORMATION
(TAPE)

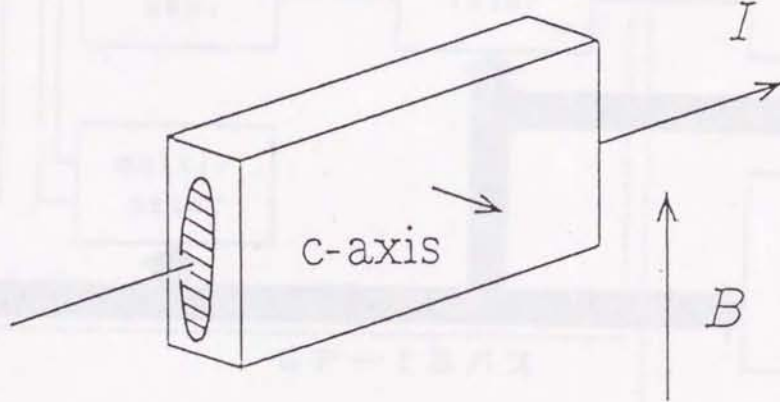


SINTERING

Fig.1-3-1



(a)



(b)

Fig. 2-1-1

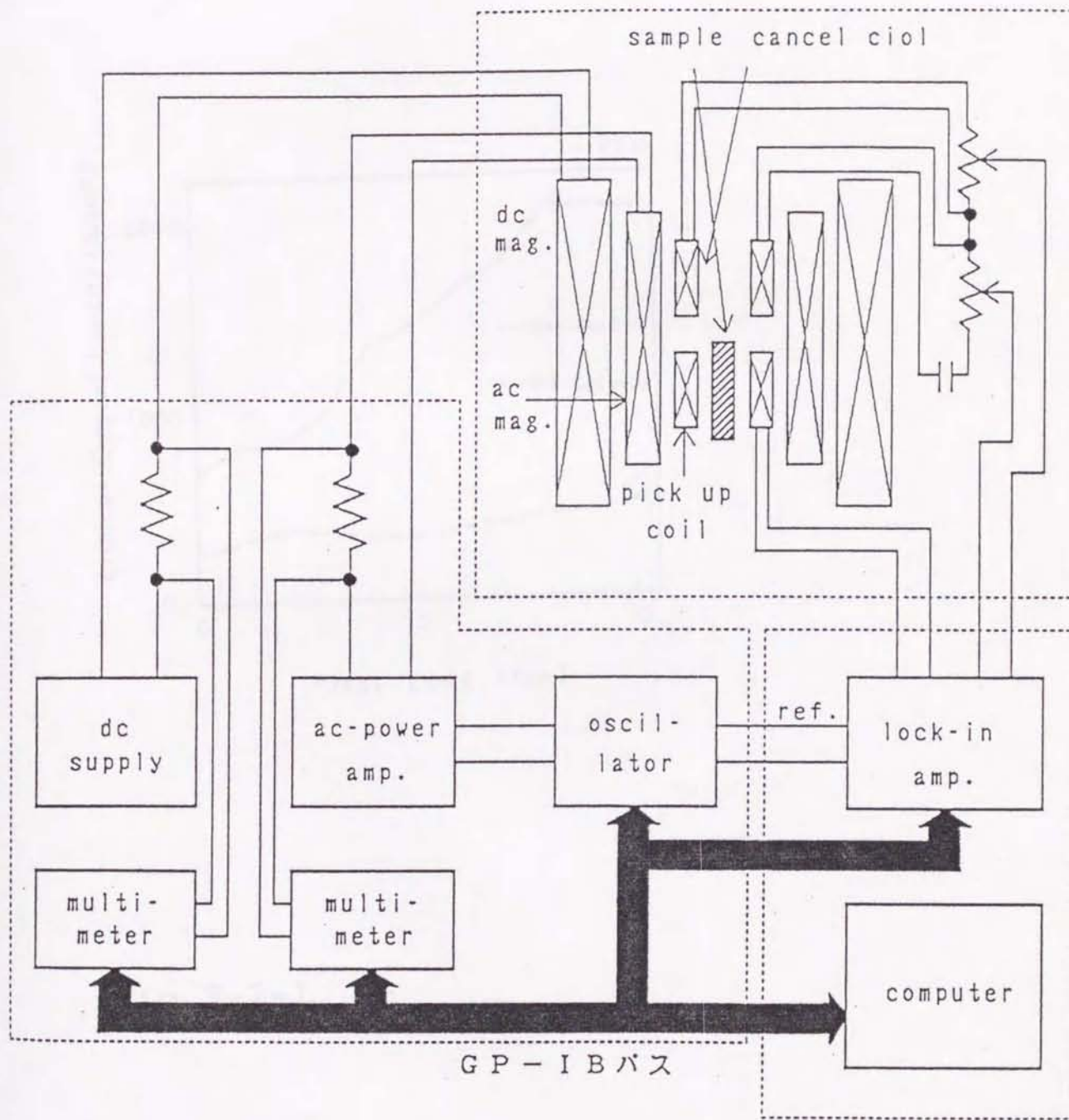


Fig.2-1-2

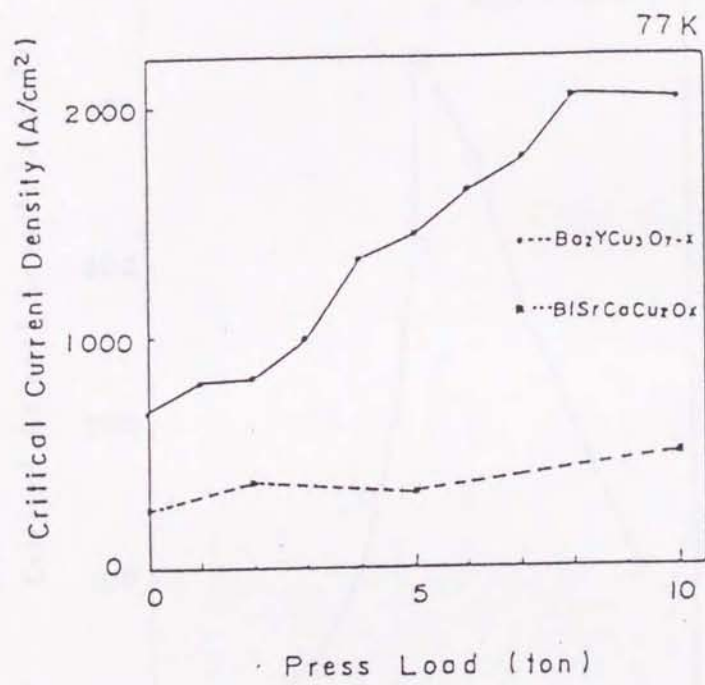


Fig.3-2-1

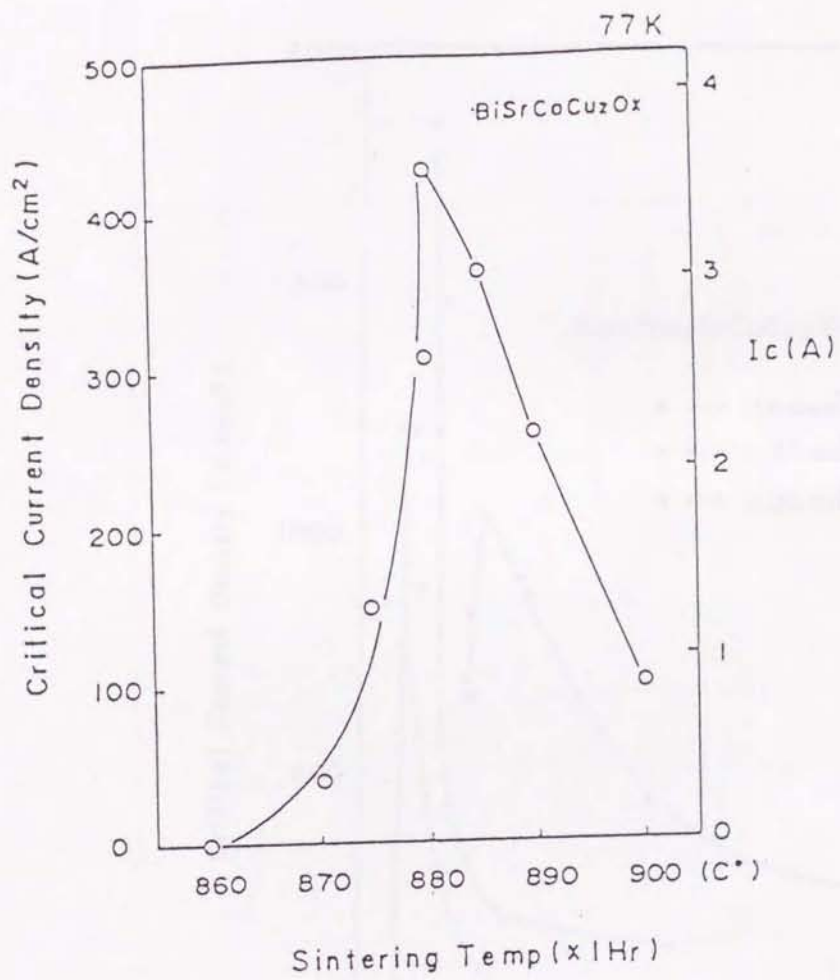


Fig.3-2-2

Fig.3-2-3

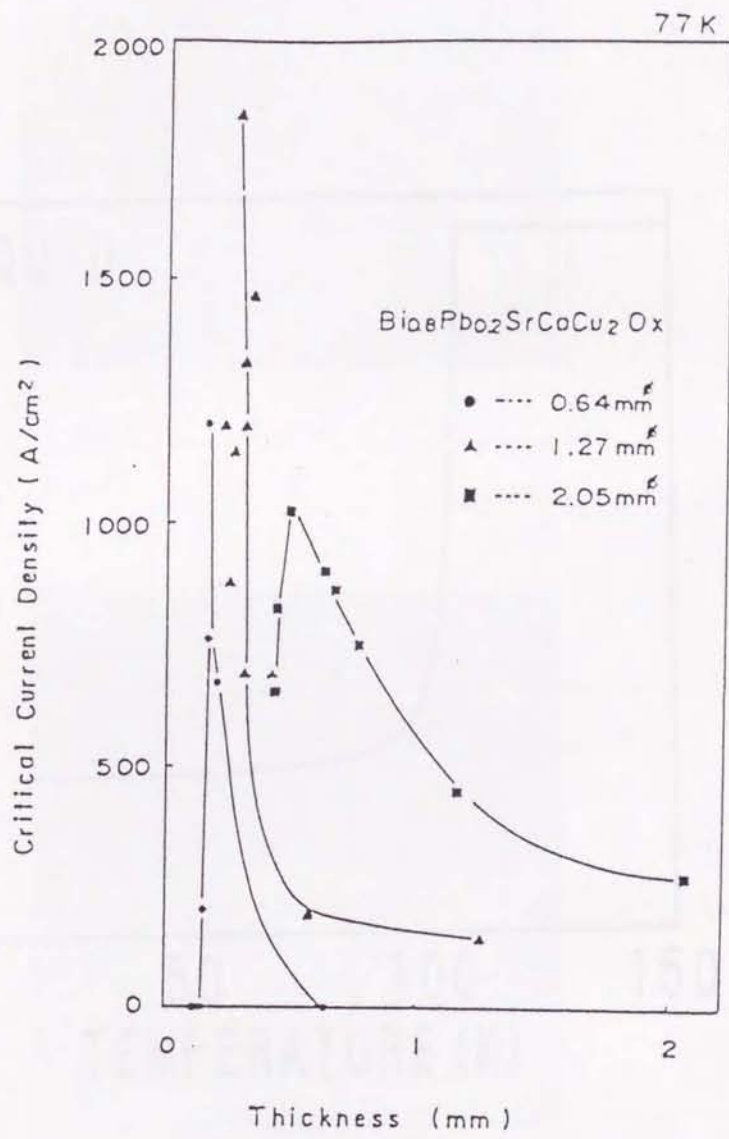


Fig.3-2-3

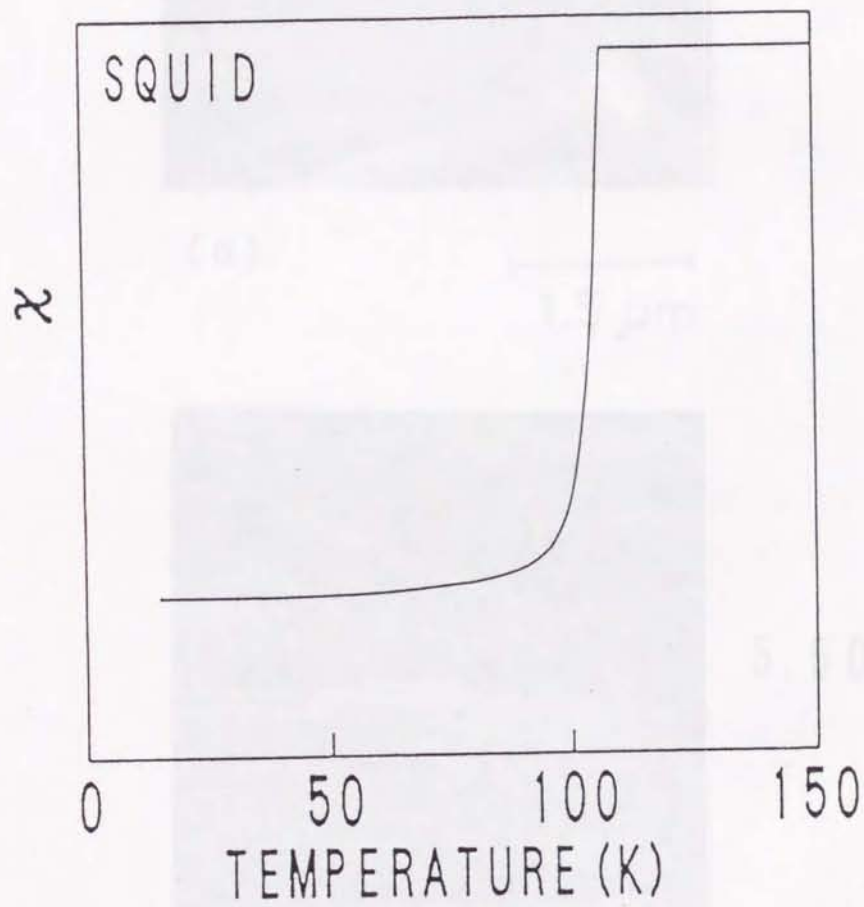
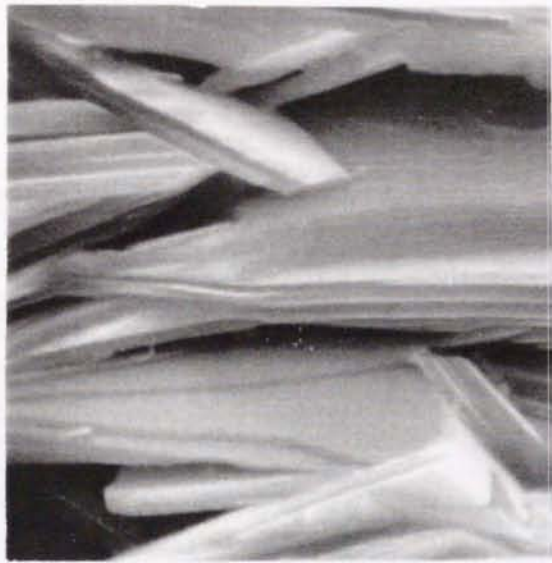


Fig.3-2-4

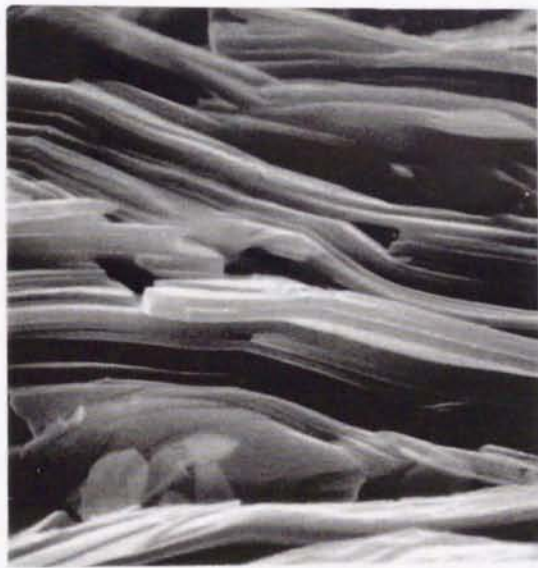
Fig.3-3-1



1,650 A/cm²

(a)

1.5 μm



5,500 A/cm²

(b)

Fig.3-3-1

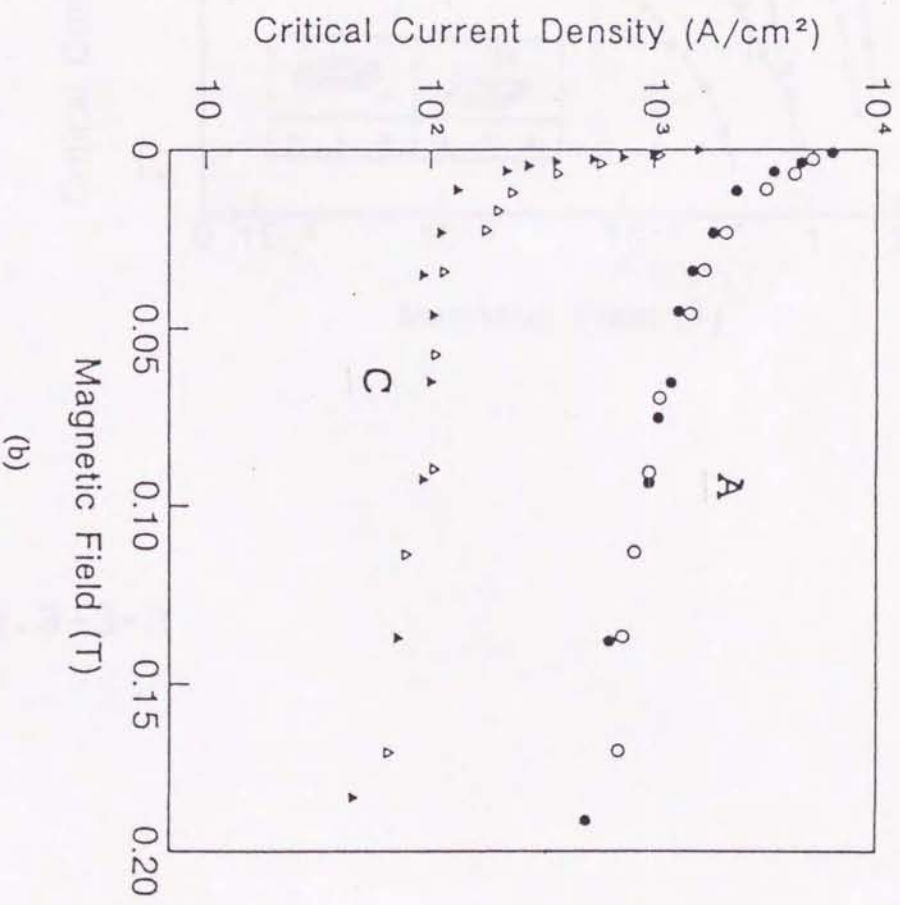
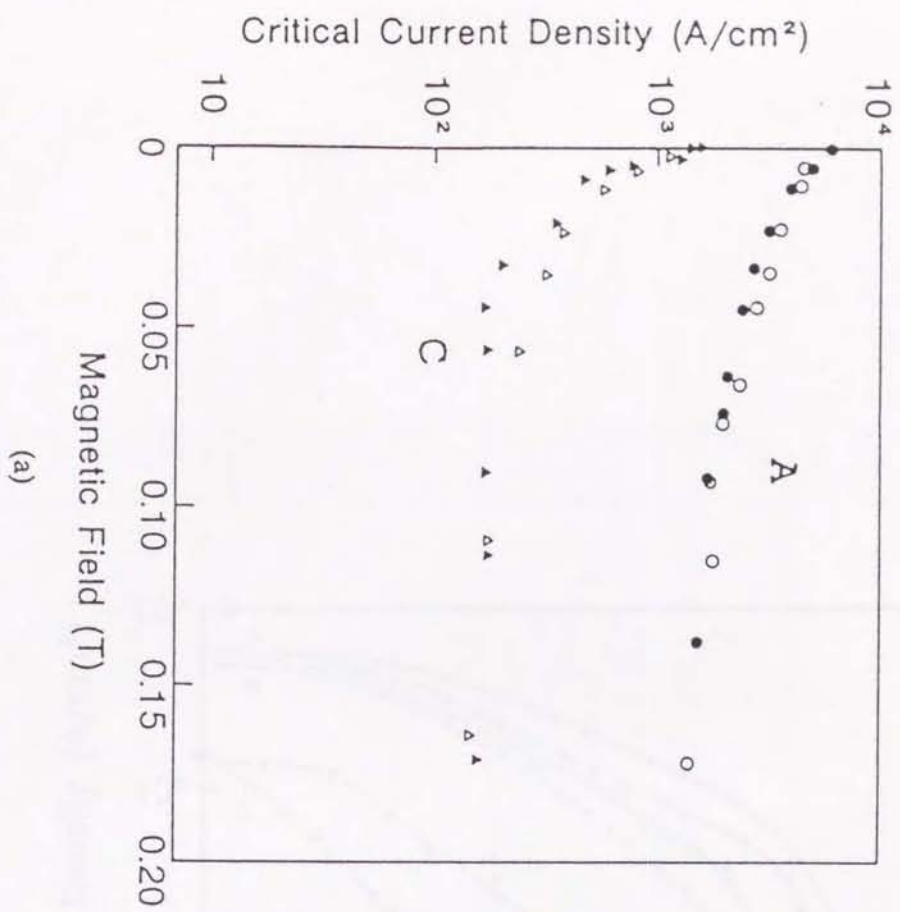


Fig.3-3-2

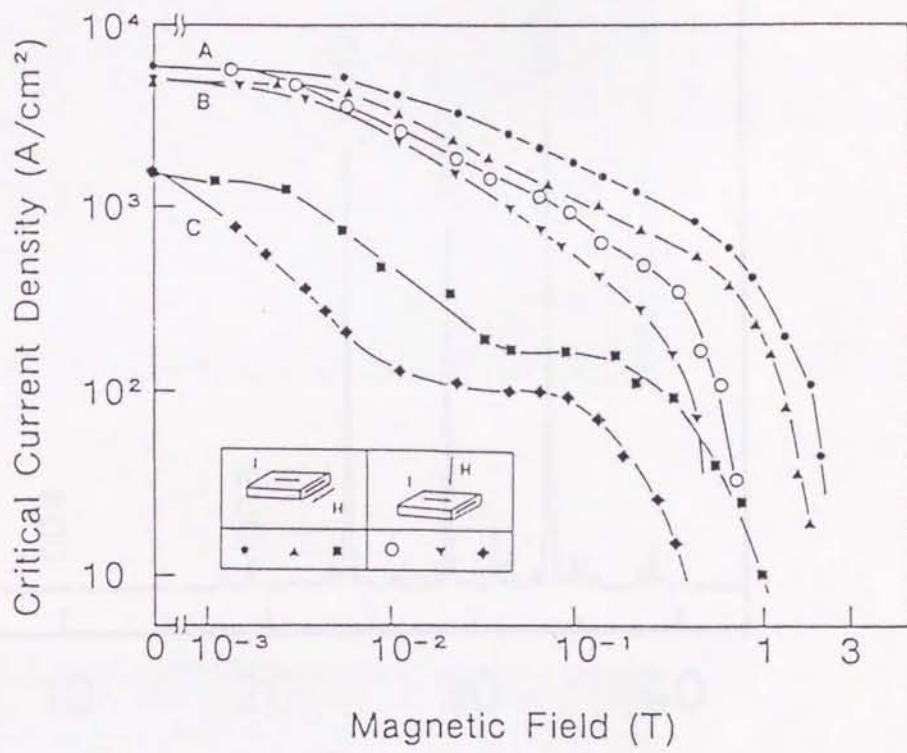


Fig.3-3-3

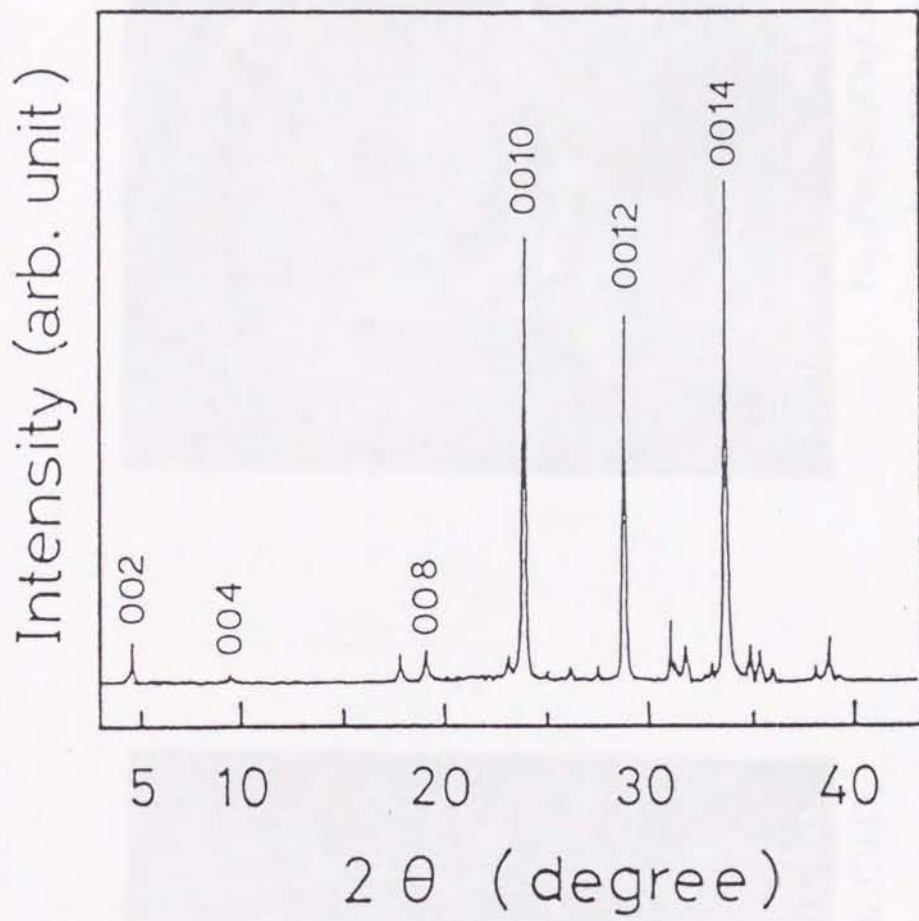
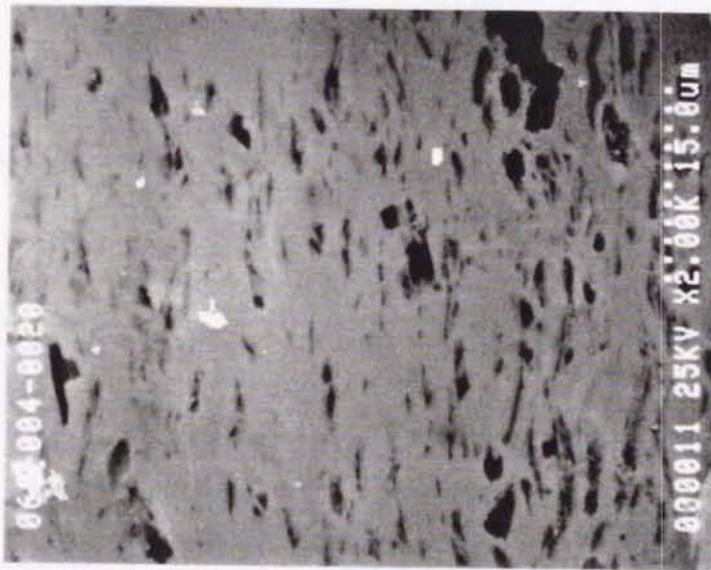


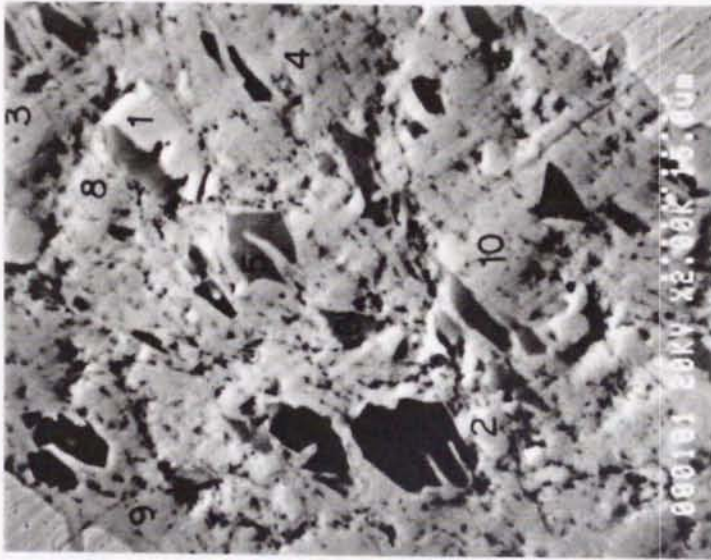
Fig.3-3-4



$\text{Bi}_{1.8}\text{Pb}_{0.4}\text{Sr}_2\text{Ca}_{2.2}\text{Cu}_3\text{O}_x$

$J_c = 14,300\text{A}/\text{cm}^2$

(a)



$\text{Bi}_{1.6}\text{Pb}_{0.4}\text{Sr}_2\text{Ca}_2\text{Cu}_3\text{O}_x$

$J_c = 5,500\text{A}/\text{cm}^2$

(b)

Fig. 3-4-1

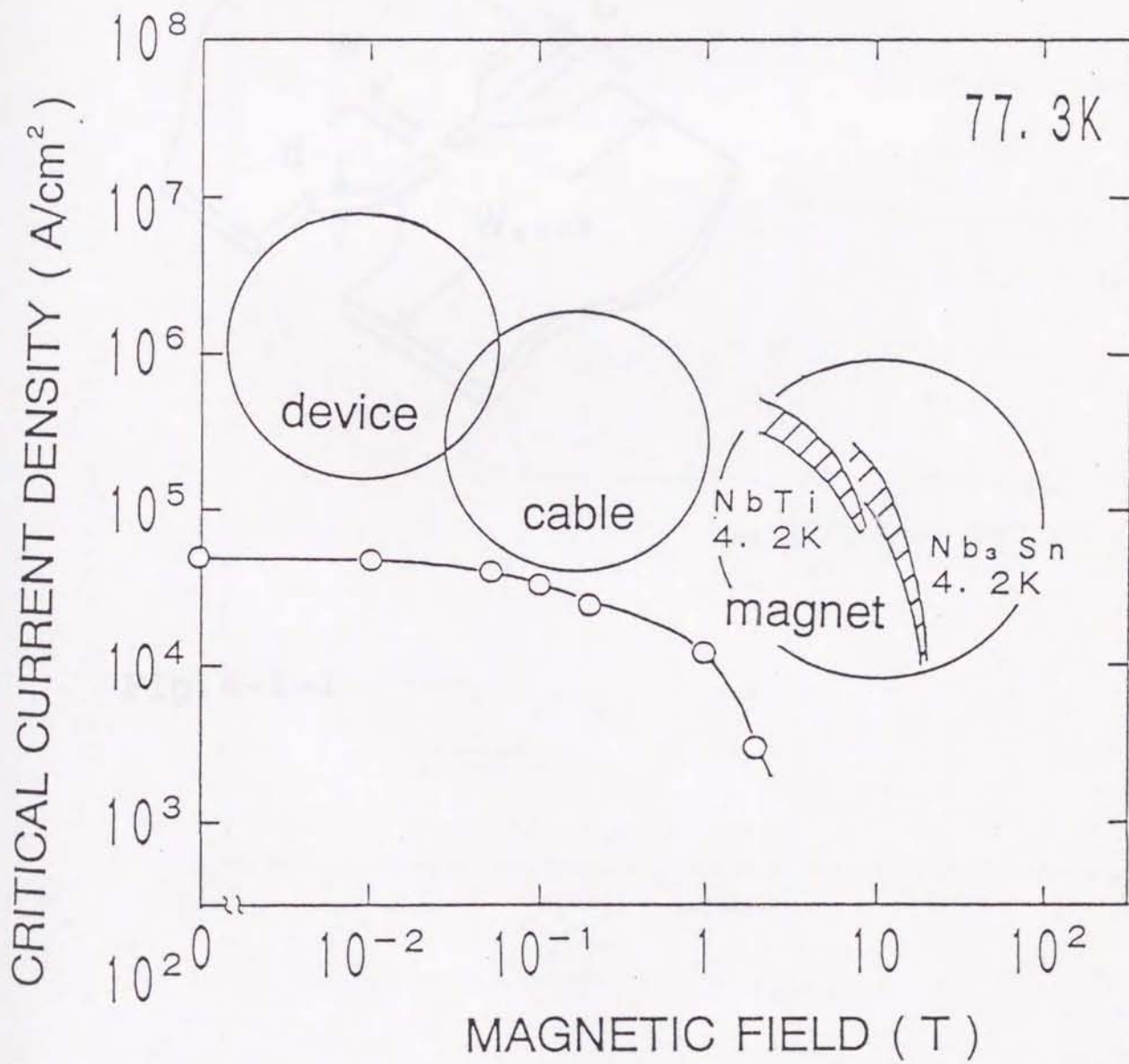


Fig.3-4-2

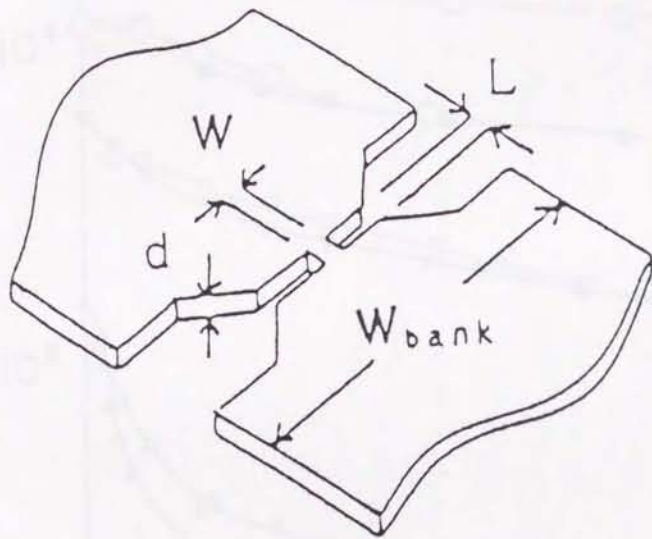


Fig.4-1-1

Fig.4-2-1

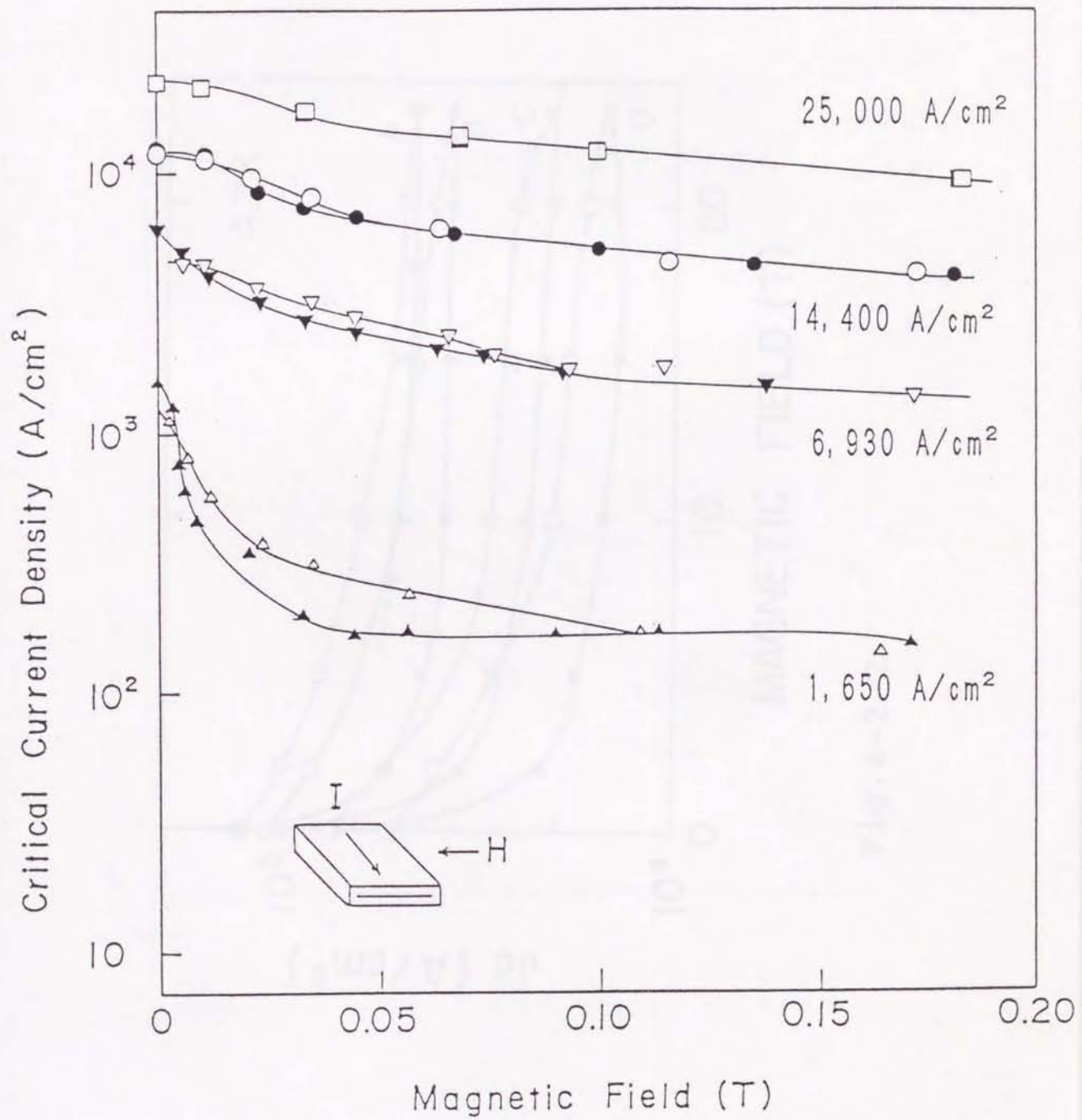


Fig.4-2-1

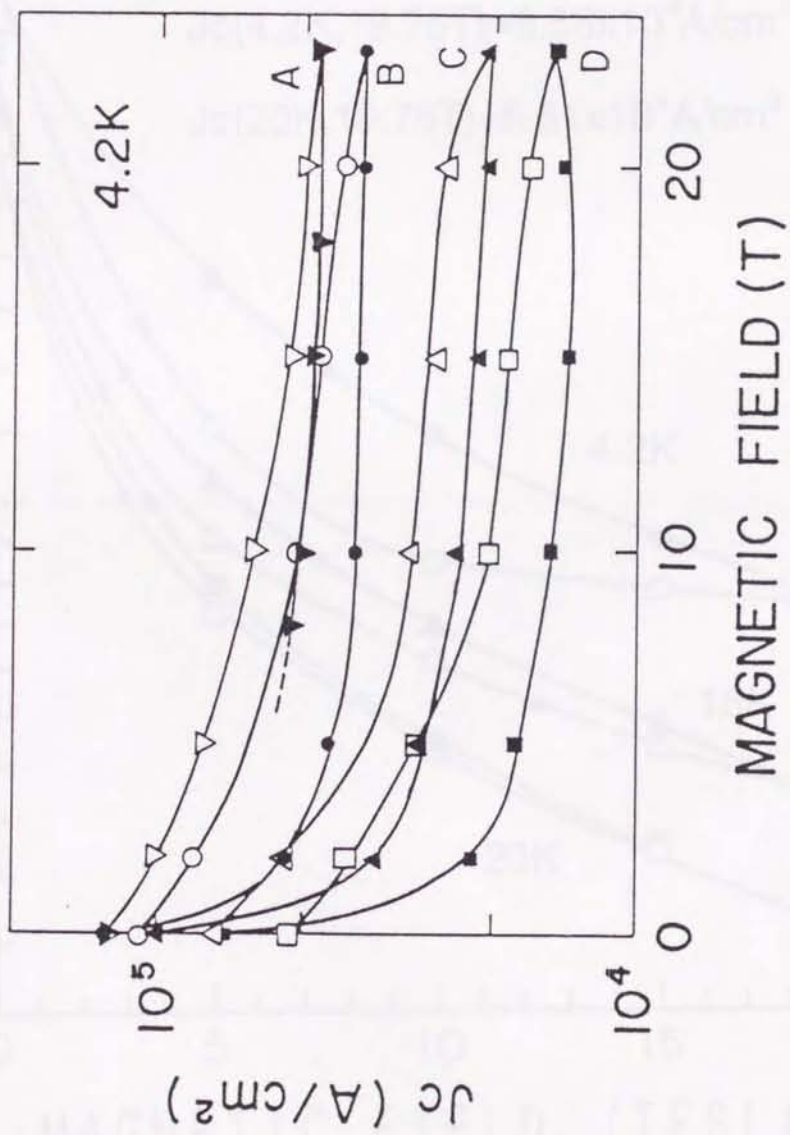


Fig. 4-2-2

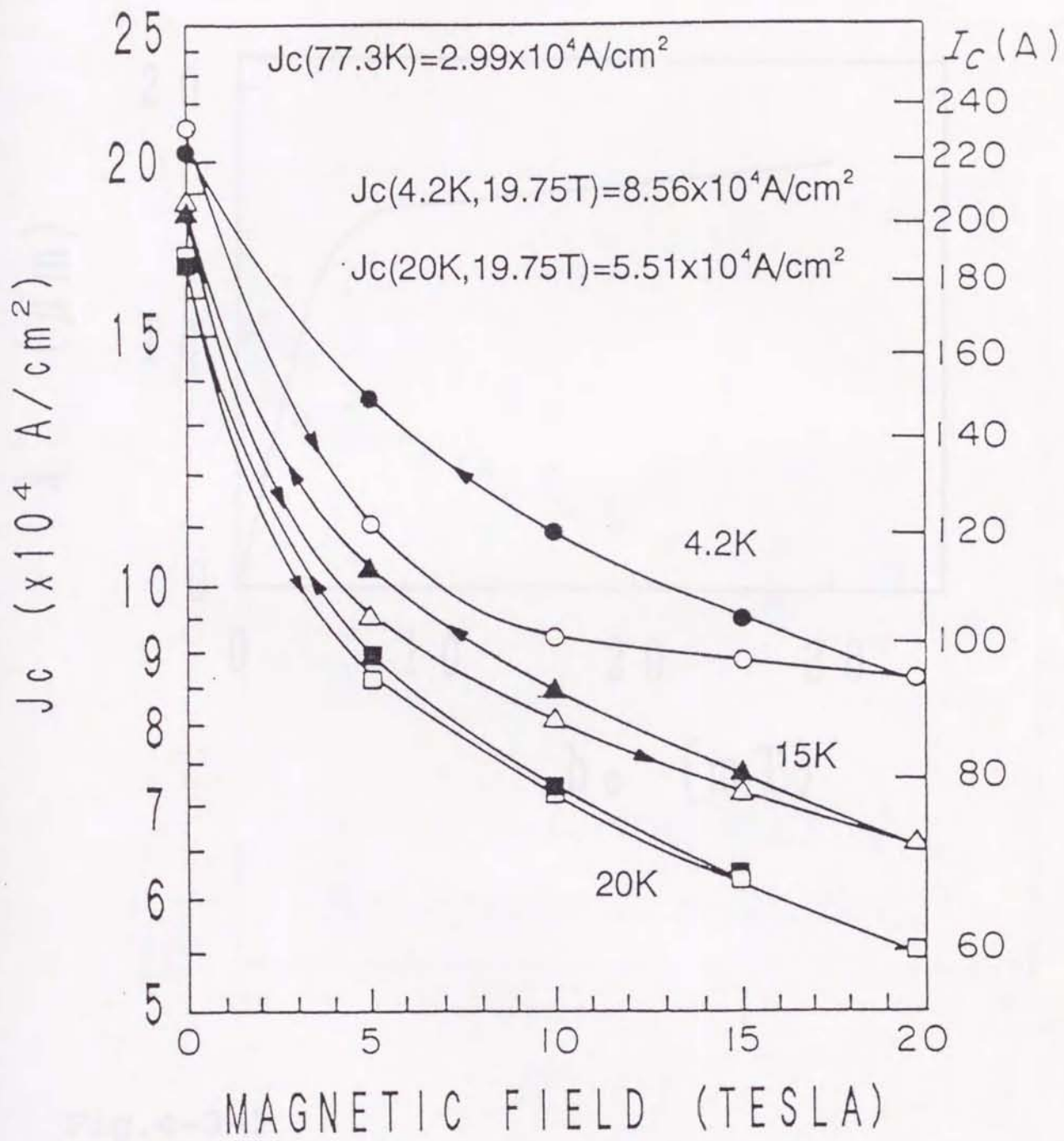


Fig.4-2-3

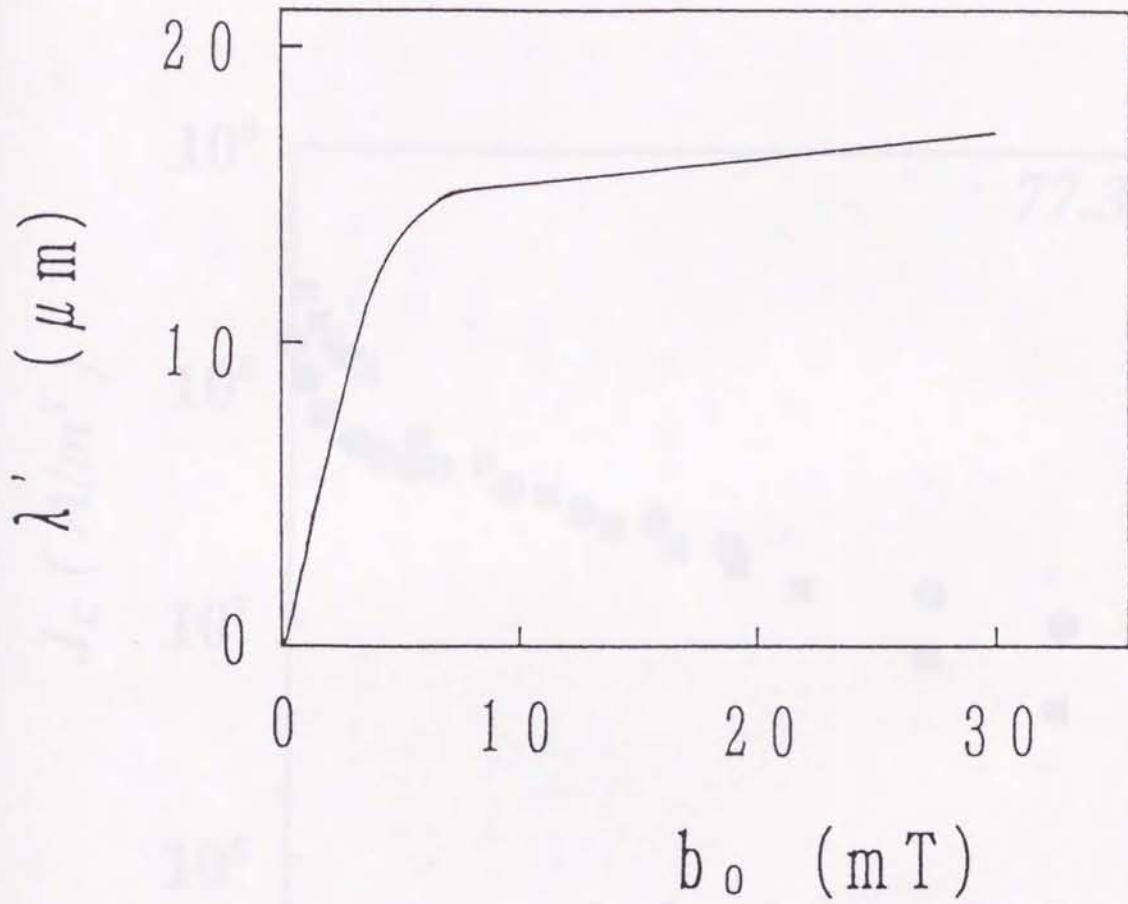


Fig. 4-3-1

Fig. 4-3-2

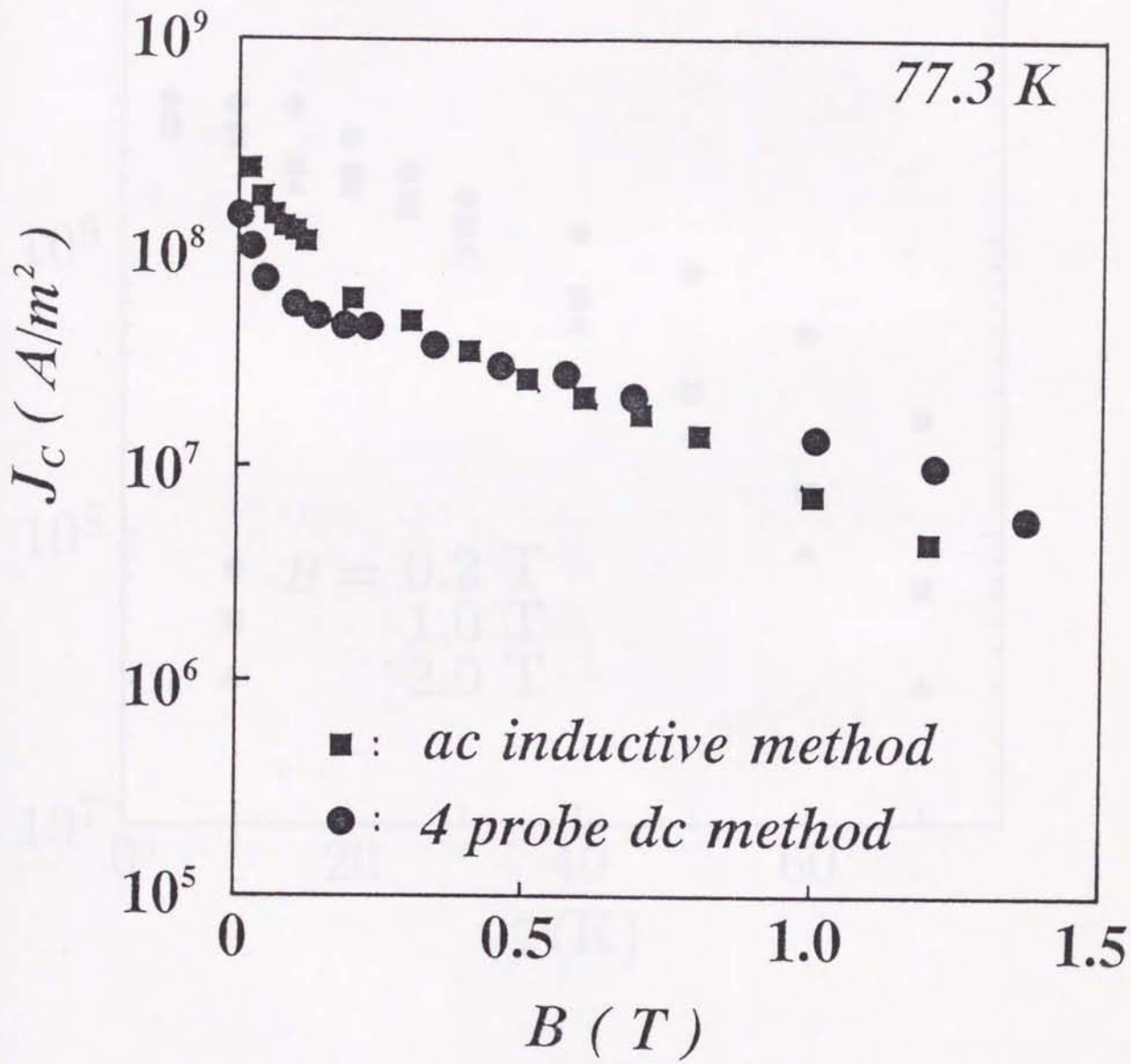


Fig. 4-3-2

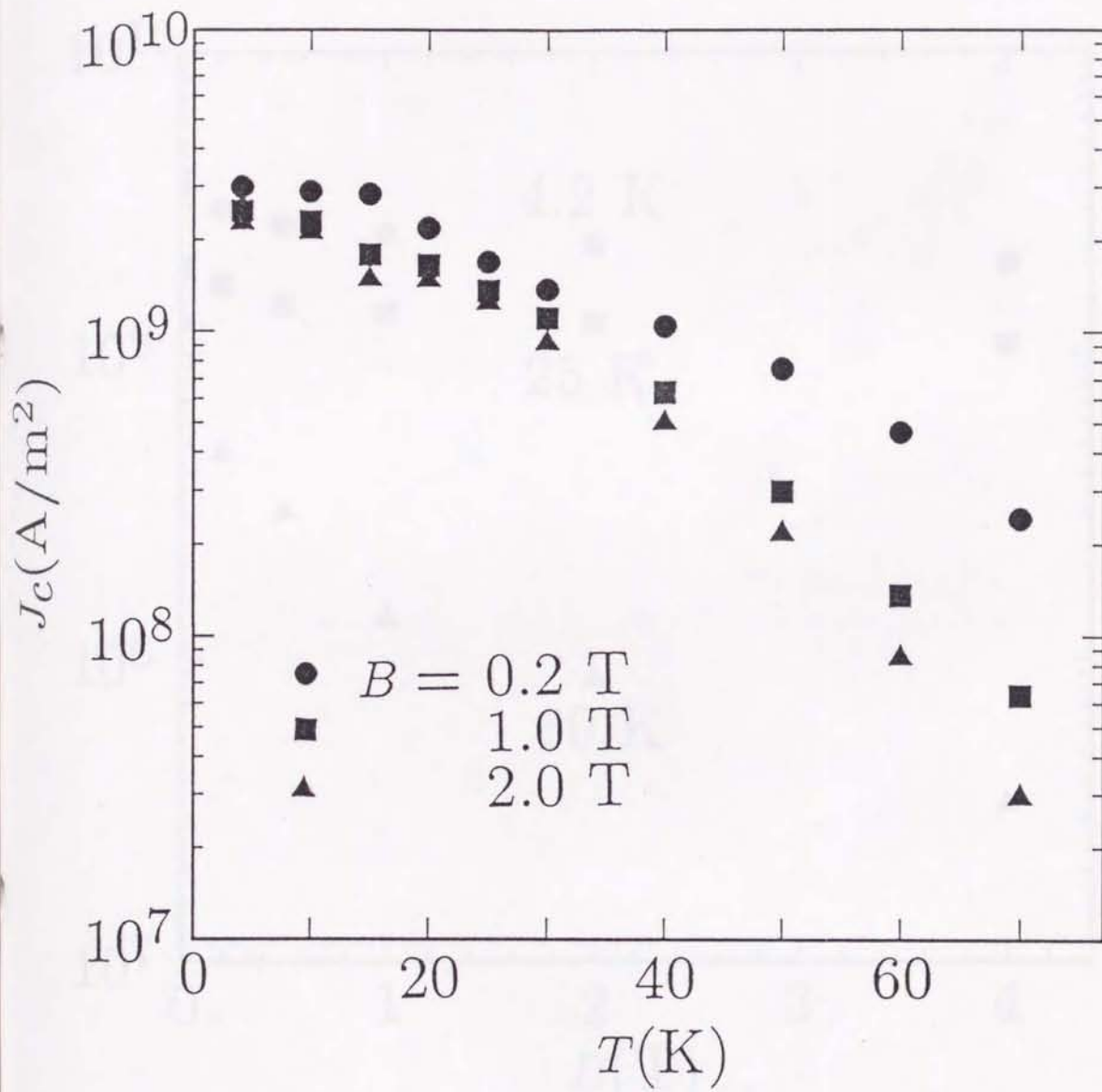


Fig. 4-3-3

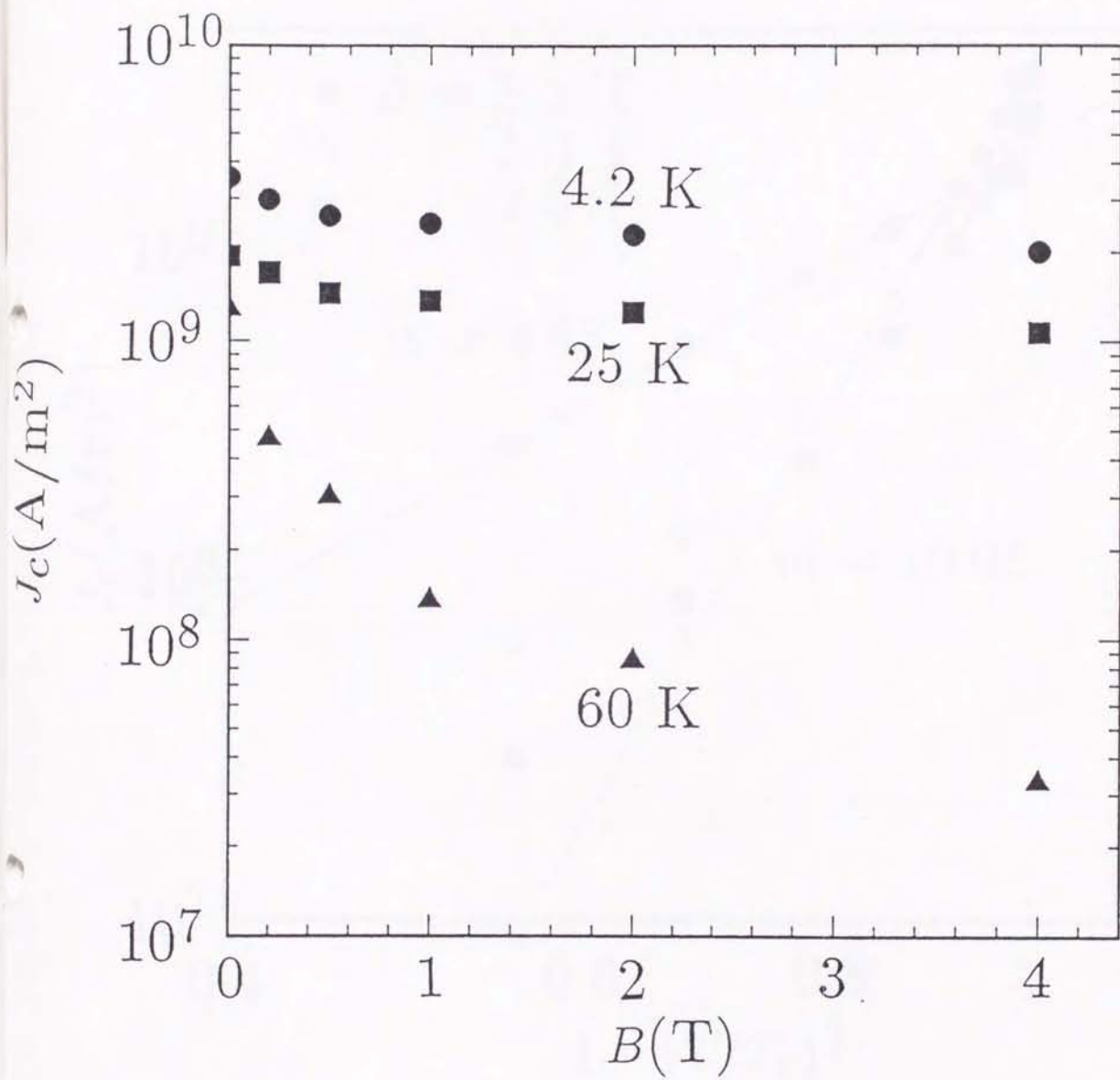


Fig. 4-3-4

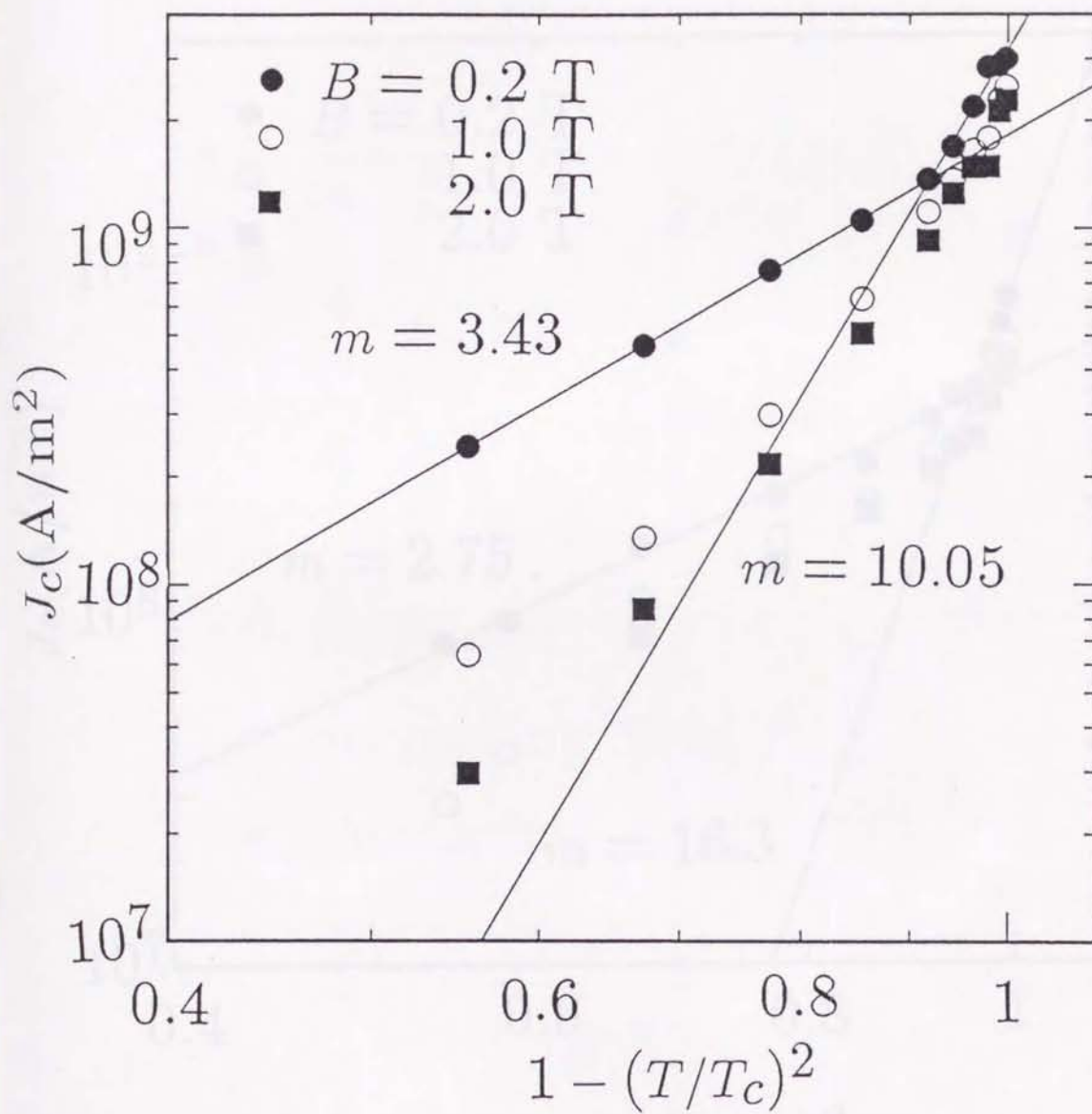


Fig.4-3-5

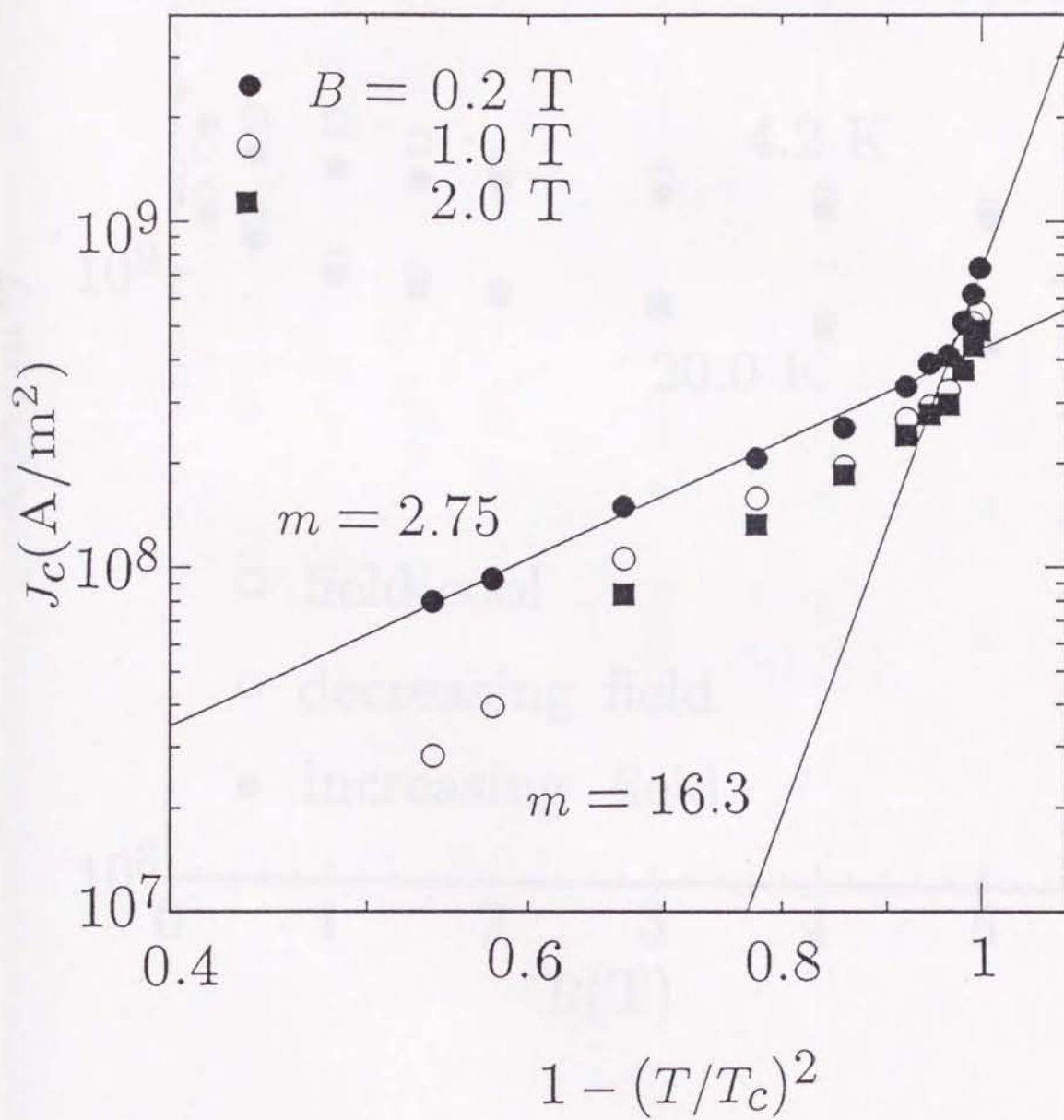


Fig.4-3-6

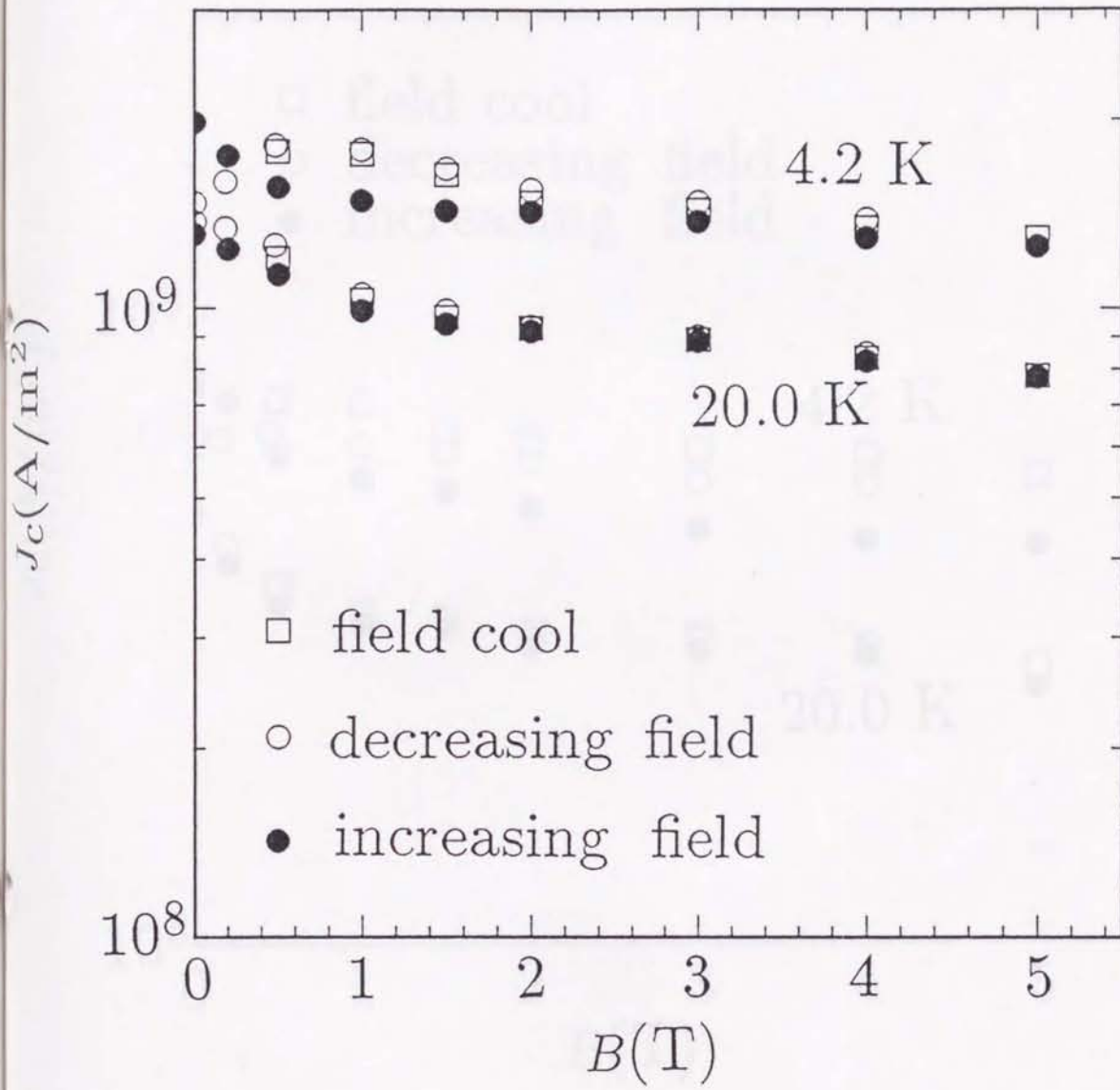


Fig.4-3-7

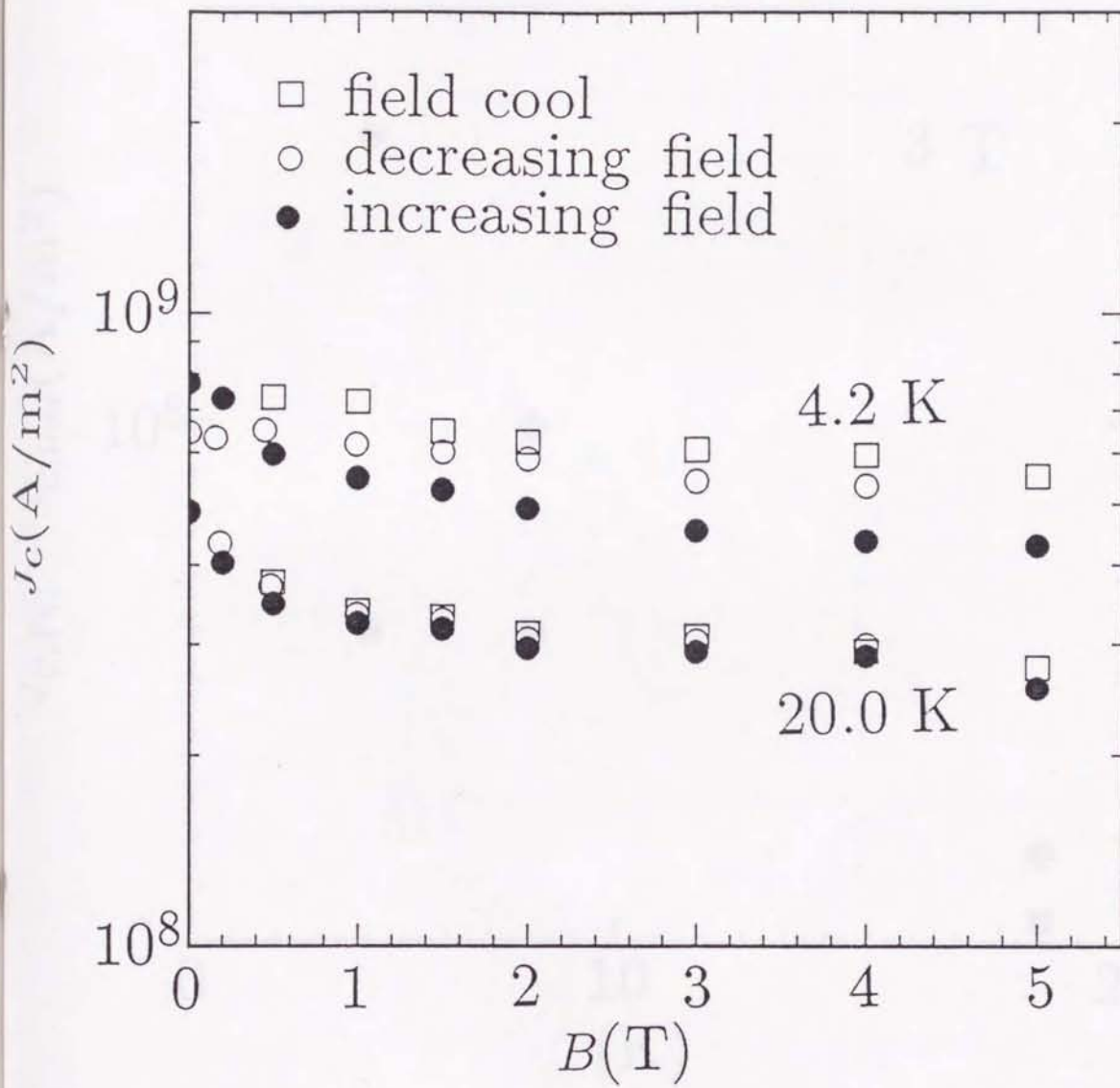


Fig. 4-3-8

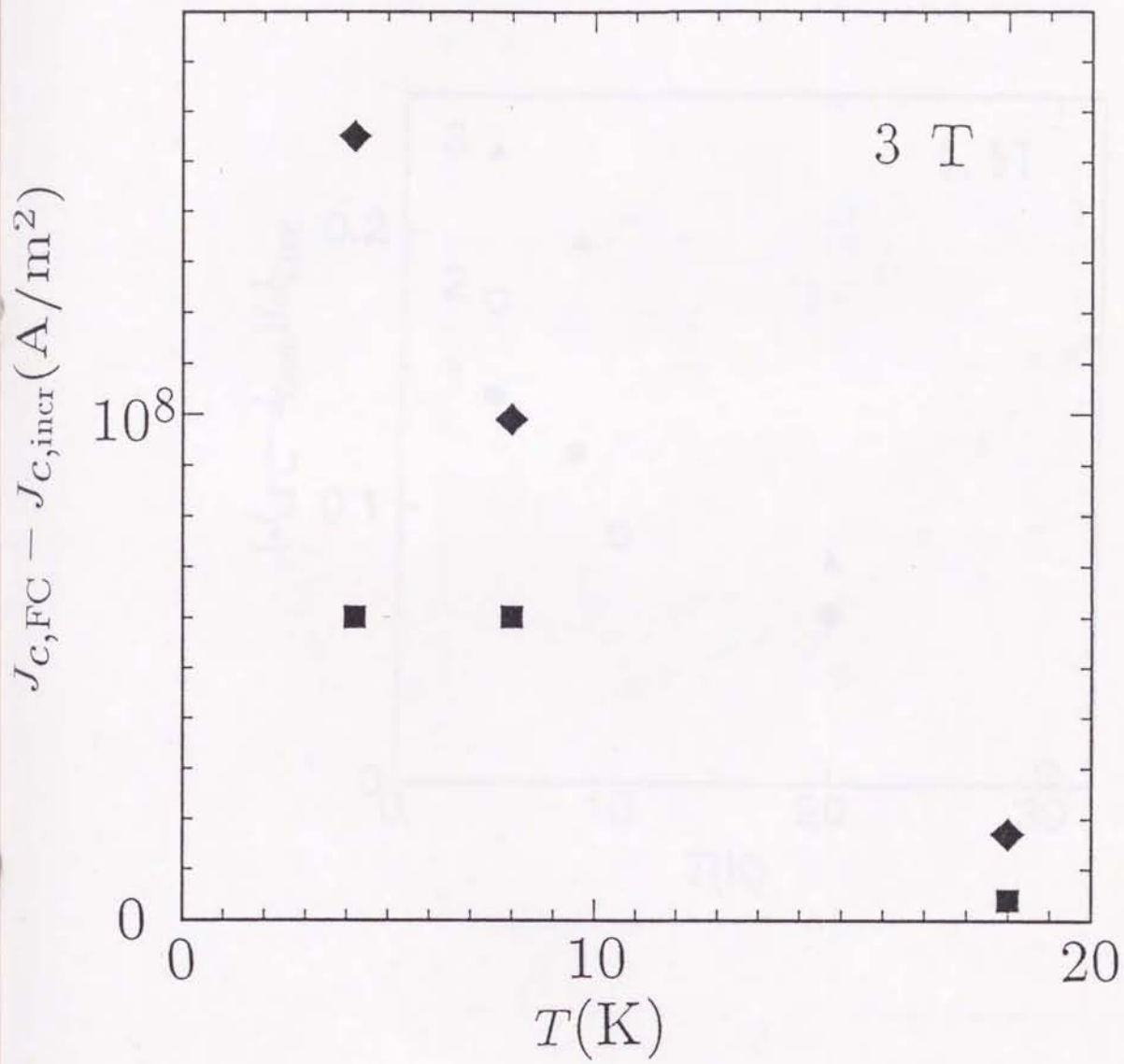


Fig.4-3-9

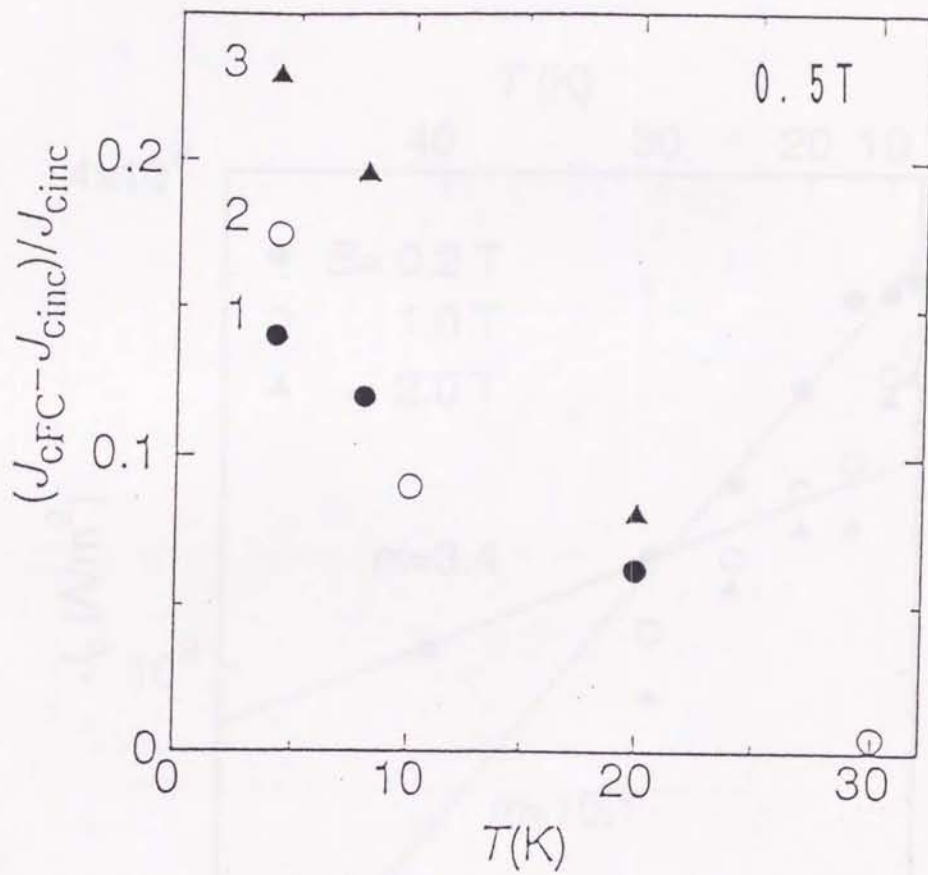


Fig. 4-3-10

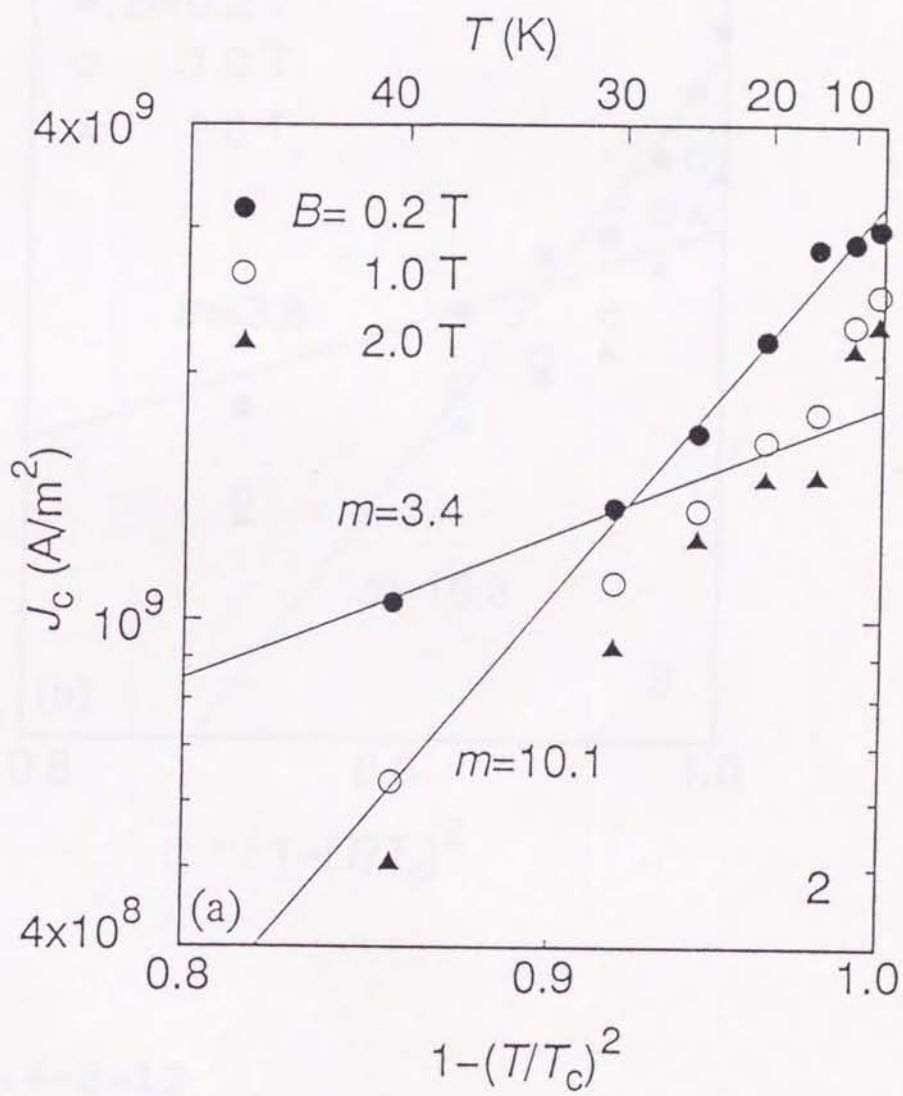


Fig. 4-3-11

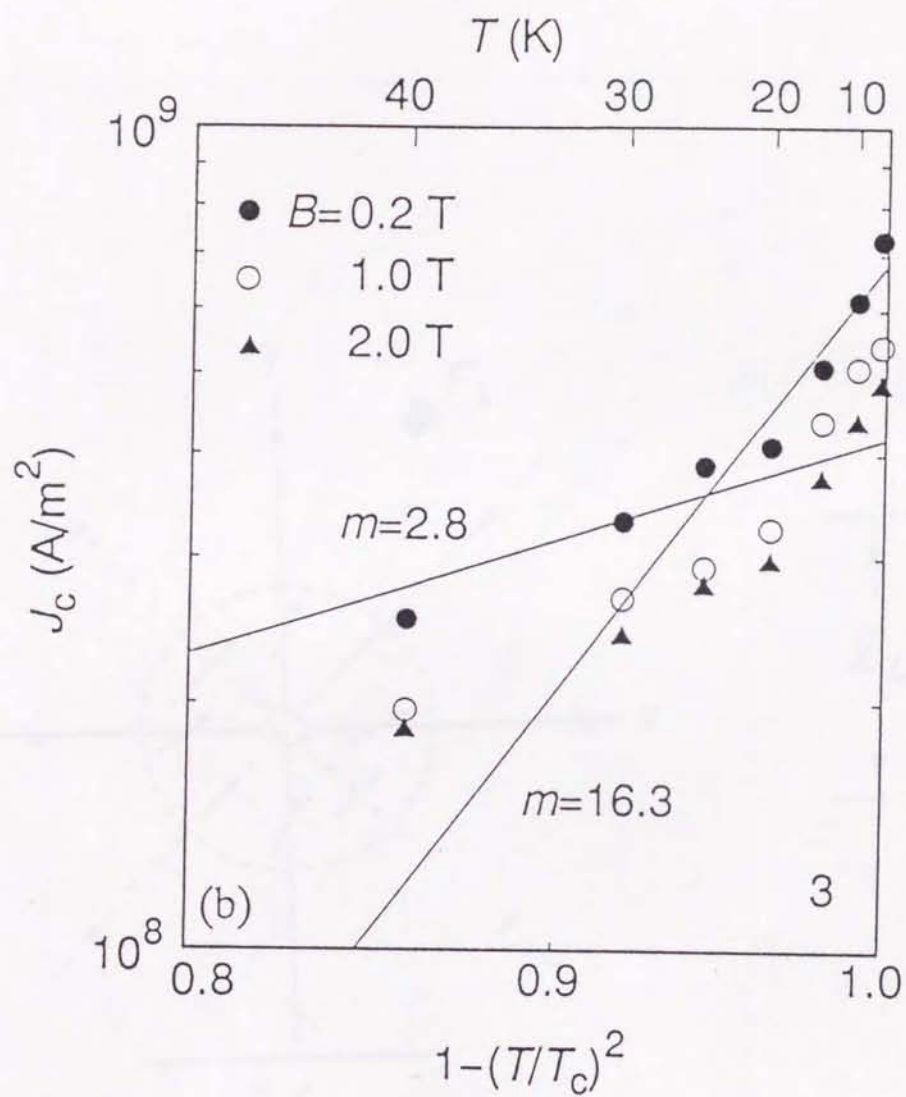


Fig. 4-3-12

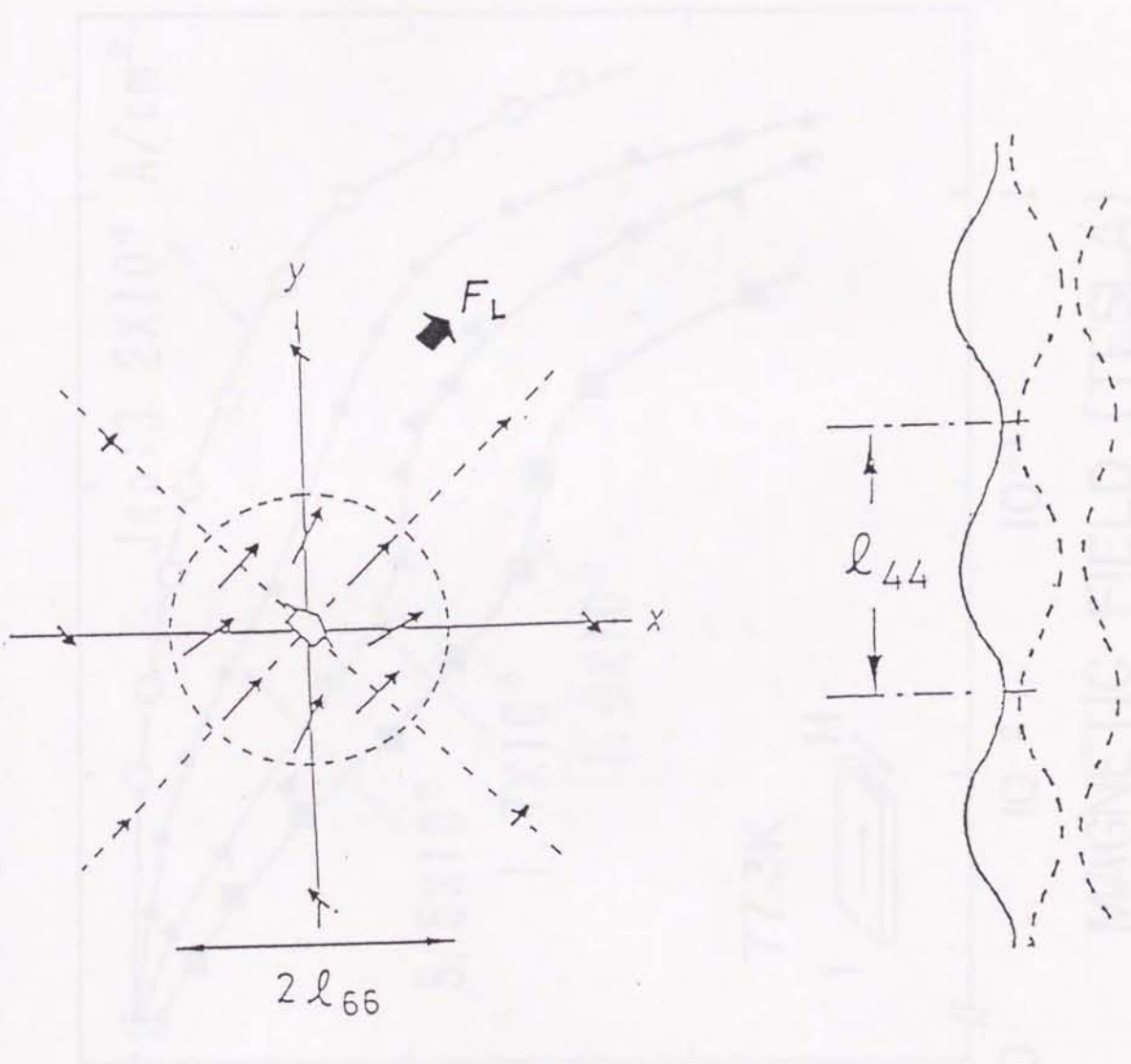
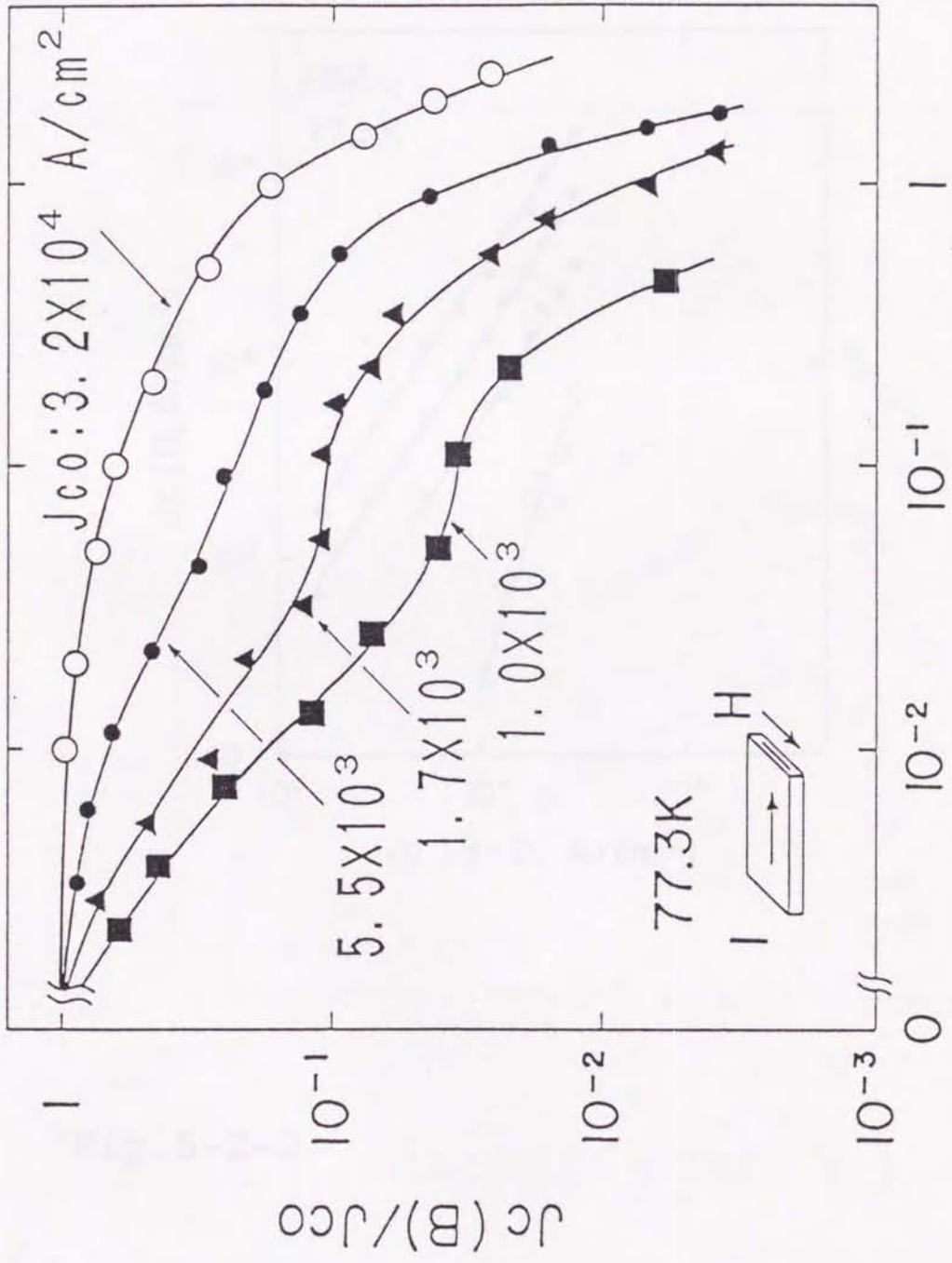


Fig. 5-1-1



MAGNETIC FIELD (TESLA)

Fig. 5-2-1

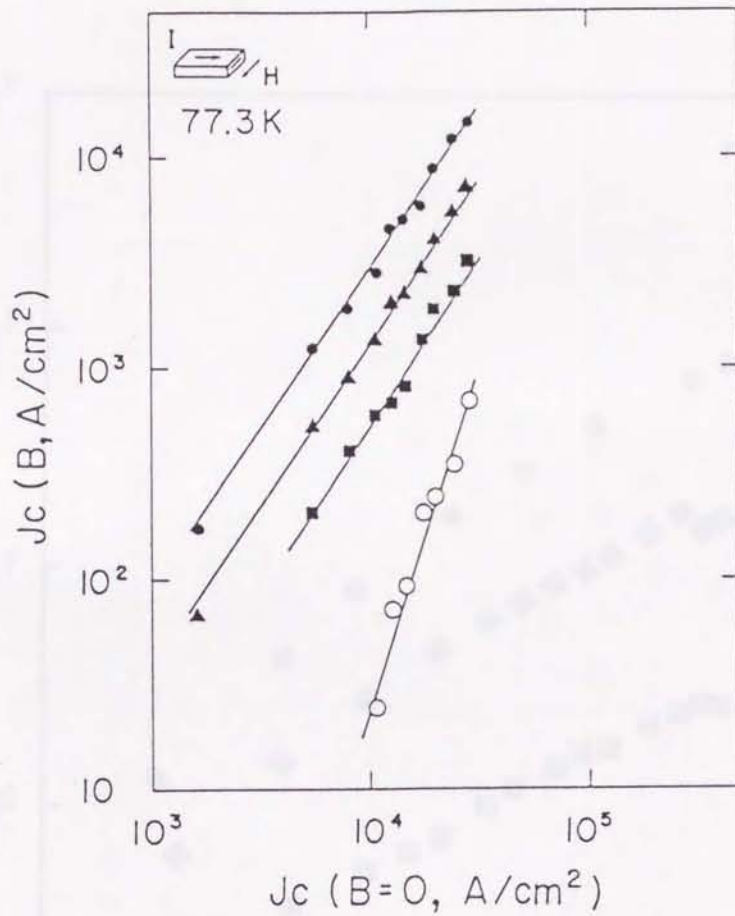


Fig. 5-2-2

Fig. 5-2-3

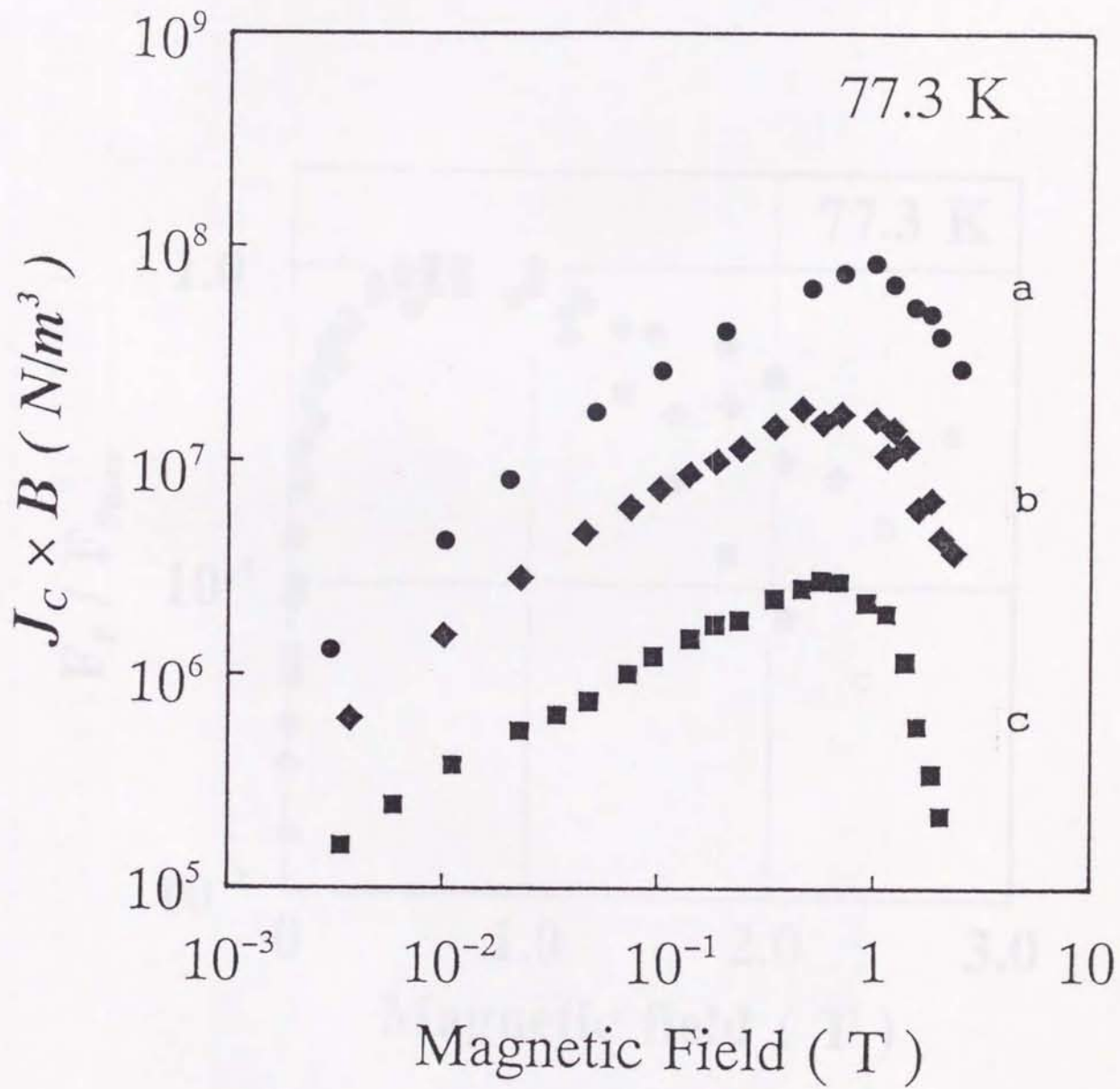


Fig.5-2-3

Fig.5-2-4

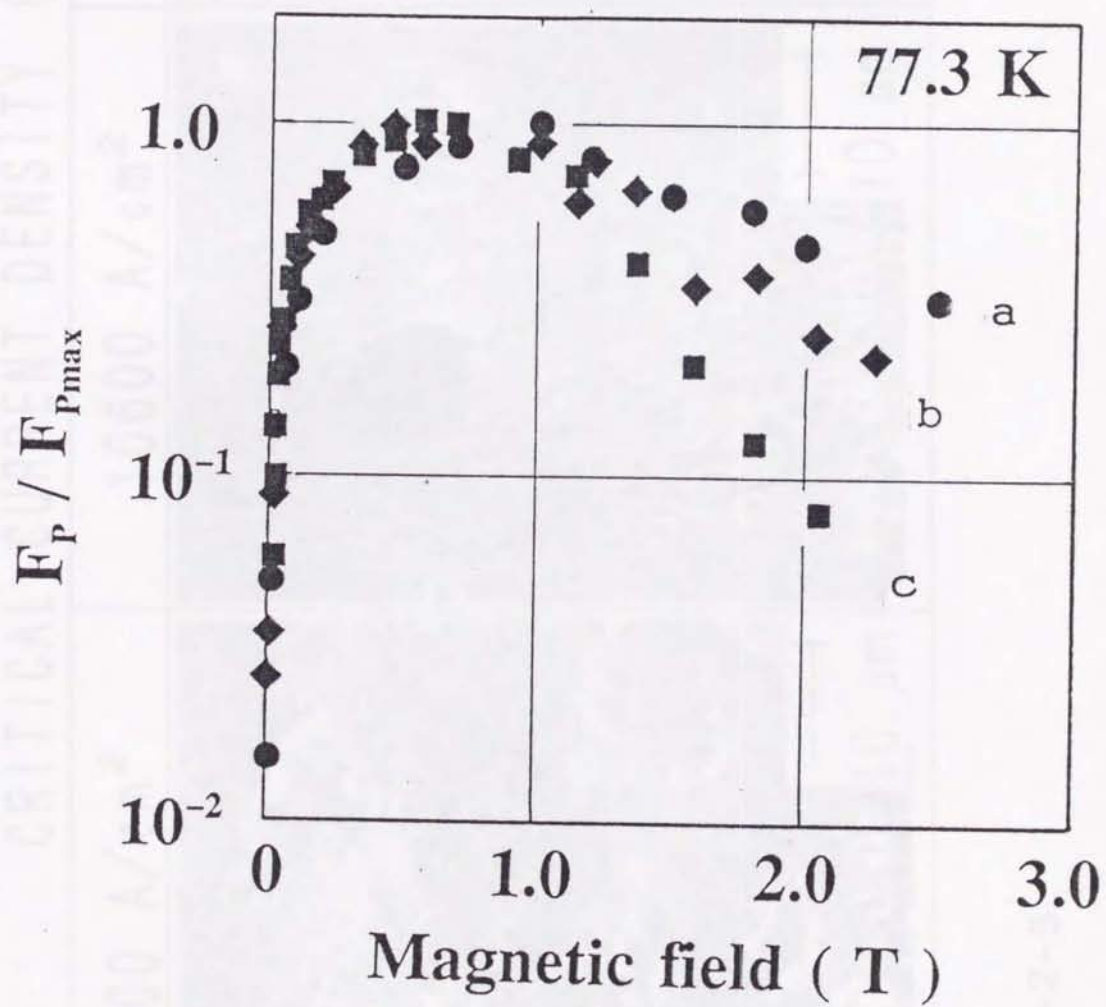


Fig.5-2-4

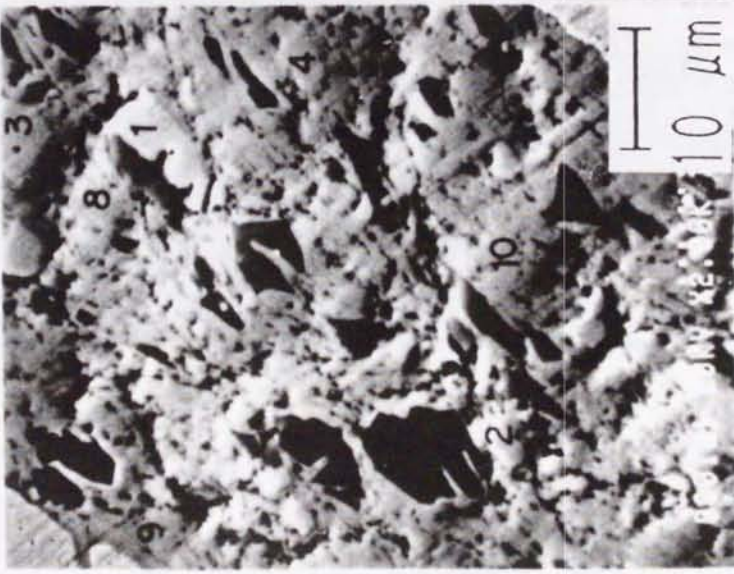
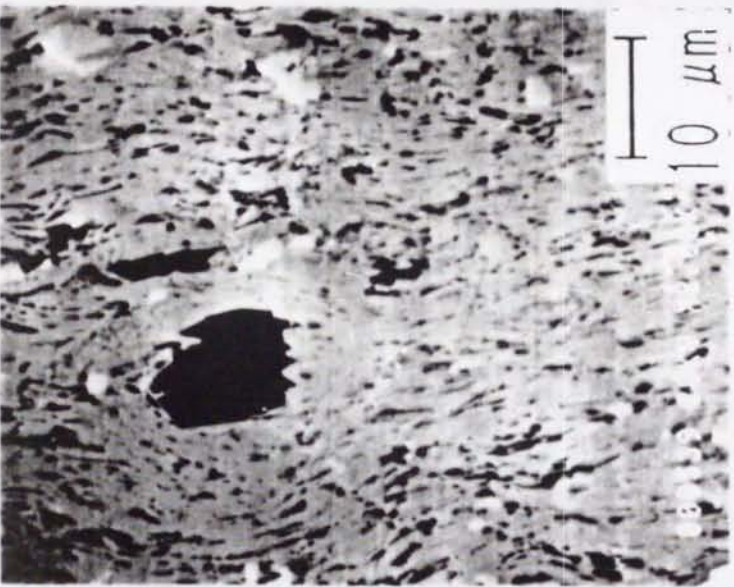
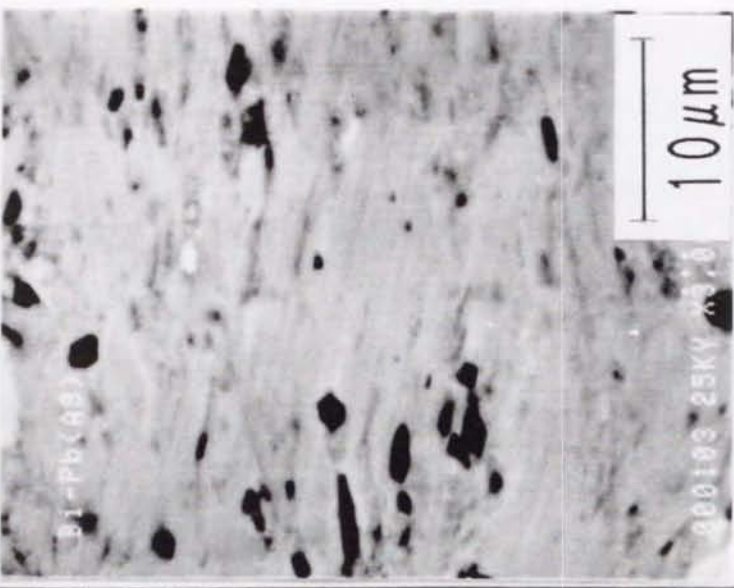
CRITICAL CURRENT DENSITY (77.3K)		
5500 A/cm ²	10600 A/cm ²	22200 A/cm ²
		

Fig. 5-2-5

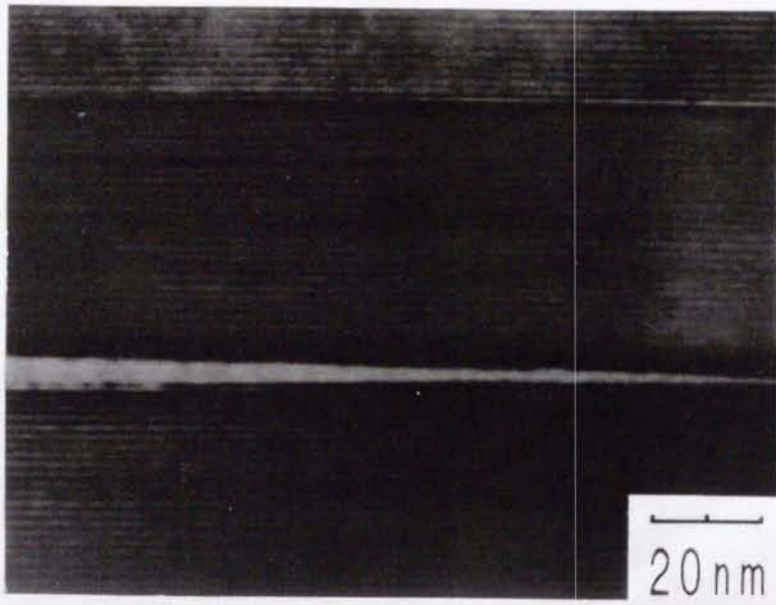


Fig.5-2-6

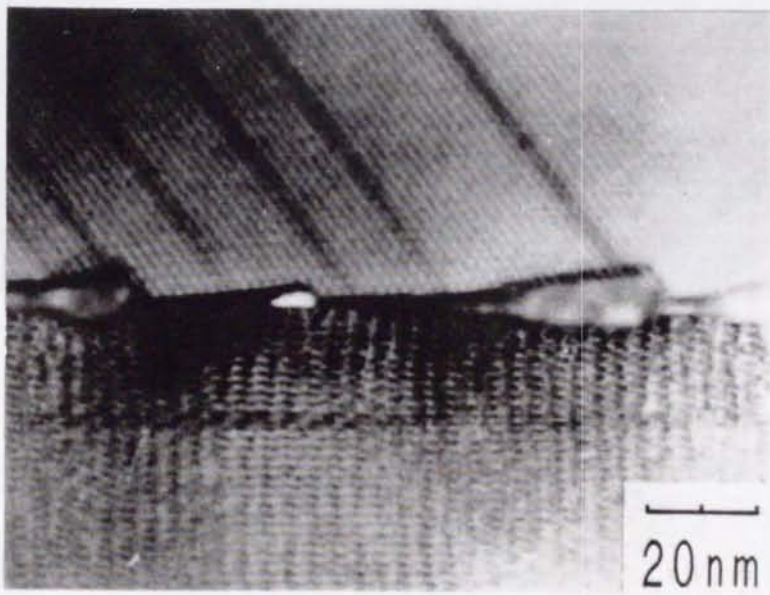
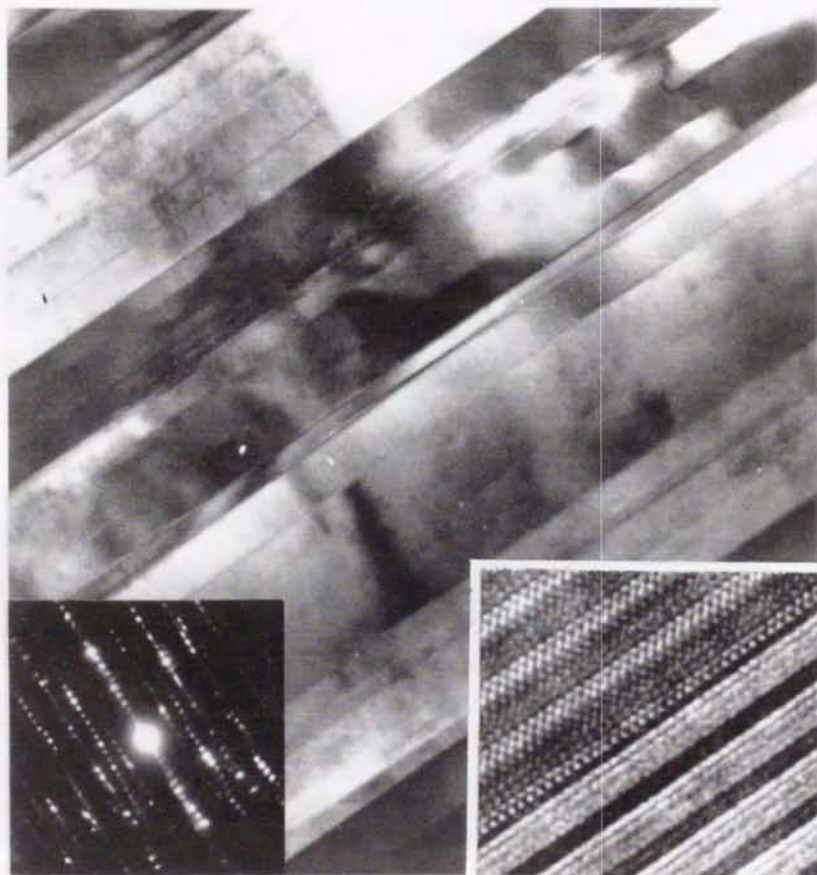


Fig.5-2-7

TEM Photograph of Ag/BiPbSrCaCuO



0.1 μm

5 nm

Fig.5-2-8

TEM Photograph of Ag/BiPbSrCaCuO

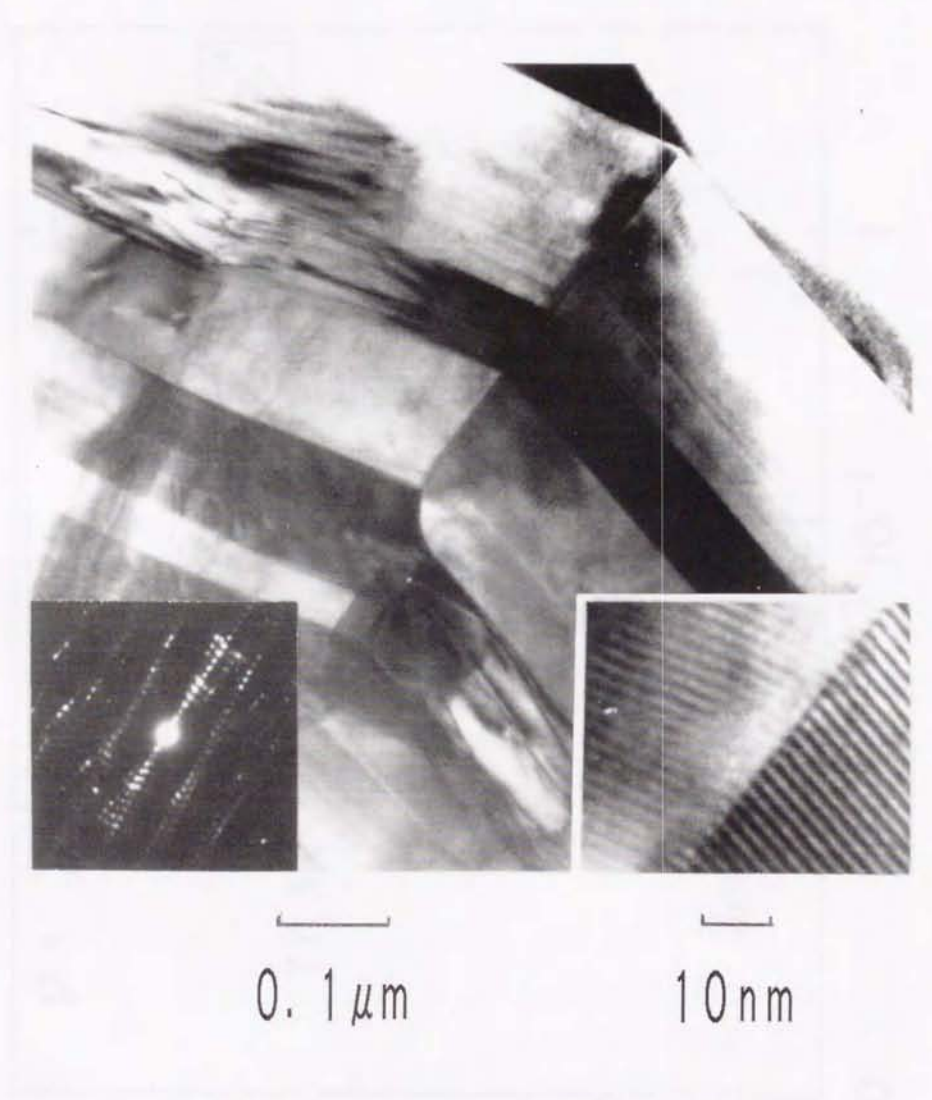


Fig.5-2-9

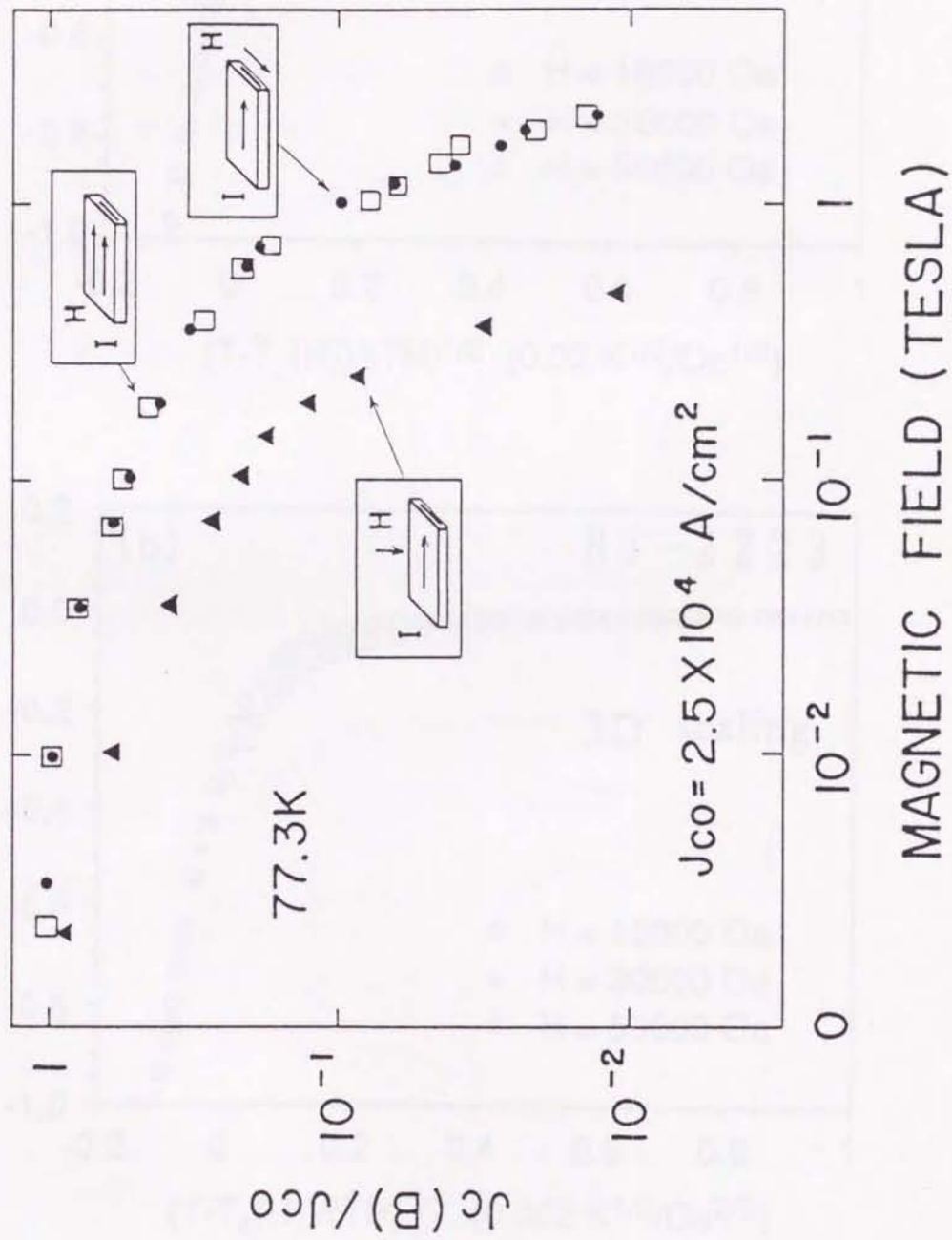


Fig. 5-2-10

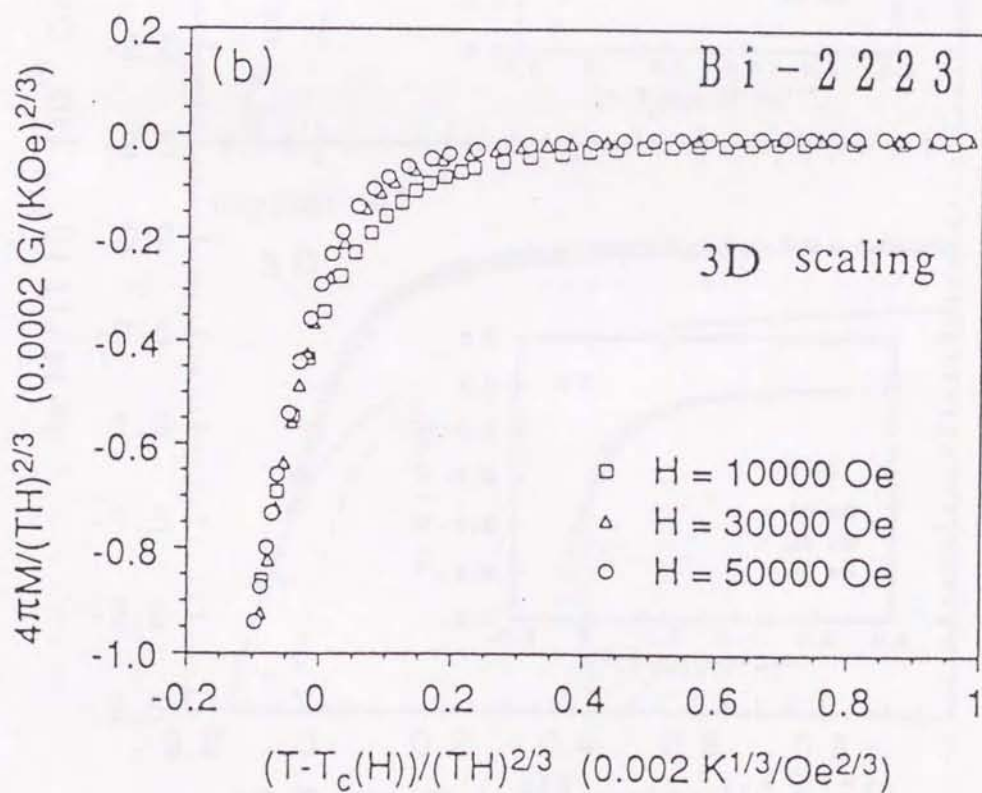
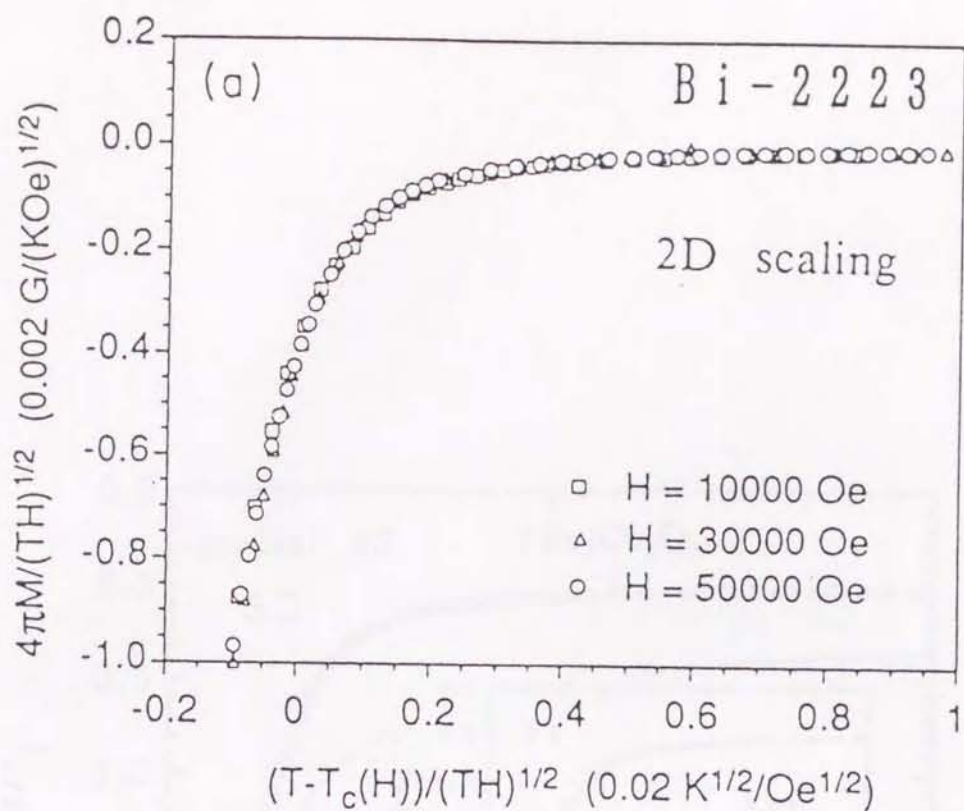


Fig. 5-2-11

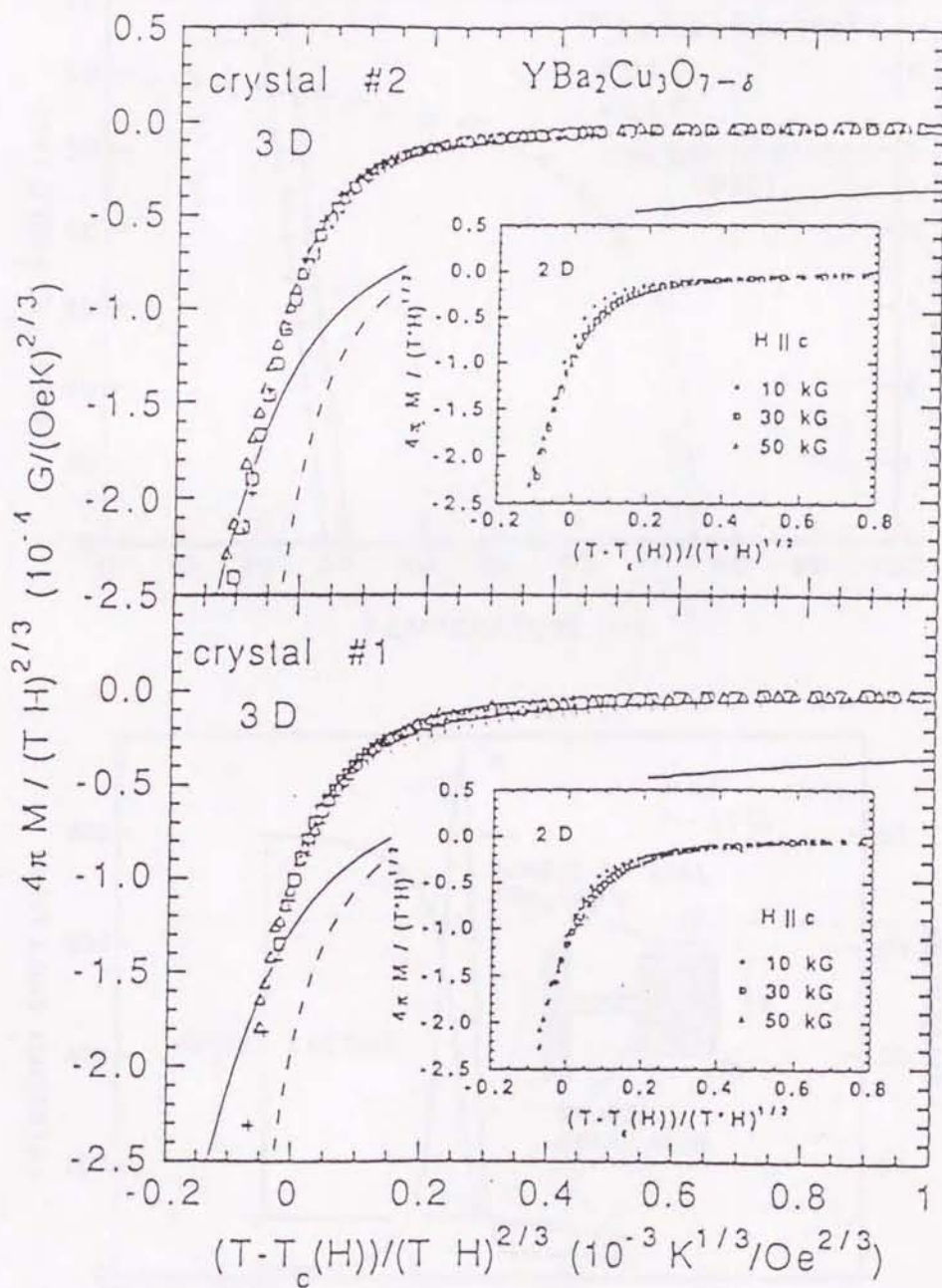


Fig.5-2-12

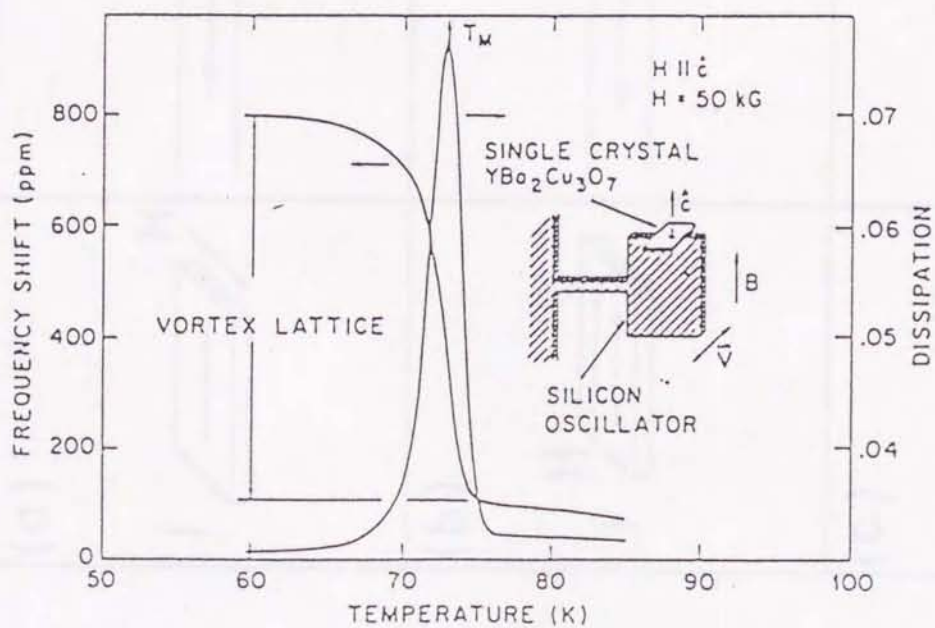
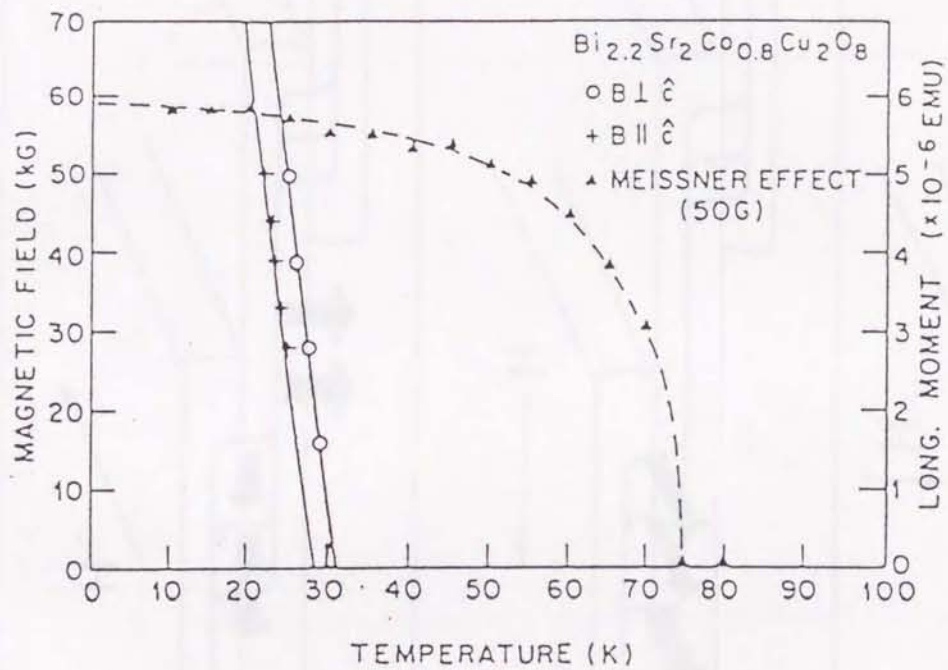


Fig. 5-2-13

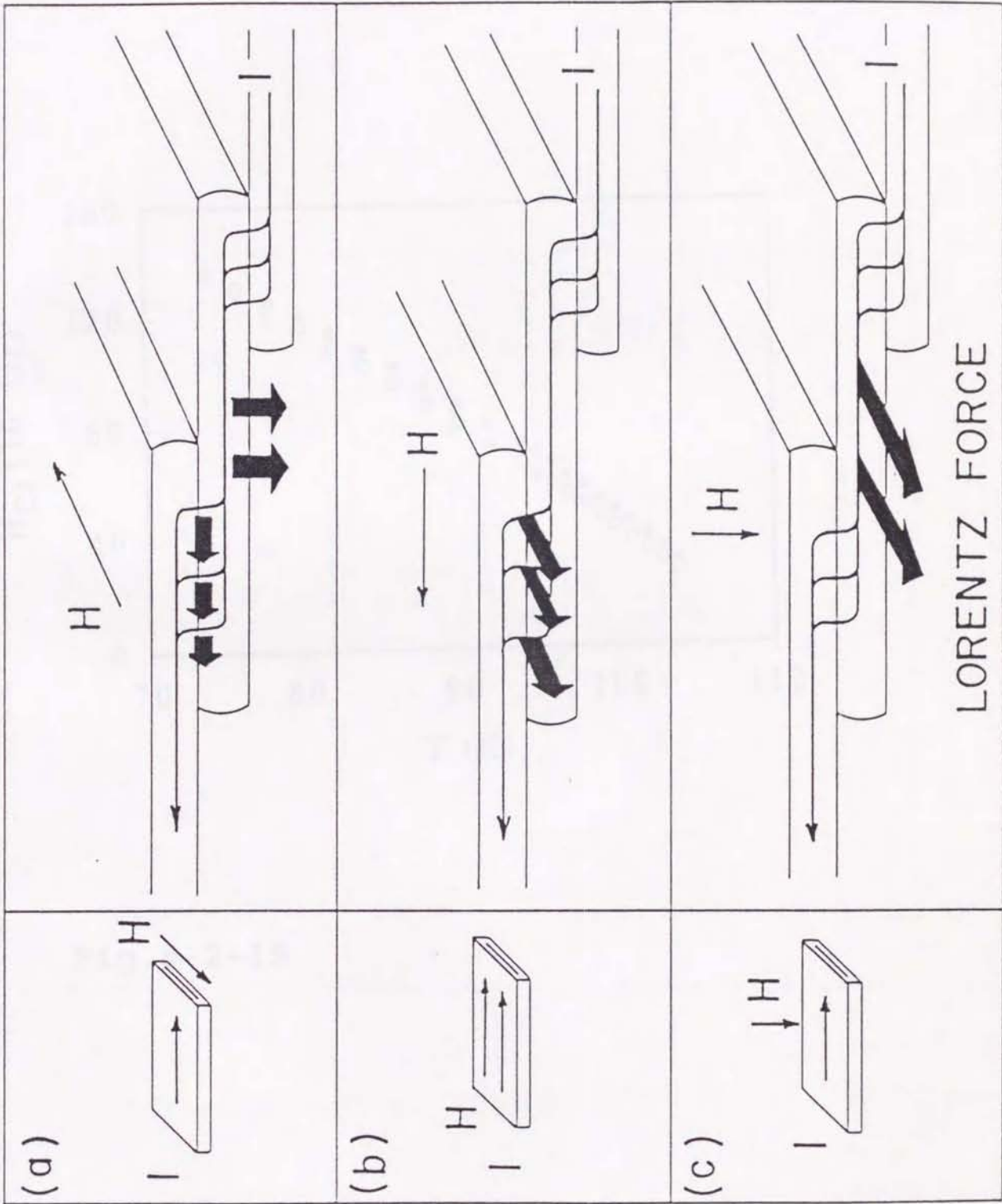


Fig. 5-2-14

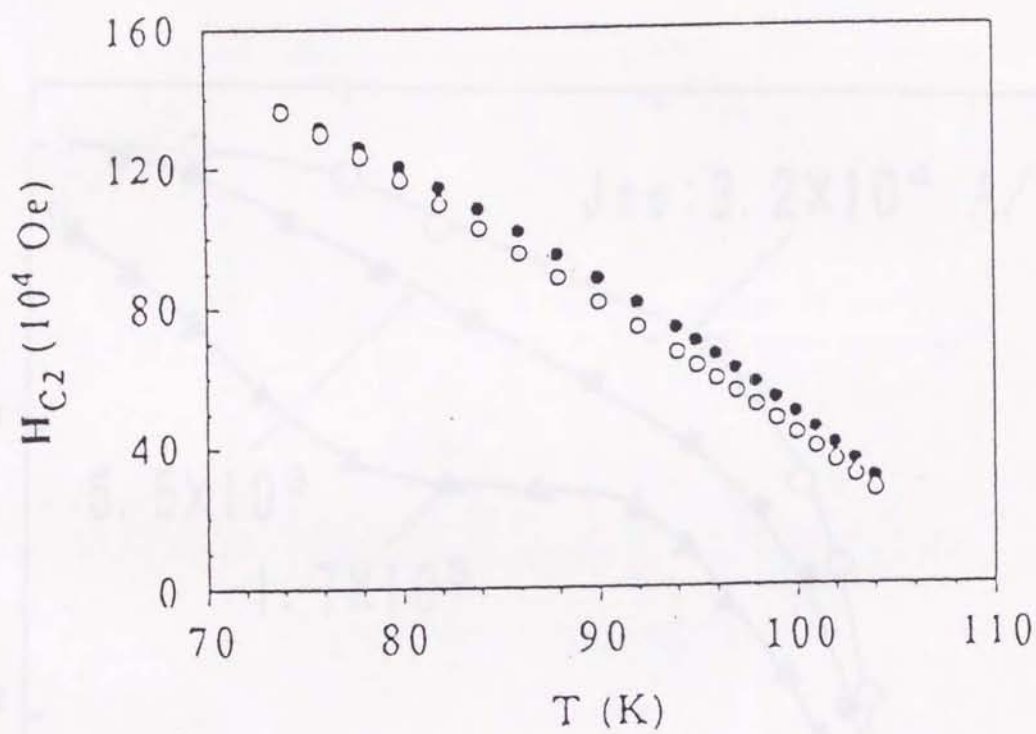


Fig. 5-2-15

Fig. 5-2-15

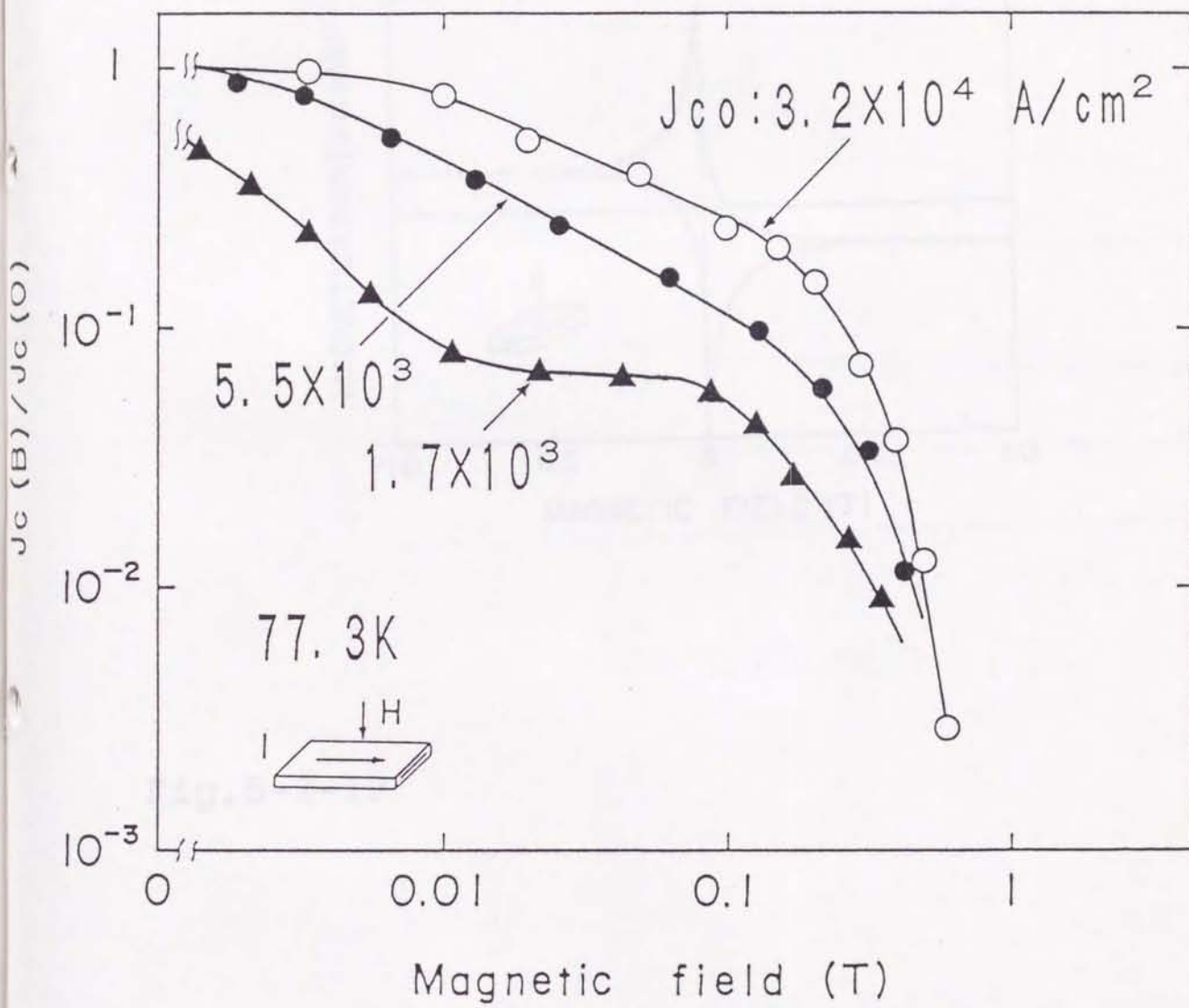


Fig.5-2-16

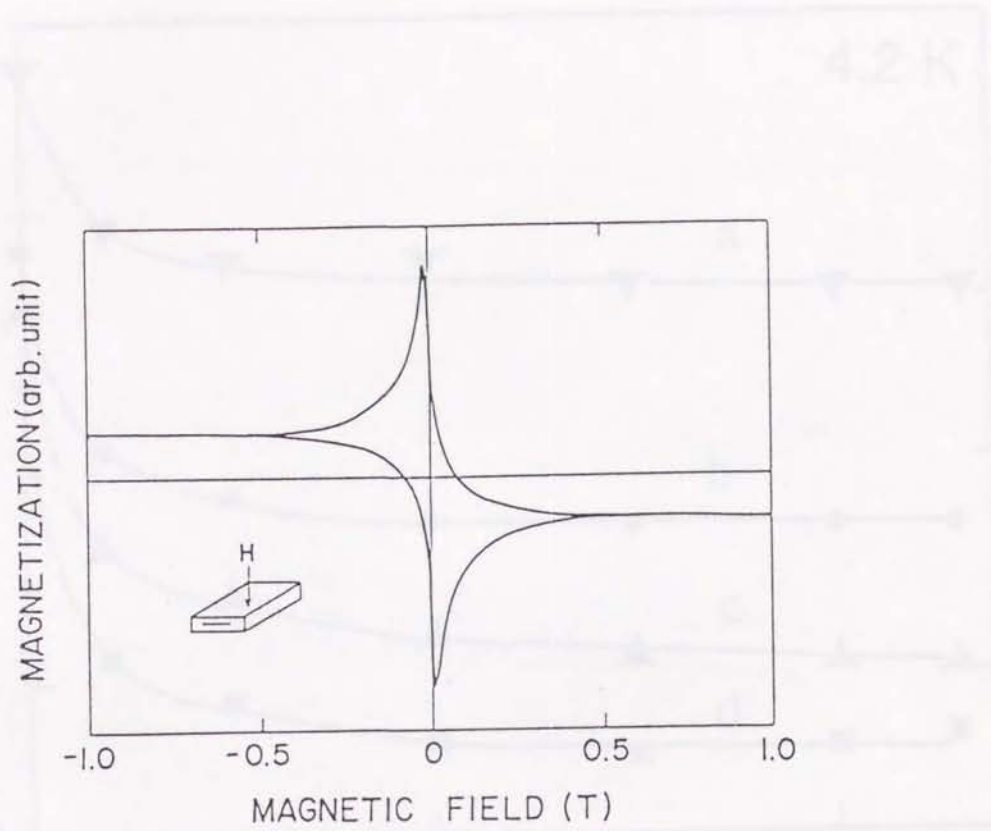


Fig.5-2-17

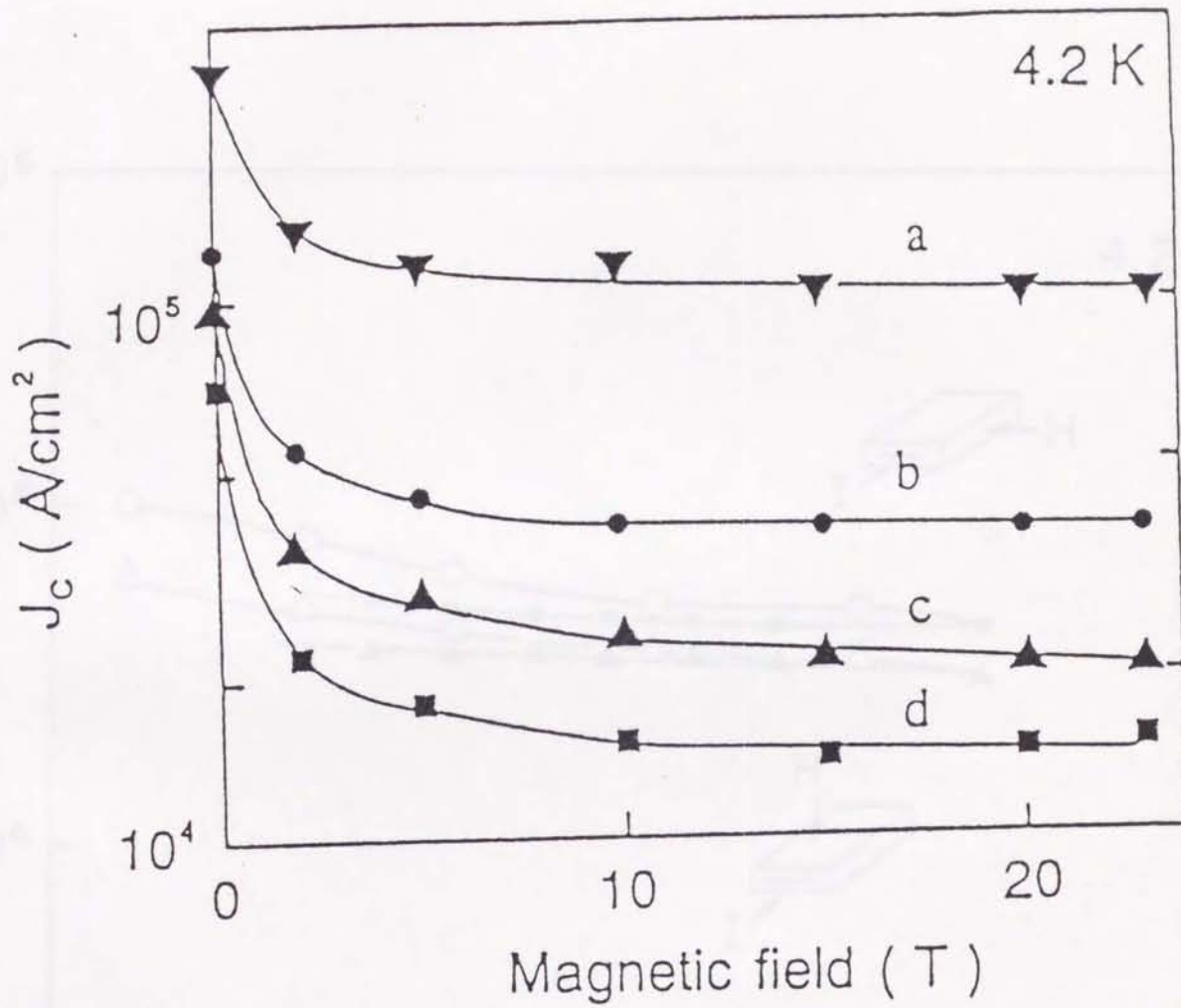


Fig.5-3-1

Fig.5-3-2

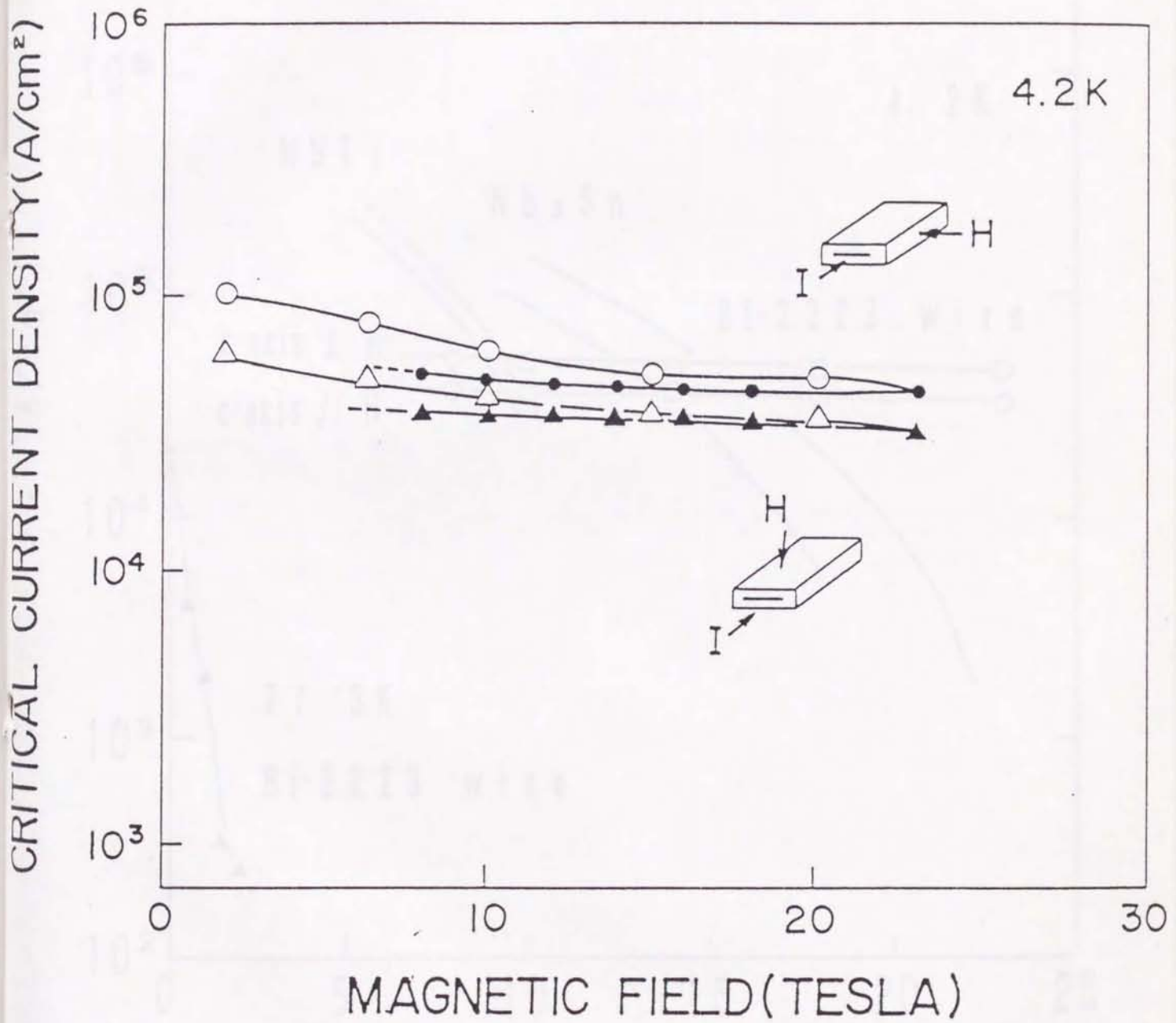


Fig.5-3-2

Fig.5-3-3

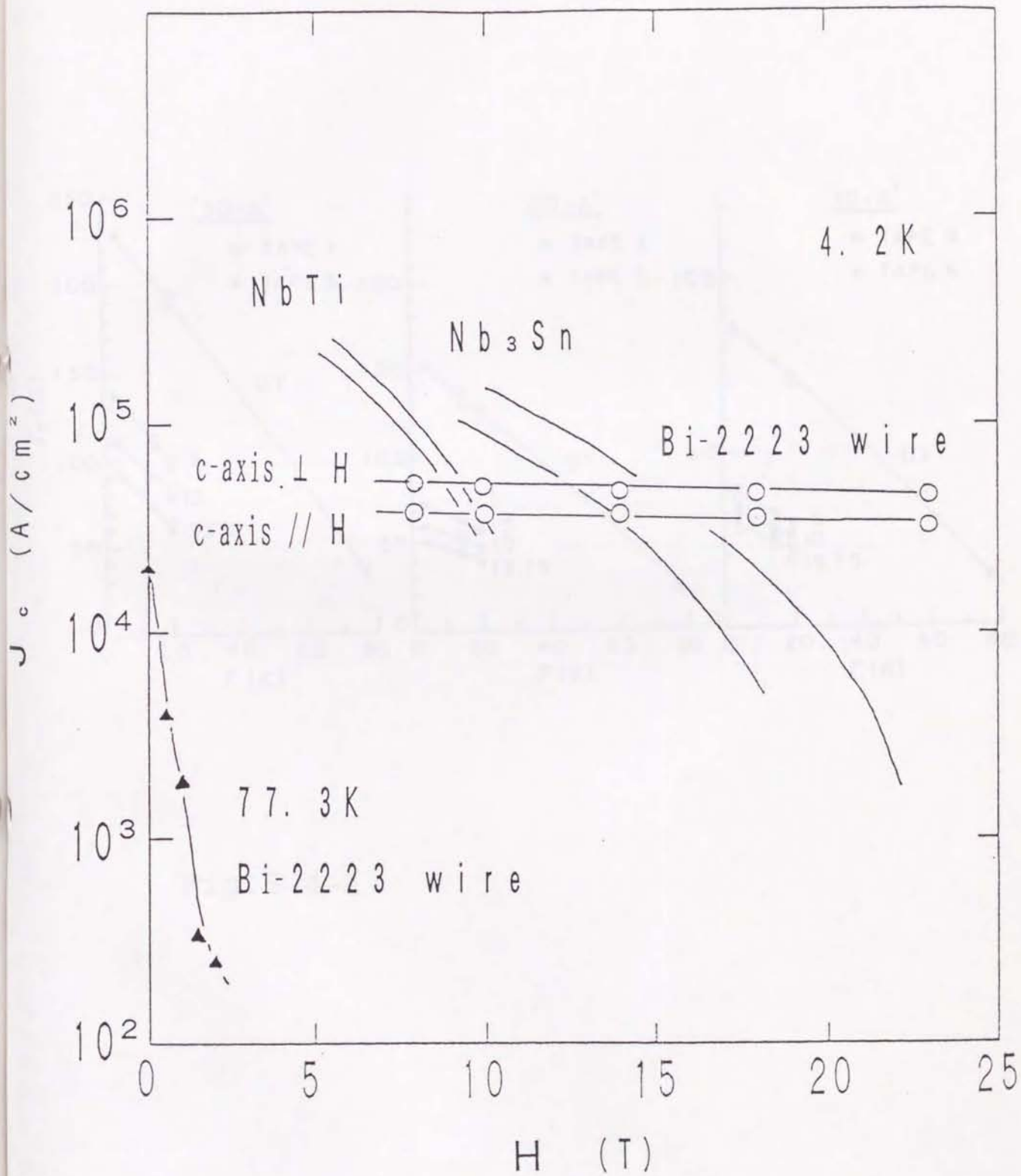


Fig.5-3-3

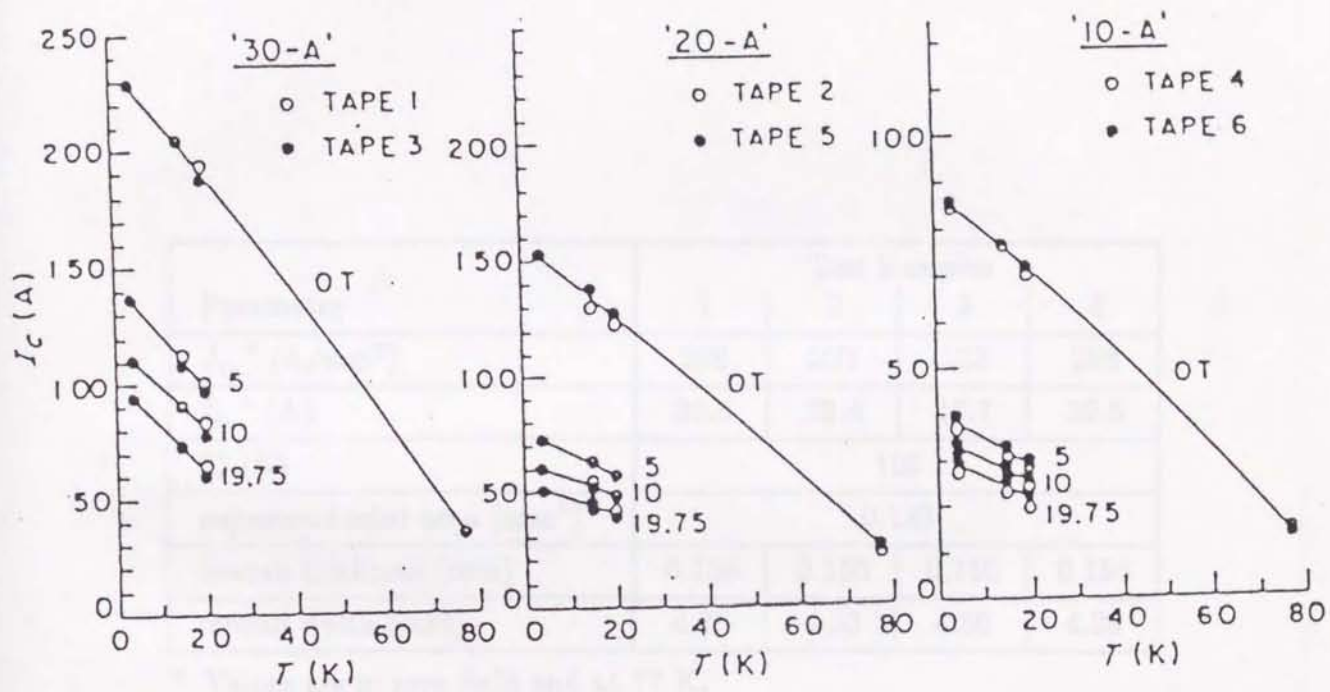


Fig.5-4-1

Parameter	Test Samples			
	1	2	3	4
$J_{c_0}^*$ (A/mm ²)	298	221	133	298
$I_{c_0}^*$ (A)	39.6	29.4	17.7	39.6
T_c (K)	106			
superconductor area (mm ²)	0.133			
overall thickness (mm)	0.156	0.155	0.150	0.156
overall width (mm)	4.35	4.50	4.50	4.35

* Values are in zero field and at 77 K.

Table 5-4-1

Fig. 5-4-2

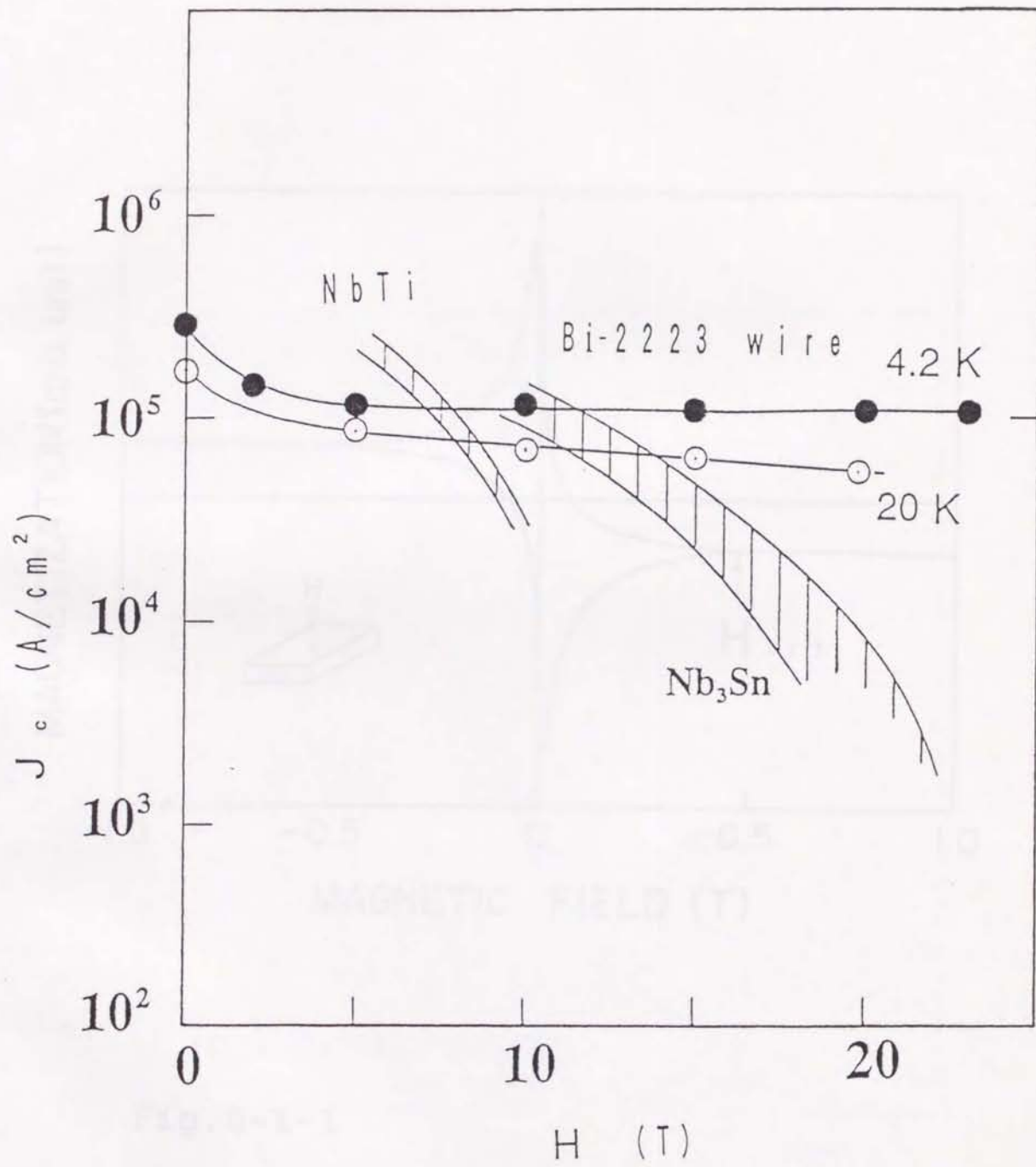


Fig.5-4-2

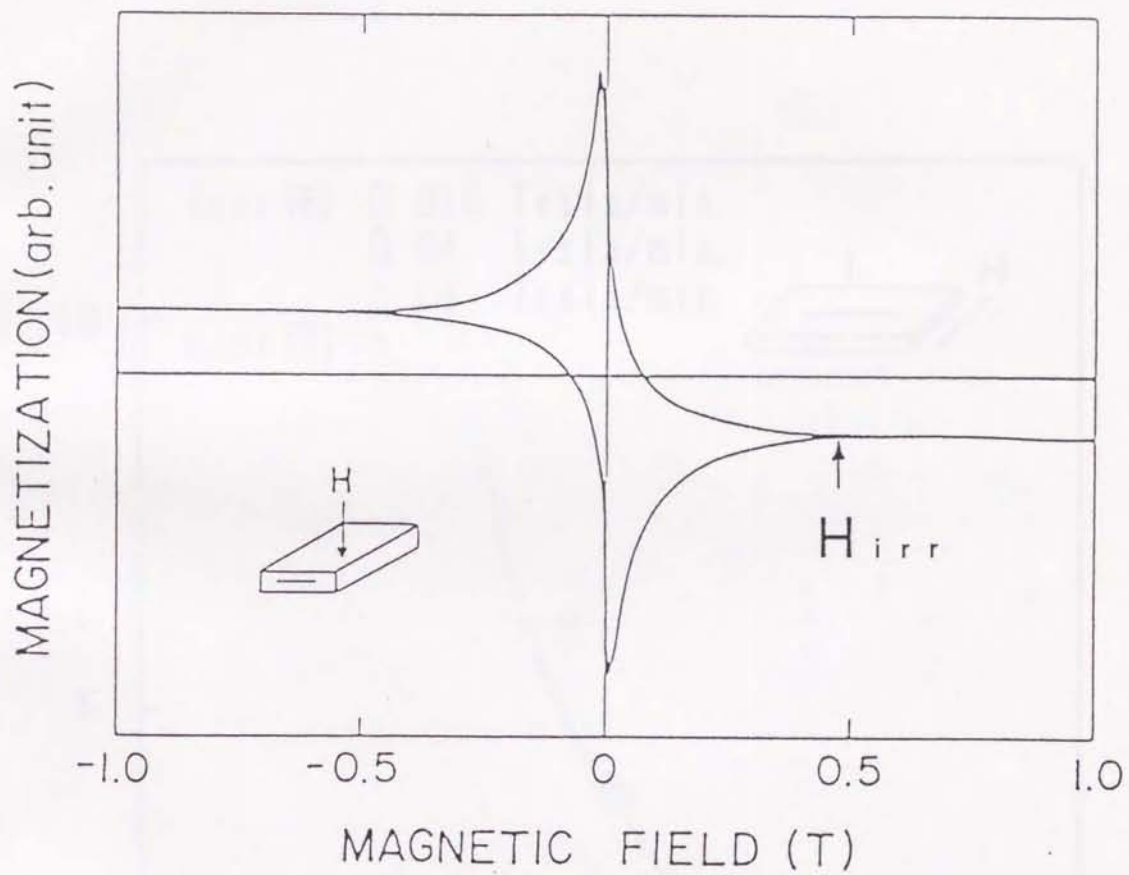


Fig.6-1-1

TEMPERATURE (K)

Fig.6-2-1

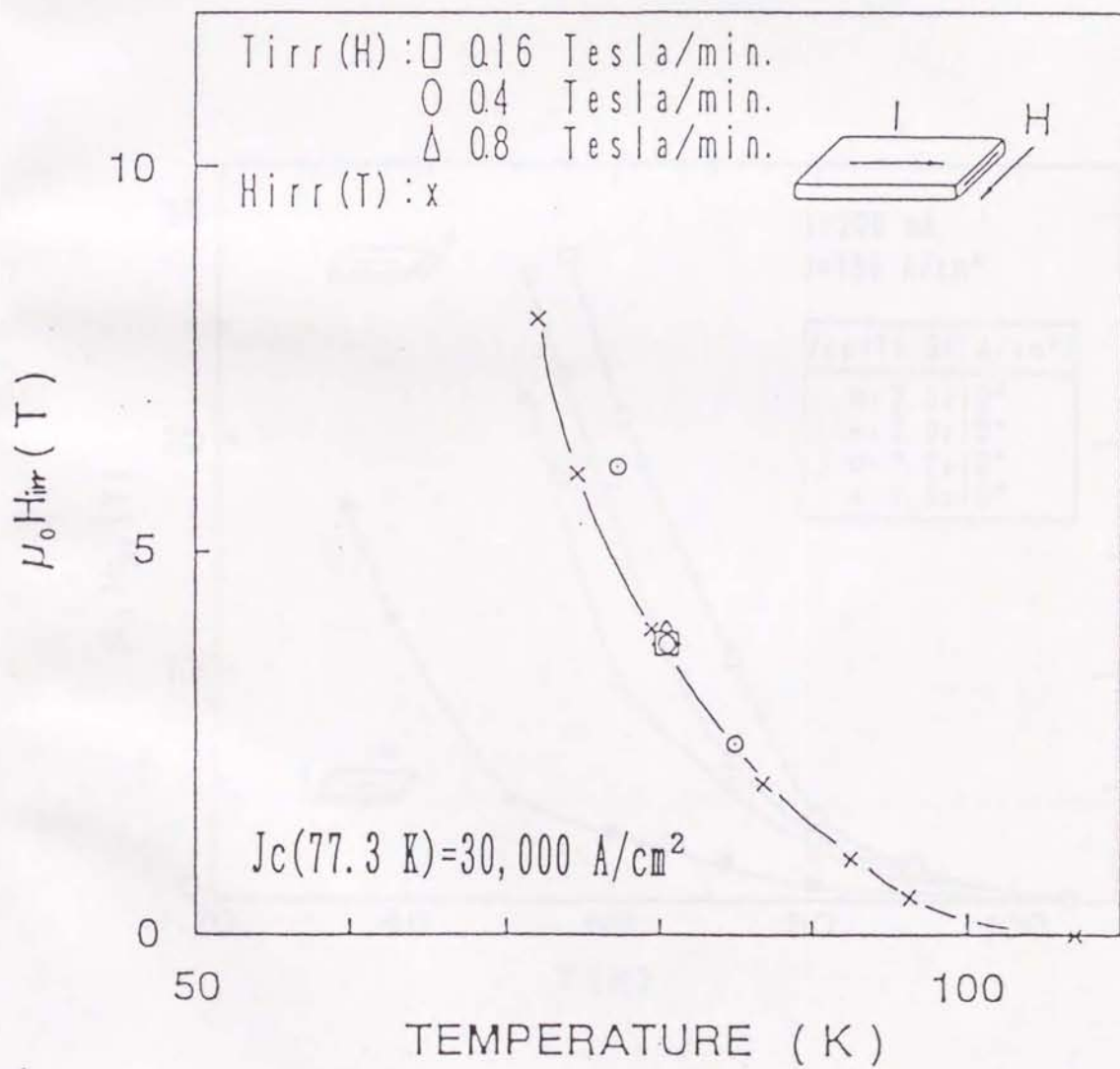


Fig.6-2-1

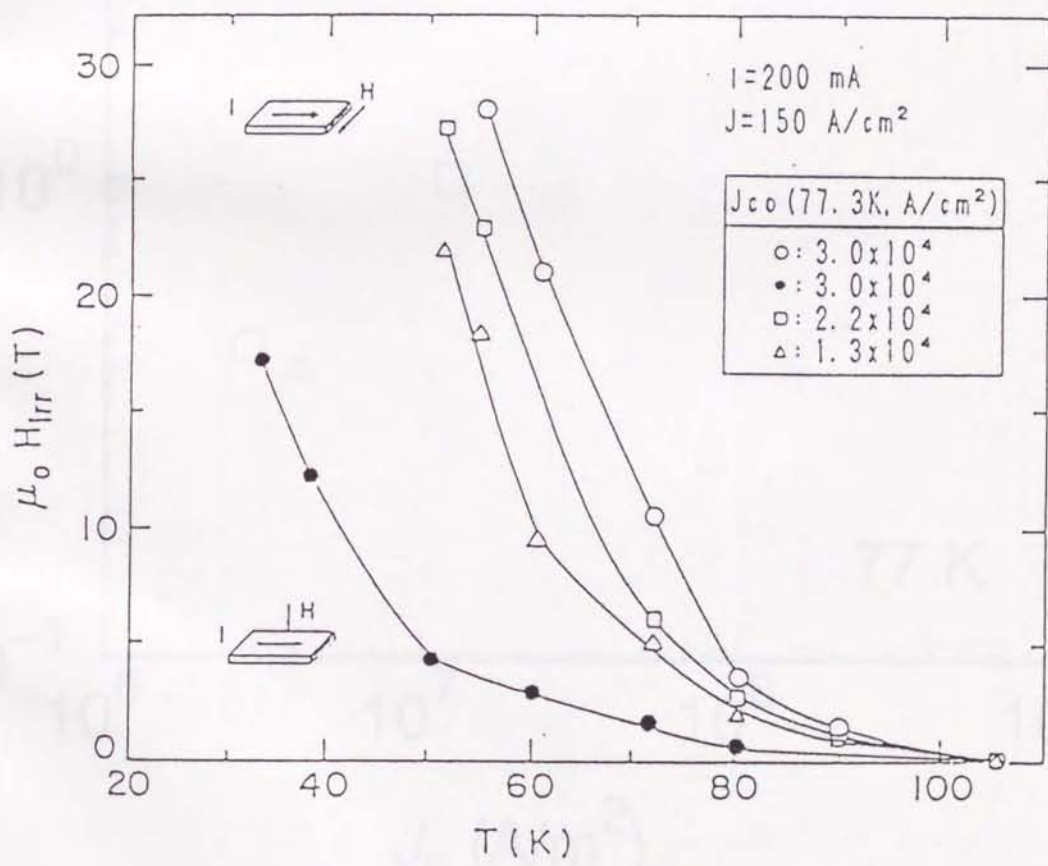


Fig.6-2-2

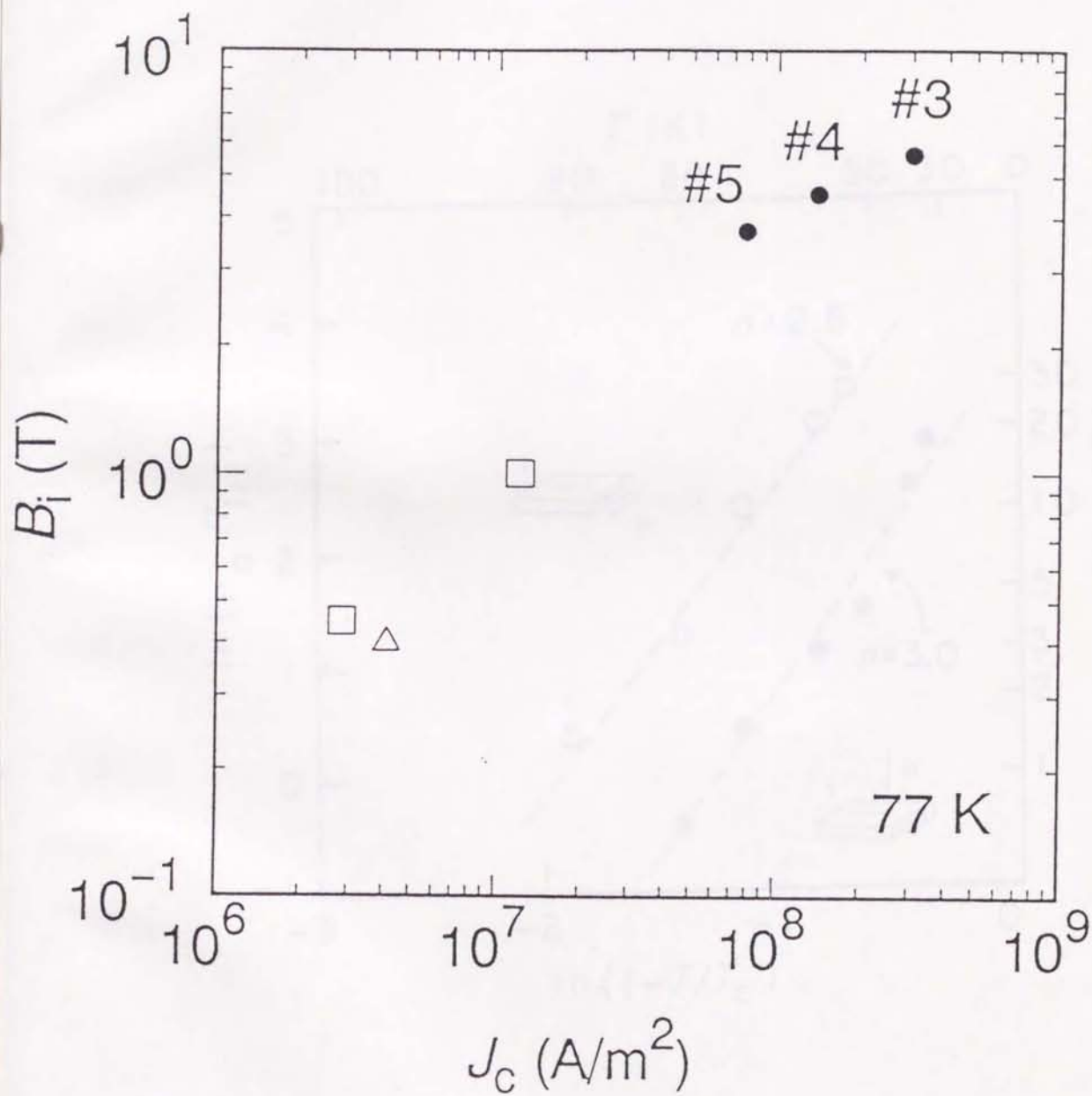


Fig. 6-2-3

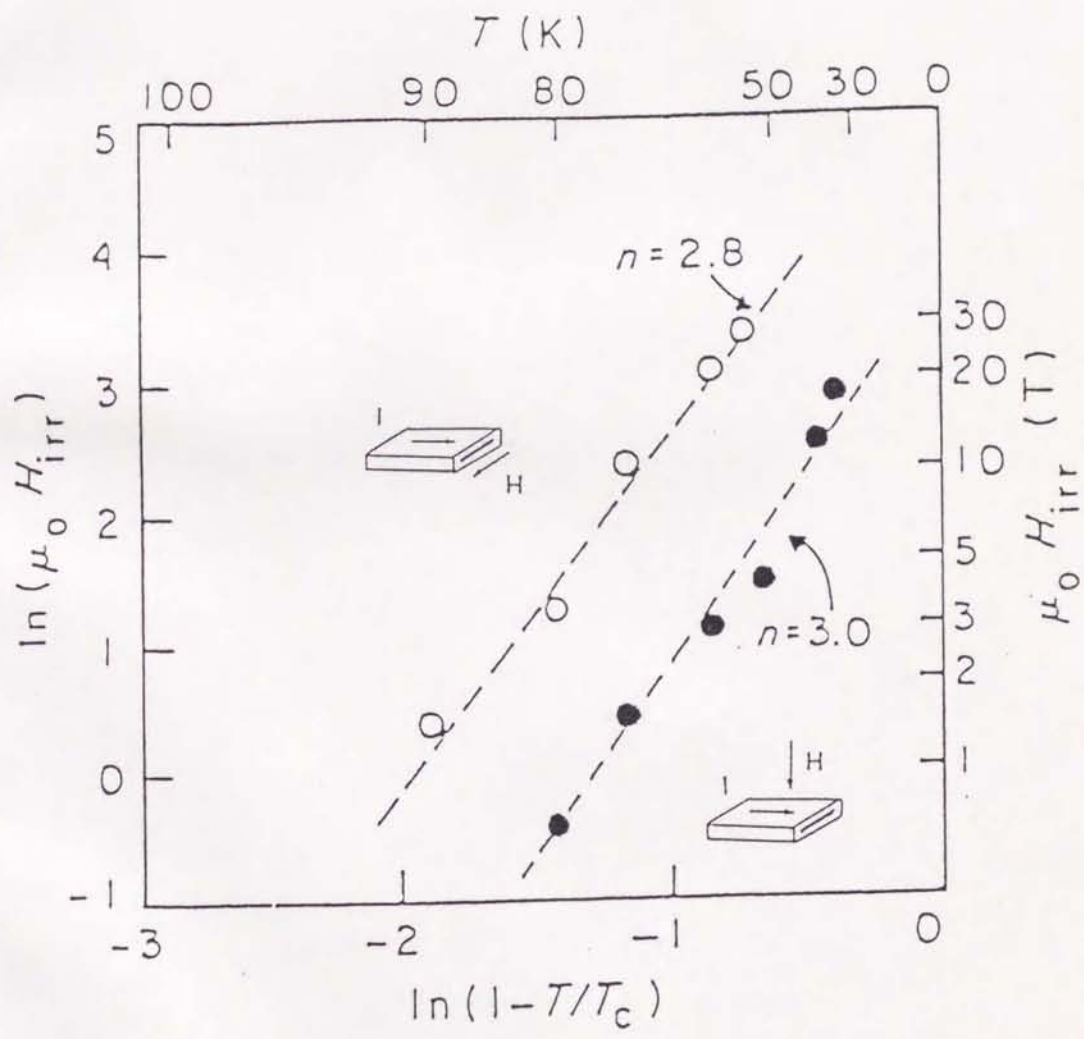
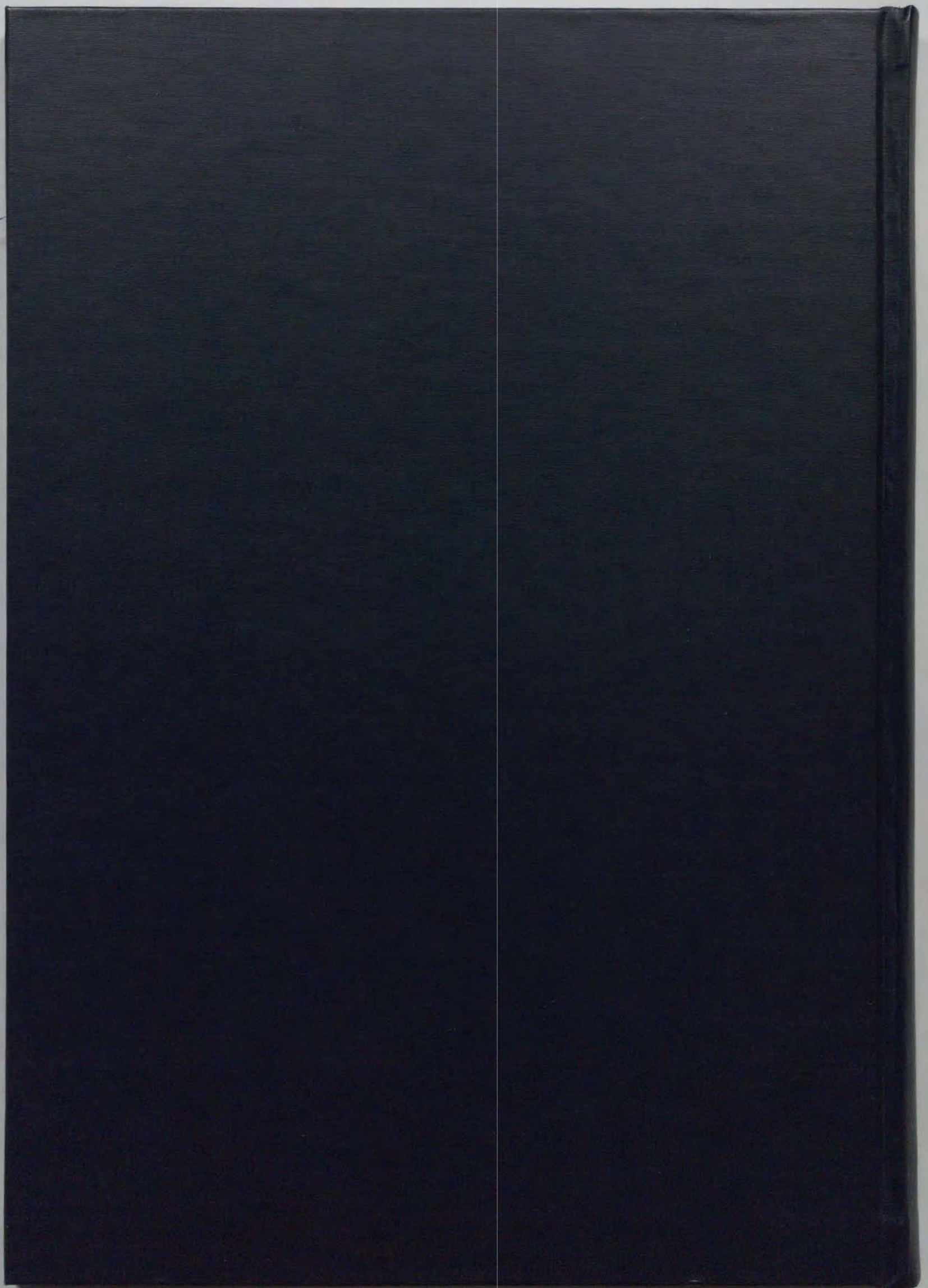


Fig.6-2-4



inches 1 2 3 4 5 6 7 8
cm 1 2 3 4 5 6 7 8 9 10 11 12 13 14 15 16 17 18 19

Kodak Color Control Patches

© Kodak, 2007 TM: Kodak



Kodak Gray Scale



© Kodak, 2007 TM: Kodak

A 1 2 3 4 5 6 **M** 8 9 10 11 12 13 14 15 **B** 17 18 19

